FINAL REPORT

Project Title:	An Innovative Titania-Activated Carbon System for Removal of VOC's & HAP's from Pulp, Paper, Paperboard Mills, and Wood Products Facilities with In-Situ Regeneration Capabilities
Covering Period:	April 1, 2003 through April 30, 2007
Date of Report:	April 30, 2007
Recipient:	University of Florida PO Box 116450 Gainesville, FL 32611 5th Congressional District
Award Number:	DE-FC36-03ID14437
Subcontractors:	MicroEnergy Systems, Inc. 300 Industrial Drive Oakland, MD 21550 Rick Sheahan (301) 334-3455 6th Congressional District. National Council for Air and Stream Improvement PO Box 141020 Gainesville, FL 32614 Ashok Jain (352) 377-4708 5th Congressional District
Other Partners:	None
Contact(s):	David W. Mazyck, (352) 846-1039, dmazyck@ufl.edu Angela Lindner, (352) 846-3033, alind@eng.ufl.edu CY Wu, (352) 392-0845, cywu@ufl.edu
Project Team:	Joe Springer (Project Manager), Golden Field Office DOE/GO Project Officer 1617 Cole Boulevard, Bldg 17/2 Golden, CO 80401 Tel: 303-275-4758/1-800-644-6735, ext. 4758 Fax: 303-275-4753

EXECUTIVE SUMMARY

Forest products provide essential resources for human civilization, including energy and materials. In processing forest products, however, unwanted byproducts, such as volatile organic compounds (VOCs) and hazardous air pollutants (HAPs) are generated. The goal of this study was to develop a cost effective and reliable air pollution control system to reduce VOC and HAP emissions from pulp, paper and paperboard mills and solid wood product facilities. Specifically, this work focused on the removal of VOCs and HAPs from high volume low concentration (HVLC) gases, particularly methanol since it is the largest HAP constituent in these gases. Three technologies were developed and tested at the bench-scale: (1) A novel composite material of activated carbon coated with a photocatalyst titanium dioxide (TiO_2) (referred to as TiO_2-coated activated carbon or TiO_2/AC), (2) a novel silica gel impregnated with nanosized TiO_2 (referred to as silica-titania composites or STC), and (3) biofiltration. A pilot-scale reactor was also fabricated and tested for methanol removal using the TiO_2/AC and STC.

The technical feasibility of removing methanol with TiO_2/AC was studied using a composite synthesized via a spay desiccation method. The removal of methanol consists of two consecutive operation steps: removal of methanol using fixed-bed activated carbon adsorption and regeneration of spent activated carbon using in-situ photocatalytic oxidation. Regeneration using photocatalytic oxidation employed irradiation of the TiO_2 catalyst with low-energy ultraviolet (UV) light. Results of this technical feasibility study showed that photocatalytic oxidation can be used to regenerate a spent TiO_2/AC adsorbent. A TiO_2/AC adsorbent was then developed using a dry impregnation method, which performed better than the TiO_2/AC synthesized using the spray desiccation method. The enhanced performance was likely a result of the better distribution of TiO_2 particles on the activated carbon surface. A method for pore volume impregnation using microwave irradiation was also developed. A commercial microwave oven (800 W) was used as the microwave source. Under 2450 MHz microwave irradiation, TTIP was quickly hydrolyzed and anatase TiO_2 was formed in a short time (< 20 minutes). Due to the volumetric heating and selective heating of microwave, the solvent and by-products were quickly removed which reduced energy consumption and processing time.

Activated carbon and TiO_2/AC were also tested for the removal of hydrogen sulfide, which was chosen as the representative total reduced sulfur (TRS) species. The BioNuchar AC support itself was a good H_2S remover. After coating TiO_2 by dry impregnation, H_2S removal efficiency of TiO_2/AC decreased compared with the virgin AC due to the change of surface pH. Under UV light irradiation, H_2S removal efficiency of TiO_2/AC composite doubled, and its sulfate conversion efficiency was higher than that of AC. The formation of sulfate is preferred since the sulfate can be removed from the composite by rising with water.

A pilot-scale fluidized bed reactor was designed to test the efficiency of methanol oxidation with TiO_2/AC in the presence of UV light. TiO_2/AC was prepared using the spray desiccation method. The TiO_2/AC was pre-loaded with (1) methanol (equivalent to about $2\%_{wt}$) and (2) methanol and water. When the TiO_2/AC loaded with methanol only was exposed to UV light for one hour in the reactor, most of the methanol remained in the carbon pores and, thus, was not oxidized. The TiO_2/AC loaded with methanol and water desorbed about 2/3 of the methanol from its pores during fluidization, however, only a small portion of this desorbed methanol was oxidized.

A biofilter system employing biological activated carbon was developed for methanol removal. The biofilter contained a mixed packing with Westvaco BioNuchar granular activated carbon, perlite, Osmocote slow release ammonium nitrate pellets, and Agrasoke water crystals in a 4:2:1:1 ratio by volume. The biofilter was inoculated with a bacterial culture collected from a Florida pulp and paperboard plant. A non-inoculated biofilter column was also tested. Use of a biological inoculum enriched from biofilm in the pulp and paper process has the potential to enhance the performance of a GAC biofilter. During testing, packing material was removed from the inlet and oulet of the biofilters and analyzed for genetic diversity using molecular techniques. The biofilter inoculated with specifically-enhanced inoculum showed higher bacterial diversity for methylotrophs and all bacteria, as compared to a non-inoculated biofilter. Mixed methylotrophic cultures, selected as potential biofilter inocula, showed increased methanol removal with highest concentrations of nitrogen provided as nitrate.

A photocatalytic reactor employing STC pellets was optimized for methanol removal at the bench scale. The following variables were manipulated to study their effect on methanol removal: (1) STC pore size, (2) TiO_2 loading of STC, (3) STC aging time during synthesis, (4) UV wavelength, (5) residence time, and (6) influent methanol concentration. Methanol removal via adsorption (in the dark) and simultaneous adsorption and oxidation (i.e., with UV light) was dependent on the pore size of the STC, with the smallest pore size (i.e., 40 Å) performing the best. Various TiO_2 loadings between 1 and 60% were studied and the results showed an optimal TiO_2 loading of 4%. A reduction in the aging time of the pellets from 2 days at room temperature and 2 days at 65 deg. C to 1 day at 65 deg. C did not affect methanol removal performance. Shorter aging times were not feasible since the pellets did not shrink enough for them to be removed from the mold for drying. Studies comparing UV light with a peak wavelength of 254 nm and 365 nm showed that the higher intensity of the 254 nm light bulb resulted in more complete oxidation. The methanol removal via adsorption and oxidation was dependent on the residence time of the gas though the reactor and influent methanol concentration. Increasing residence time resulted in lower effluent methanol concentrations. When the STC was irradiated with UVC light, 90% methanol removal was achieved with a 4.3 second residence time and influent methanol concentration of 50 ppm_v. The design of the pilot reactor was modified to simulate these reactor conditions at a flow rate of 40 ACFM.

The fluidized bed pilot reactor as modified into a fixed bed configuration and the STC technology was tested for methanol removal. The STC synthesis procedure was scaled-up so that large quantities of the STC pellets could be produced. The testing conditions included a residence time of 4.3 seconds, influent methanol concentration of 50 – 100 ppm_v, and influent relative humidity of 95-99%. Over a 24 hour period, methanol removal rates ranged from 65 to 95%. Production of intermediate oxidation byproducts (i.e., formaldehyde) was low (< 1 ppm_v). The methanol removal rate was dependent on the UV intensity in the packed bed. Testing conducted with minimum UV intensity resulted in a steady state methanol removal rate of 20-40%. In order to increase methanol oxidation rates when using photocatalytic reactors for large flow rates, the development of a novel silica-titania coated packing (STCP) material began. A second generation pilot reactor was fabricated for testing the STCP. Initial testing showed 99% removal of methanol.

A life cycle analysis of the technologies developed during this work is being conducted. The goal of the LCA is to compare the environmental impact associated with the current state of volatile emissions from pulp and paper mills with that of a system employing photocatalytic oxidation followed by a biofilter polisher.

TABLE OF CONTENTS

PROJECT OBJECTIVE

The goal of the proposed work is to develop a cost-effective and reliable air pollution control system to remove VOCs (volatile organic compounds) and HAPs (hazardous air pollutants) in emissions from pulp, paper and paperboard mills, and solid wood products facilities. The focus of our proposed control system is a novel composite material of activated carbon coated with a photocatalyst titanium dioxide (TiO_2), herein referred to as TiO_2-coated activated carbon.

BACKGROUND

Forest products provide essential resources for human civilization, including energy and materials. Compared to fossil fuels, such as coal and oil, the resources from forest products are more sustainable and diverse. In processing forest products, however, unwanted by-products, such as VOCs and HAPs, are generated. Effective control of these emissions is of seminal importance to the continuing development of the forest product industry.

Currently thermal oxidation is the most commonly applied technique for the control of VOC and HAP emissions from the forest products industry sources. While effective, these measures require a constant fuel supply to support the thermal energy requirements. Considering its operating cost involving intensive resources and the formation of NOx, thermal oxidation is not favorable in the long run. In certain facilities, the gas stream is directed to a boiler for treatment. Although the fuel cost is reduced in comparison to thermal oxidation technologies, the transport of the gas stream and the ductwork building is still costly. Hence, a cost-effective technique for in-situ treatment of these pollutants is needed.

The goal of this work was to develop a cost-effective and reliable air pollution control system to reduce VOC and HAP emissions from pulp, paper and paperboard mills and solid wood products facilities. Specifically, this work focused on the removal of VOCs and HAPs from high volume low concentration (HVLC) gases, particularly methanol since it is the largest HAP constituent in these gases. The focus of the control system is a novel composite material of activated carbon coated with a photocatalyst titanium dioxide (TiO_2), herein referred to as TiO_2-coated activated carbon. Activated carbon has been shown to be effective in removing VOCs and HAPs from various sources, and its effectiveness is attributed to its high surface area (e.g., > 1000 m^2/g). For example, the Department of Defense chose to use activated carbon to remove VOCs and HAPs, such as methyl ethyl ketone (MEK) and methyl isobutyl ketone (MIBK), from military paint spray booths in Barstow, CA (Cannon et al., 1996).

Despite its ability to effectively adsorb VOCs and HAPs, activated carbon does have a finite service life, and, once exhausted, regeneration is necessary to return this spent material back to (or as close as possible to) its virgin (new) capacity. Typically, regeneration of activated carbon is performed ex-situ by exposing the carbon to high temperatures in an oxidizing environment. To minimize the down time due to regeneration and to lower the energy requirements and costs associated with ex-situ regeneration, this work focused on coating the activated carbon with a photocatalyst and using low-energy UV light to regenerate the carbon in-situ. In traditional thermal or microwave regeneration, pollutants are simply desorbed. Regeneration in the TiO_2-coated activated carbon system will be achieved by photocatalytic oxidation of pollutants (Sadeghi et al., 1996; Wu et al., 1998), thus no post-treatment is needed for the desorbed pollutants. Additionally, titania can photocatalytically oxidize high molecular weight organics, hence preventing the glazing coating problem commonly encountered in an adsorption bed (Fujii et al., 1997).

In addition to the development of TiO_2-coated activated carbon, two other technologies were evaluated for the removal of VOCs and HAPs: (1) silica-titania composites (STC), which consist of a porous, high surface area silica-gel substrate that is transparent to UV light and impregnated with photocatalyst particles (i.e., TiO_2) and (2) a biofilter comprised of biologically active activated carbon. These technologies were evaluated for their feasibility for use as a polishing step after the TiO_2-coated activated carbon. In addition, the STC was evaluated for its use as the primary removal process for VOCs and HAPs.

TITANIA-COATED ACTIVATED CARBON (TiO_2/AC)

Removal of Methanol Using TiO_2/AC Adsorption and Photocatalytic Oxidation

The objective of this study was to investigate the technical feasibility of the removal and destruction of methanol at the laboratory scale using combined adsorption and photocatalytic regeneration. The process consists of two consecutive operational steps: removal of methanol using fixed-bed activated carbon adsorption and regeneration of spent activated carbon using in-situ photocatalytic oxidation. To facilitate the regeneration, the activated carbon was coated with a TiO_2 photocatalyst (Degussa P25) by a spray desiccation method, which would allow the composite to act as both an adsorbent for capturing the methanol and a photocatalyst for destroying the methanol during regeneration. The activated carbon concentrates the pollutants around the photocatalyst to improve the photocatalytic efficiency and reduce energy consumption.

Materials and Methods. TiO_2 photocatalyst (P25, Degussa); methanol/air mixture (1000 ppm_v, Praxair); activated carbon (Bio-Nuchar 120, wood based chemically activated carbon, effective particle size 1.1 - 1.3 mm, MeadWestvaco). The Bio-Nuchar 120 was selected because it possesses the best methanol adsorption capacity among various carbons tested.

TiO_2/AC composite was prepared by a spray desiccation method, which is simple and employs a high performance commercial photocatalyst (Degussa P25 TiO_2) directly. A TiO_2 slurry was sprayed on activated carbon and then dried in a rotary kiln. The amount of TiO_2 and activated carbon added in this procedure depended on the experimental conditions. The TiO_2 loading on the activated carbon was estimated by the apparent/true density of the carbon before and after the coating.

The specific surface area and pore size distribution of the carbon and TiO_2/AC samples were obtained by N_2 adsorption/desorption isotherms performed at 77 K (NOVA 1200, Quantachrome). All samples were dried at 105 ^oC for 2 hours prior to measurement. The specific surface area was determined by multipoint BET using the adsorption data in the relative pressure (P/P_0) range of 0.05-0.30. The isotherms were used to determine the pore size distribution using the Barrett, Joyner, and Halenda (BJH) method with cylindrical pore size. The surface morphology of TiO_2/AC composites was characterized by Scanning Electron Microscopy (JSM6330F, JEOL). The true density of the activated carbon with and without TiO_2 was measured by gas displacement (Ultrapyc 1000 Gas Pycnometer, Quantachrome).

In order to simulate the emissions from paper mills, a low methanol concentration and high humidity (80 ± 2%) were chosen. The experimental set up is shown in Figure 1. One gram of TiO_2/AC was placed on the frit in the reactor which was equipped with an 8 watt UVA lamp (peak wavelength at 365 nm) in the center of the reactor. The distance between the UV lamp and the inner wall of the reactor was 9 mm. The outer diameter of the reactor was 48 mm. The methanol concentration in the influent and effluent of the reactor during the experiment was measured according to the NCASI Chilled Impinger Method CI/SG/PULP-94.02 (NCASI, 1998). The methanol in the air flow was first collected by drawing it through two midget impingers (Analytical Research Systems, Inc.) in series, which were filled with 10 mL of water. The impingers were kept in an ice water bath (2^oC) during sampling to enhance collection efficiency. The sampling time was one hour.

The methanol concentration in the impingers was analyzed by direct injection into a gas chromatograph (Clarus 500, Perkin Elmer) equipped with a flame ionization detector (GC/FID). The methanol removal performance was evaluated by the concentration of methanol in the effluent. Formaldehyde is one of the possible byproducts of methanol photocatalytic oxidation. The Chilled Impinger Method was used to measure formaldehyde concentration. A 2.0 mL aliquot of the impinger sample was mixed thoroughly with 2.0 mL of acetylacetone reagent and reacted in a water bath at 60 ^oC for 10 minutes. After cooling to room temperature, the absorbance at 412 nm was measured by spectrophotometer (DR/4000U, HACH). Formaldehyde concentration was calculated according to standard calibration curve which was prepared and measured previously.

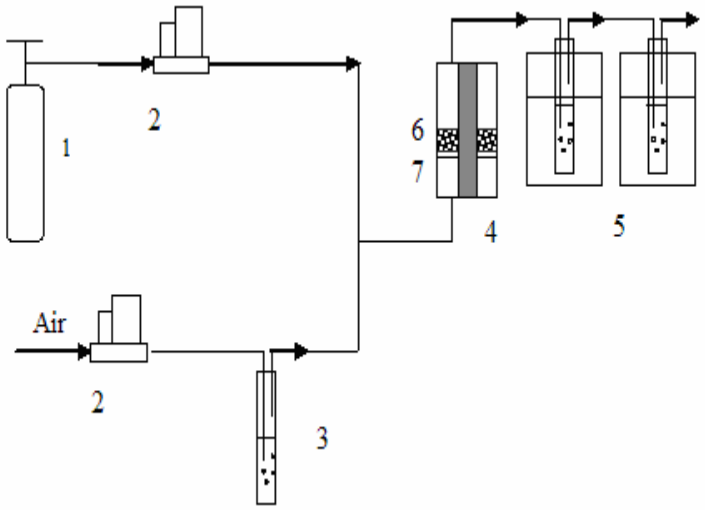

1. Methanol/Air mixture cylinder (1000 ppm_v MeOH); 2. Mass flow controller; 3. Water bubble bottle; 4. Photocatalytic reactor (equipped with 8 W black light UV lamp); 5. Impingers in ice bath; 6. TiO_2/AC; 7. Frit

Figure 1. Experiment Set-up of Methanol Removal Evaluation using TiO_2/AC

The TiO_2/AC sample was pre-adsorbed with moisture until saturated by passing humid air through the reactor at the rate of 0.4 L/min for 16 hours. Humid methanol-laden air was then passed through the fixed bed of TiO_2/AC with and without UV light for 6 hours. The empty bed contact time (EBCT) was about 0.35 s. Table 1 lists the adsorption column parameters. In order to investigate the effect of EBCT, methanol removal performance in 7.00 g TiO_2/AC column with or without UV irradiation was also tested. Before testing the TiO_2/AC sample was pre-adsorbed with humidity until saturated similar to other samples for 44 hours. The adsorption column parameters are listed in Table 1.

Table 1. Adsorption Column Parameters

Parameters	1 g TiO_2/AC	7 g TiO_2/AC
EBCT (s)	0.35	2.45
Bed depth (cm)	0.4	2.8

Methanol Removal Evaluation. In order to evaluate the effect of humidity on methanol adsorption and photocatalytic oxidation, experiments were carried out without pre-saturation of moisture and/or without humidity. Table 2 lists the operation conditions.

Table 2. Operational Conditions for Methanol Removal

Set	Pre-saturation	Humidity	Operation
1	With Moisture	80%	6 hours, w/o UV light
2	no	80%	6 hours, w/o UV light
3	no	0%	6 hours, w/o UV light

In order to reduce the operation cost, adsorption followed by periodic photocatalytic regeneration of TiO_2/AC was tested. To evaluate the effectiveness of photocatalysis on regeneration, experiments were carried out following similar procedures. Methanol-laden air was then passed through the fixed bed of

1.00 g TiO_2/AC without UV light for 6 hours. Then the flow was cut off and the UV light was turned on to regenerate the spent carbon for 3 to 9 hours. Table 3 lists the operation conditions. The adsorption-regeneration cycle was repeated four times. The methanol adsorption capacity of each cycle was calculated. The effect of purge air flow rate in regeneration was also investigated.

Table 3. Operational Conditions for Adsorption/Regeneration Cycles

Set	Pre-saturation	Humidity	Adsorption	Regeneration
4	With Moisture	80%	6 hours	9, 6, 3 hours between each two cycles respectively without purge air
5	No	80%	6 hours	3 hours, without purge air
6	No	0%	6 hours	3 hours, without purge air
7	No	0%	6 hours	3 hours, with 0.1 LPM purge air
8	No	0%	6 hours	3 hours, with 0.2 LPM purge air

TiO_2/AC Characterization. Degussa P25 (specific surface area 50 m^2/g, mean primary particle diameter 20 nm, density = 4 g/cm^3, ~80% anatase phase), is a good photocatalyst cited in numerous articles. Figure 2 shows the SEM images of the TiO_2/AC composite prepared by the described method. The SEM image of the external surface indicates the P25 TiO_2 particles were coated on the AC surface by the described method. Although the particle size of P25 is about 20 nm, the P25 nanoparticles agglomerated on the carbon surface. The difference between the SEM images of the external and internal surface of the TiO_2/AC particle indicates the TiO_2 was mainly coated on the outer surface of the AC particles. Table 4 lists the specific surface area, pore size distribution, and density of the AC before and after TiO_2 coating. From the difference between the true density of AC before and after TiO_2 coating, the TiO_2 loading was estimated to be 9.51%$_{wt}$. The TiO_2 coating did not significantly decrease the BET surface area and the total pore volume of the carbon. The volume of micropores increased due to the micropores formed between the TiO_2 nanoparticles.

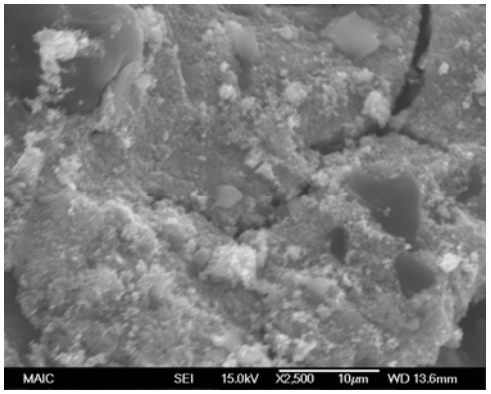

(a) External Surface

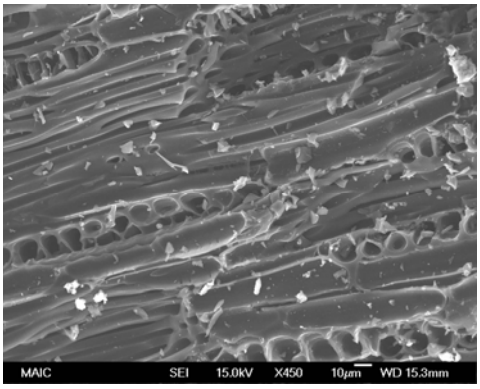

(b) Internal Surface

Figure 2. SEM Images for the TiO_2/AC composite

Table 4. The Effect of Calcination Conditions

	BET Surface Area (m^2/g)	Total Pore Volume (cc/g)	Micropores (<20Å) (cc/g)	Mesopores (200-500Å) (cc/g)	True Density (g/cm^3)	Bulk Density (g/cm^3)
AC	1472	1.45	0.46	0.84	1.668	0.253
TiO_2/AC	1380	1.33	0.54	0.79	1.766	0.270

Methanol Removal w/o UV Light. The methanol removal by the original AC and TiO_2/AC composites with and without UV light was carried out in order to compare their ability to remove methanol via simultaneous adsorption and oxidation. The effluent methanol concentration profiles are shown in Figure 3 for the virgin AC and TiO_2/AC when using 1.00 g of adsorbent. The influent methanol concentration was 31.0 ppm_v. It is apparent from Figure 3 that the effluent methanol concentration increased quickly when treated by the virgin AC with and without UV light. When treated by TiO_2/AC without UV light irradiation, a similar adsorption profile was observed, and the methanol adsorption capacities for the virgin AC and TiO_2/AC composite were similar. However, when methanol was treated by the TiO_2/AC with UV light irradiation, the methanol concentration did not reach saturation for the duration of the experiment. The effluent methanol concentration increased during the first 2 hours and then maintained about 35% removal.

Figure 4 displays the methanol effluent concentration when using 7.00 g TiO_2/AC composite. The influent methanol concentration was 36.4 ppm_v. Apparently, increasing the EBCT increased the methanol removal. Under UV irradiation, the methanol removal efficiency maintained around 90% after 12 hours.

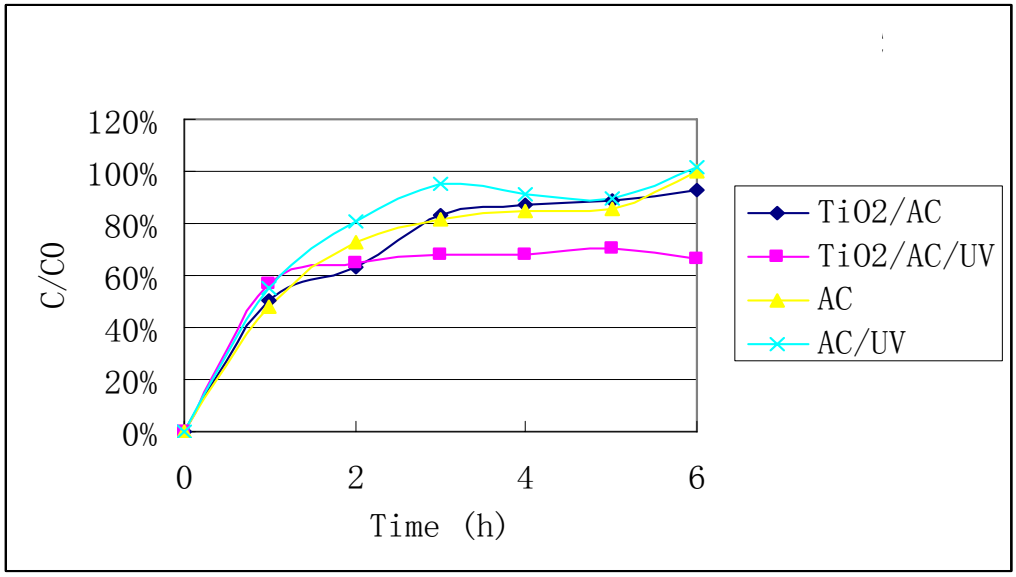

Figure 3. Methanol Effluent Concentration for AC and TiO_2/AC with 1 g of Adsorbent

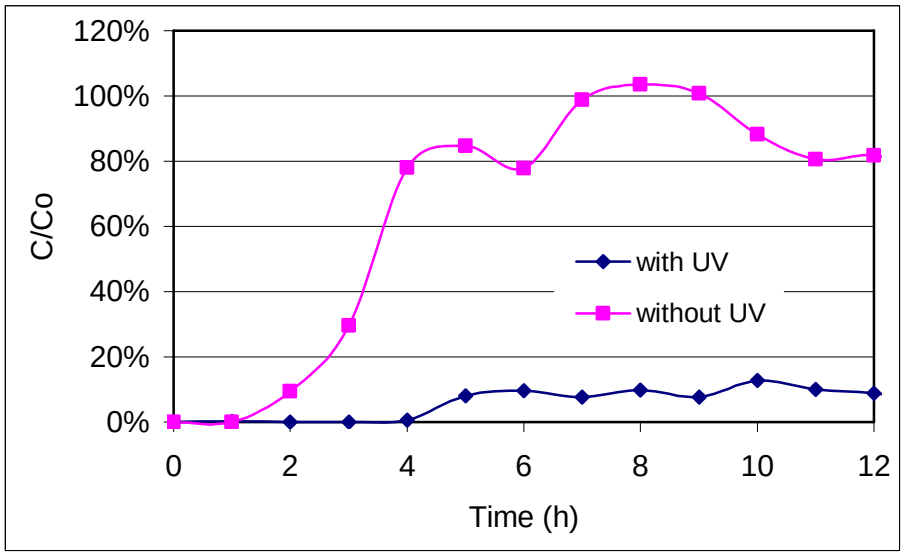

Figure 4. Methanol Effluent Concentration of TiO_2/AC with 7 g of Adsorbent

These two sets of experiments show photocatalytic oxidation can be used to destroy methanol adsorbates simultaneously and extend the AC's usage life.

Effect of Humidity. In order to investigate the effect of humidity on methanol adsorption and photocatalytic oxidation, experiments listed in Table 2 were carried out. The influent methanol concentration was 31.0 ppm_v; 1.00 g TiO_2/AC adsorbent was used in each experiment. Figures 5a and 5b show the relative effluent methanol concentration with and without UVA light.

The results of methanol removal without UV light show that moisture greatly hindered the methanol adsorption on TiO_2/AC. The adsorption capacity of set 3 was much higher than that of set 1 and set 2. The methanol adsorption of set 2 was lower than that of set 1 in the beginning but increased slowly. For set 1, TiO_2/AC was saturated with moisture and TiO_2/AC surface was covered by water molecules and part of the pores were filled with water due to capillary condensation. The water film increased the methanol adsorption in the beginning due to the affinity of methanol for water and decreased the methanol adsorption later because the available adsorption sites were used up. For set 2, because of the competitive adsorption between water vapor and methanol on the carbon surface, the methanol adsorption of set 2 in the beginning was lower than that of set 1. The methanol adsorption of set 2 increased slower than that of set 1 because the adsorbent was not saturated with water vapor.

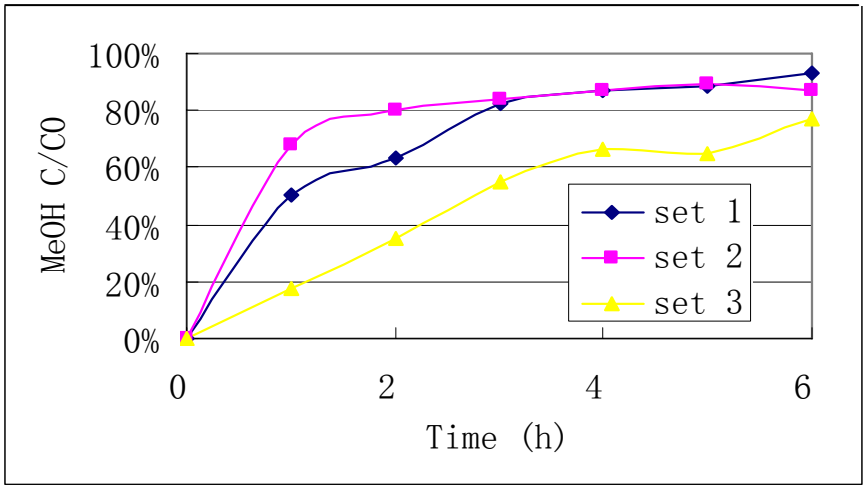

Figure 5a. Normalized Effluent Methanol Concentration of TiO_2/AC without UV Light

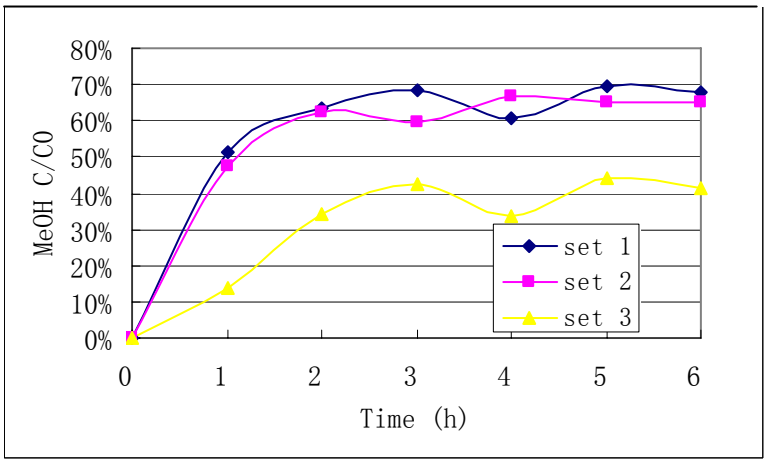

Figure 5b. Normalized Effluent Methanol Concentration of TiO_2/AC with UV Light

The results of methanol removal with UV light show that moisture greatly hindered the methanol oxidation on TiO_2/AC. This result is concord with that of Kim et al. (2002), who showed that the photocatalytic degradation rate of methanol was relatively high in lower water vapor concentration and high humidity hindered the photocatalytic degradation of methanol. The methanol removal of set 2 was similar to that of

set 1. This might be because with UV light the photocatalytic oxidation is the main mechanism of methanol removal.

Regeneration Performance. The advantage of the integration of adsorption and photocatalytic regeneration are that the photocatalytic oxidation on TiO_2/AC will be accelerated by the high concentration of pollutants eluted from the adsorbent and then reduce the UV irradiation time, thus improving the economy of the process. Moreover, the regeneration process can be operated in-situ at ambient conditions. Figure 6 shows the adsorption breakthrough curves of methanol from fresh and regenerated beds of TiO_2/AC of set 4 (C_0 =31.0 ppm). Figure 7a, 7b, and 7c show the calculated adsorption capacity of each cycle of set 4, 5 (C_0= 34.3ppm) and 6 (C_0 =27.6 ppm).

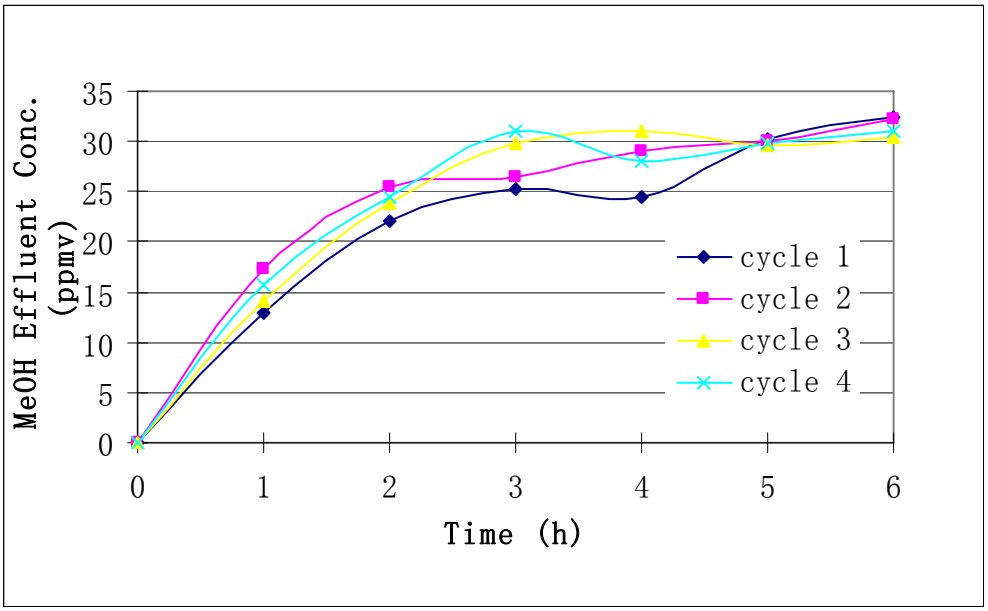

Figure 6. Breakthrough Curves of Set 4

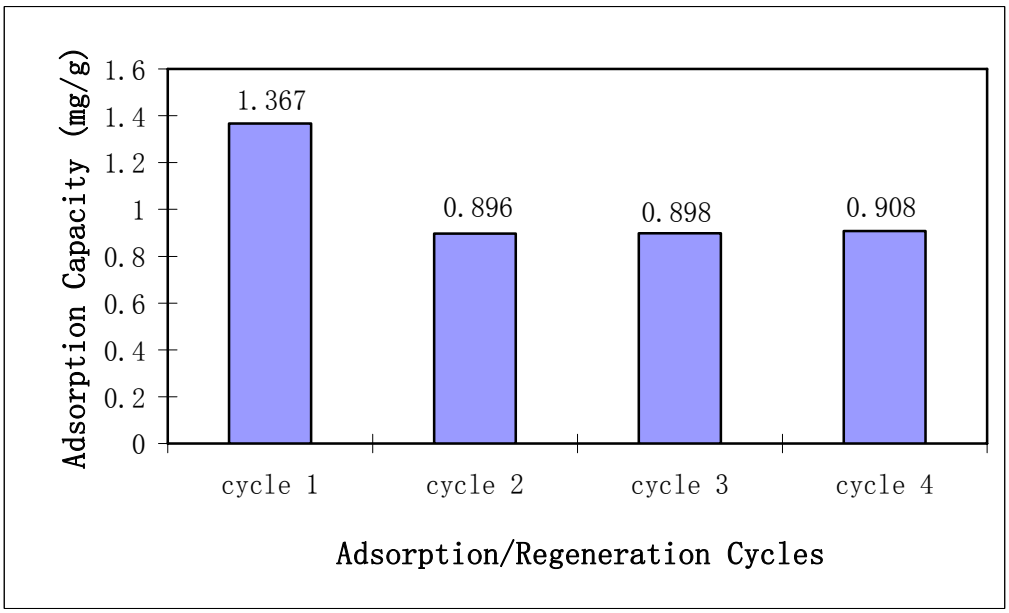

Figure 7a. Adsorption Capacity of Set 4

For set 4, Figure 6 and Figure 7a show that around 60% of the virgin capacity of the TiO_2/AC was regenerated and an increase in the regeneration time did not increase the regeneration capacity. Therefore, 3 hours of regeneration was used in set 5 and set 6. For set 5, the virgin capacity was similar to that of set 4. This result was consistent with the result of Figure 5a. The regeneration capacity of cycle 2, 3 and 4 of set 5 was around 80%, 74% and 60% of the virgin capacity of set 4 respectively. In the first 3 cycles of adsorption, the TiO_2/AC did not saturate with water vapor. That resulted in the increase of capacity. After 3 cycles of adsorption, the TiO_2/AC was almost saturated with water vapor. Therefore the regeneration capacity of the 4^{th} cycle of set 5 was similar to that of set 4. For set 6, Figure 7c shows that the virgin capacity was 1.77 times of the virgin capacity of set 4. This is because the TiO_2/AC used in set 6 was not pre-saturated with moisture and no moisture was added in the air streams. Thus, the entire adsorbent surface was available for the methanol in the beginning. The regeneration capacity of set 6 was quite similar to that of set 4. That indicated just the outer layer of the TiO_2/AC was regenerated where the UV light can reach and the TiO_2 coating was. Crittenden et al. (1997) proved the photocatalytic regeneration process was limited by the desorption of the adsorbate from the interior of the carbon. A possible way to increase the regeneration capacity is to increase the desorption rate through purging or heating. Therefore, purge air was used to increase the desorption rate and the effect of purge air flow was investigated.

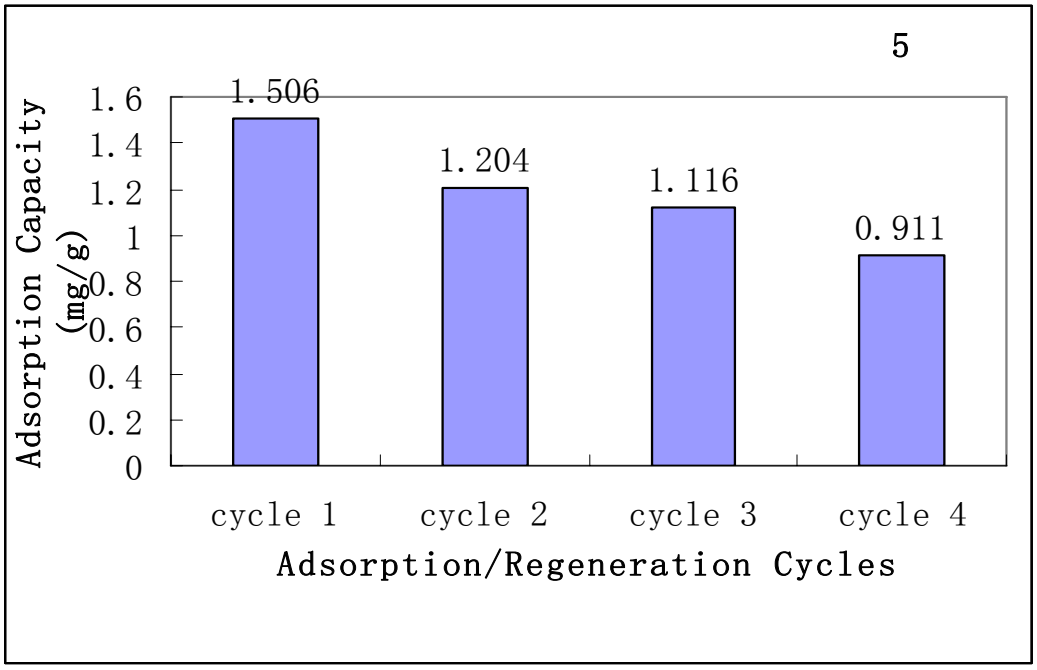

Figure 7b. Adsorption Capacity of Set 5

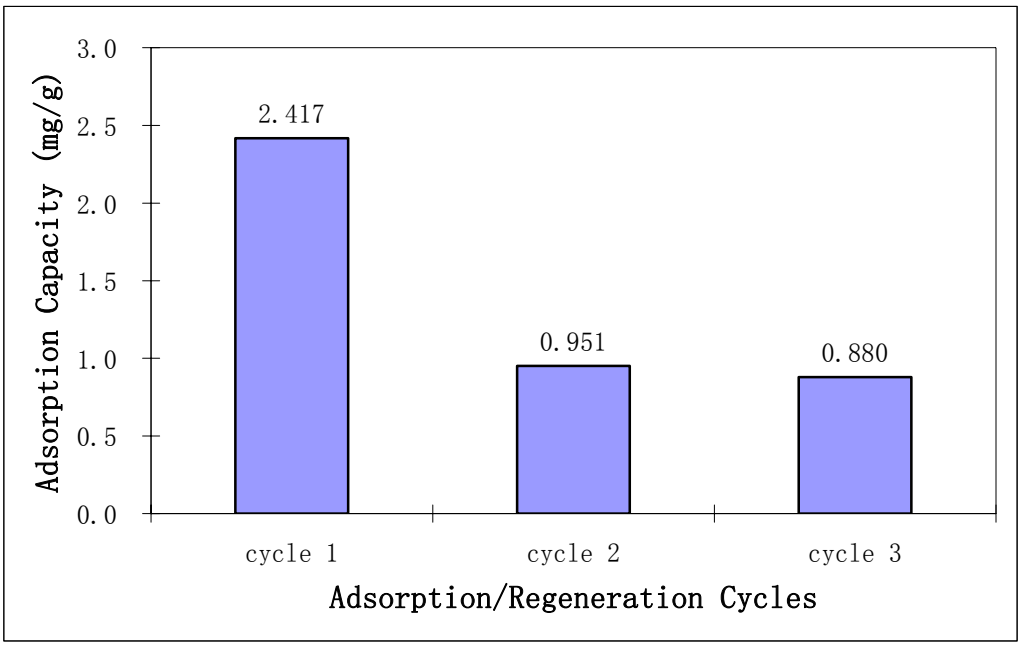

Figure 7c. Adsorption Capacity of Set 6

Figure 8a and 8b show the calculated adsorption capacity of each cycle of sets 7 (C_0= 23.7 ppm_v) and 8 (C_0 =23.7 ppm_v). During regeneration, the methanol and formaldehyde in reactor effluents were collected and measured by the NCASI Chilled Impinger Method. The methanol desorption amount and formaldehyde formation amount in the regeneration are also shown in Figures 8a and 8b.

When using 0.2 LPM purge air (set 7), around 77% of the original capacity was regenerated after 3 hours regeneration. Around 52% regeneration capacity resulted from direct desorption. When using 0.1 LPM purge air (set 8), around 80% of the original capacity was regenerated after 3 hours of regeneration. Around 24% regeneration capacity resulted from direct desorption. Without purge air (set 6), only 40% of the original capacity was regenerated after 3 hours UV irradiation.

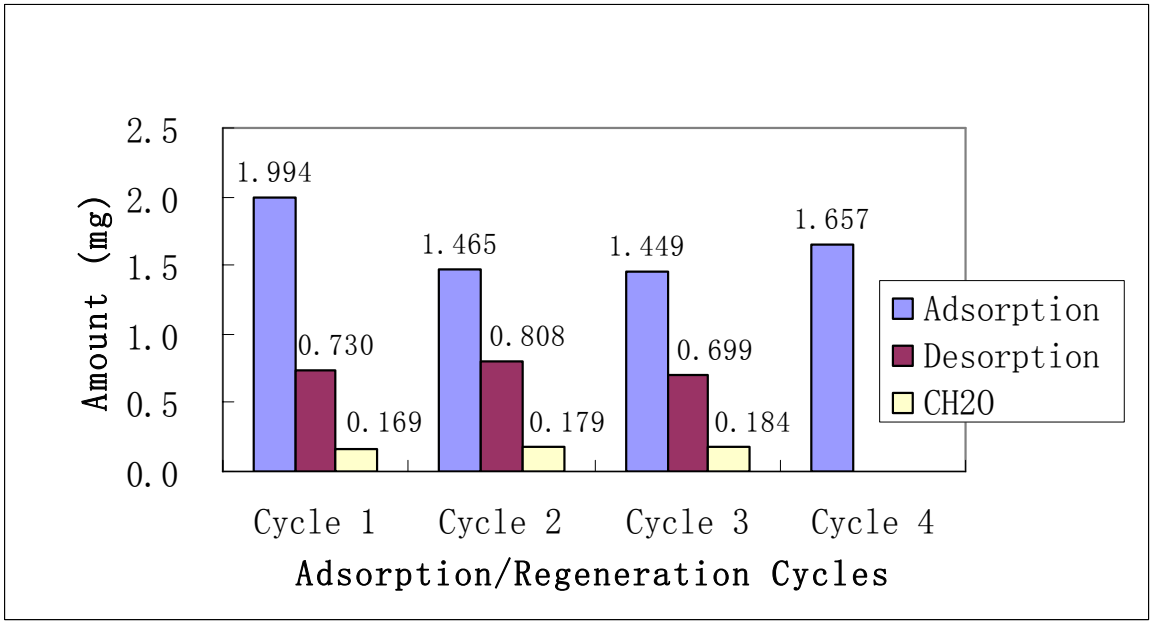

Figure 8a. Adsorption/Regeneration of Set 7

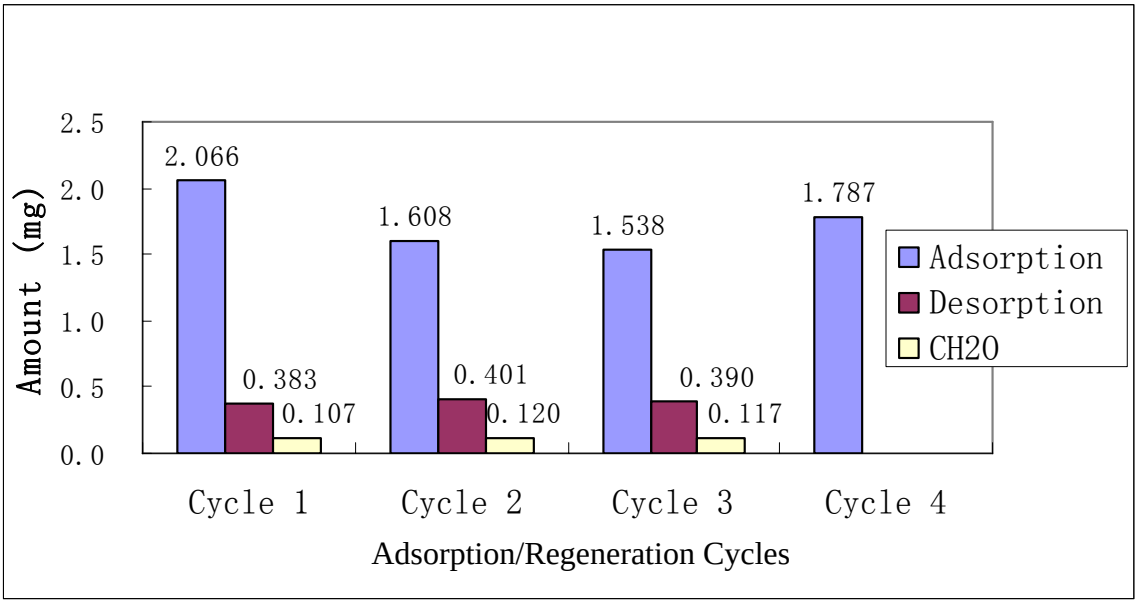

Figure 8b. Adsorption/Regeneration of Set 8

Photocatalytic regeneration of activated carbon ascribe to both desorption and photocatalytic degradation of the adsorbate. Therefore, the desorption rate and degradation rate both affected the regeneration efficiency. Without purge air, desorption rate was so low that the methanol adsorbed on the carbon could not effectively transfer to the TiO_2 photocatalyst. Therefore, the photocatalytic regeneration process was limited by the desorption rate. With 0.1 LPM purge air, the regeneration efficiency was greatly increased. However, the desorption rate was higher than the degradation rate. Therefore, part of the methanol directly desorbed without degradation. With 0.2 LPM purge air, the desorption rate was further increased. But the regeneration efficiency decreased because degradation rate decreased resulting from the decrease of contact time. The formaldehyde formation of set 7 was higher than that of set 8. This may indicate the contact time was not enough for complete photocatalytic oxidation. Based on the above mentioned results, the photocatalytic degradation should reach maximum when the degradation rate and the desorption rate match with each other.

Conclusions. Photocatalytic oxidation can be used to regenerate a spent adsorbent (Bio-Nuchar120 AC) and destroy methanol simultaneously. The amount of photocatalyst loaded onto the AC had no significant impact on the adsorption capacity of the AC. Increasing the EBCT from 0.35 s to 2.45 s can significantly increase the efficiency of the simultaneous adsorption and photocatalytic oxidation. The high humidity significantly hinders the methanol adsorption and simultaneous adsorption and photocatalytic oxidation on TiO_2/AC because of the competitive adsorption between water vapor and methanol. Without purge air, high humidity had no significant impact on the photocatalytic regeneration. The regeneration capacity for an influent methanol of 31.0 ppm_v (RH = 80%) is about 60% of virgin capacity of prepared TiO_2/AC (saturated with water vapor). Increasing the regeneration time from 3 hours to 9 hours did not increase the regeneration capacity. This indicated that the regeneration process is limited by the desorption of adsorbate from the interior surface of the carbon. Increasing the desorption rate can greatly increase the regeneration capacity. However, when desorption rate is greater than photocatalytic oxidation rate, part of the methanol directly desorbs.

Dry Impregnation of Titania onto Activated Carbon

The spray desiccation coating method described above can effectively coat commercially available TiO_2 on AC. However, the nanoparticles of TiO_2 were agglomerated on the carbon surface, which can result in reduced photocatalytic efficiency. In addition, since the spray dessication method is a physical method, the TiO_2 particles were coated on the carbon surface by weak physical force. In order to improve the photocatalytic efficiency and the adherence between TiO_2 photocatalyst and carbon support, dry impregnation method was used to prepare TiO_2/AC composite photocatalyst.

Impregnation is a commonly used method in supported catalyst preparation. The impregnation method involves three steps: (1) contacting the support with the impregnating solution for a certain period of time, (2) drying the support to remove the imbibed liquid and (3) activating the catalyst by calcination, reduction or other appropriate treatment (Perego et al., 1997). Although impregnation method has been adopted in TiO_2/AC preparation before, very few studies have been carried out on how to prepare TiO_2/AC composite using titanium tetra-isopropoxide precursor and information about the preparation details is very limited. The effects of various preparation parameters (e.g., hydrolysis temperature, hydrolysis time, water vapor concentration) were studied. The prepared TiO_2/AC composite photocatalyst was also evaluated by removing low concentration methanol from a humid air stream.

Material and Methods. The TiO_2/AC composite photocatalysts were prepared by pore volume impregnation using a TTIP solution (with 20% by volume of 2-propanol) followed by hydrolysis and calcination. The principle of this coating method is that the volume of the precursor solution used in the impregnation is equal to the pore volume of the support, which results in a better distribution of the solute on the support surface. Before coating, the activated carbon was heated at 105^{o}C for 4 hours to remove water vapor. The Bionuchar, wood-based activated carbon (pore volume of 1.45 cc/g), was then impregnated with TTIP solution followed by hydrolysis in a hydrolysis reactor, as shown in Figure 9. The diameter of the reactor was 1 inch and the support frit size was 25 -50 m to better distribute air flow through the column. Carbon impregnated with TTIP solution (3.5 g) was placed in the reactor and air saturated with water from a water bubble bottle was passed through the reactor at 0.75 L/min for 2 or 24 hours. The EBCT was approximately 0.8 s. The temperature of the water bubble bottle was controlled at 25 and 90 ^{o}C via a hot plate. The temperature of the reactor was controlled at 25, 90, and 175 ^{o}C by heating tape wrapped around the reactor. The various hydrolysis conditions are summarized in Table 5. For convenience, notations in the first column are used to present different samples. The first number stands for the temperature of the water bubble bottle; the second number represents the temperature of the hydrolysis reactor; the third part represents the treatment time. For example, 25-25-2 represents the sample being hydrolyzed at 25^{o}C for 2 hours while the water bubble bottle was kept at 25^{o}C. After hydrolysis, the samples were dried at 105^{o}C for 4 hours to evaporate the adsorbed 2-propanol and then calcined at 300^{o}C for 2 hours in air. The specific surface areas of samples after calcination and the TiO_2 loading amount measured by Thermogravimetric Analysis are also listed in Table 5.

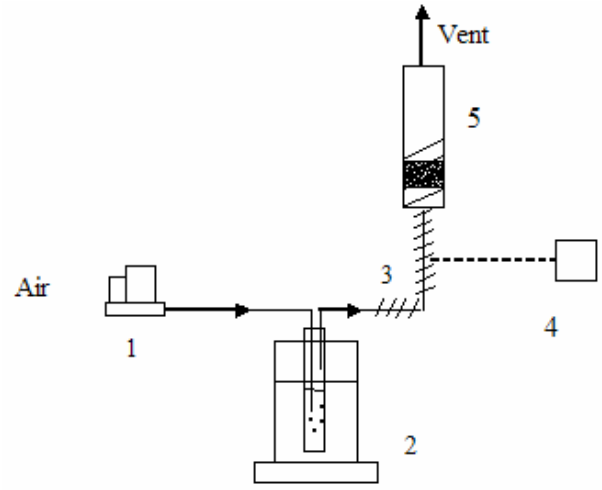

1. Mass flow controller; 2. Water bubble bottle with water bath and hot plate; 3. Heating tape; 4. Temperature controller; 5. Reactor (with carbon)

Figure 9. Schematic of the Hydrolysis Reactor for the Synthesis of TiO_2/AC

Table 5. Hydrolysis Conditions and Surface Area of TiO_2/AC

Sample	Water bath Temp (^oC)	Hydrolysis Temp. (^oC)	Hydrolysis time (hour)	Surface area (m^2/g)	TiO_2 Amount ($\%_{wt}$)
25-25-2	25	25	2	1113	6.38%
25-25-24	25	25	24	1150	4.60%
25-90-2	25	90	2	1140	5.09%
25-175-2	25	175	2	1018	2.38%
90-90-2	90	90	2	1265	8.33%

Characterization of TiO_2/AC. Hydrolysis is the key step that promotes the formation of titanium dioxide. Temperature, reaction time, and the concentration of reactant all affect the hydrolysis reaction. The rate of hydrolysis reaction positively related to the temperature and the reactant concentration (water vapor concentration); increasing the reaction time increased the degree of hydrolysis reaction. Moreover, the hydrolysis conditions affected the loading amount and the morphology of TiO_2.

Table 5 shows that the loading of TiO_2 decreased with the increase of temperature due to the increase of the evaporation of TTIP (boiling point: 220^oC). The TiO_2 loadings of 25-25-2, 25-90-2, and 25-175-2 are 6.38%, 5.09%, and 2.38%, respectively. Increasing the hydrolysis time also resulted in lower TiO_2 loadings; e.g. 4.60% vs. 6.38% for 25-25-24 and 25-25-2. The higher anatase peaks shown in Figure 10 were created with the higher degree of TTIP hydrolysis. Although the degree of TTIP hydrolysis of 25-25-2 was lower than that of 25-25-24, the TiO_2 loading of 25-25-2 was higher than that of 25-25-24. Perhaps this occurred from the unhydrolyzed TTIP remaining on the carbon that decomposed during the following calcination process. The evaporation of TTIP should work the same way under the hydrolysis conditions of 25-90-2 and 90-90-2. The TiO_2 loading of 90-90-2 (8.33%) is higher than that of 25-90-2 (5.09%), which indicates that the TiO_2 loading positively correlates to the rate of hydrolysis when the evaporation of TTIP works the same. It should be noted that the theoretical TiO_2 loading (assuming all the TTIP on the carbon converts to TiO_2) is 8.24%.

TiO_2 morphology is also important. Figure 11 shows the SEM images of different samples. TiO_2 forms a particulate film on 25-25-24 and 25-175-2, and a solid film on 25-25-2, 25-90-2 and 90-90-2. Interestingly, the first two samples have much lower loadings and higher degree of hydrolysis (Figure 10). One possible explanation is that the solid film forms when the TTIP evaporation rate is lower than the hydrolysis rate (90-90-2) and the particulate film forms when the evaporation rate is higher than the hydrolysis rate (25-25-24, 25-175-2). Another possible explanation is the solid film forms when unhydrolyzed TTIP is left on the carbon and is converted to TiO_2 during the calcination (25-25-2, 25-90-2). The SEM image for the sample prepared by boil deposition method (9% P25/AC) is also shown in Figure 11. Although the particle size of P25 is about 50 nm, the P25 nanoparticles agglomerated on the carbon surface. The distribution of P25 is not as good as that of TiO_2 on the sample prepared by the described method.

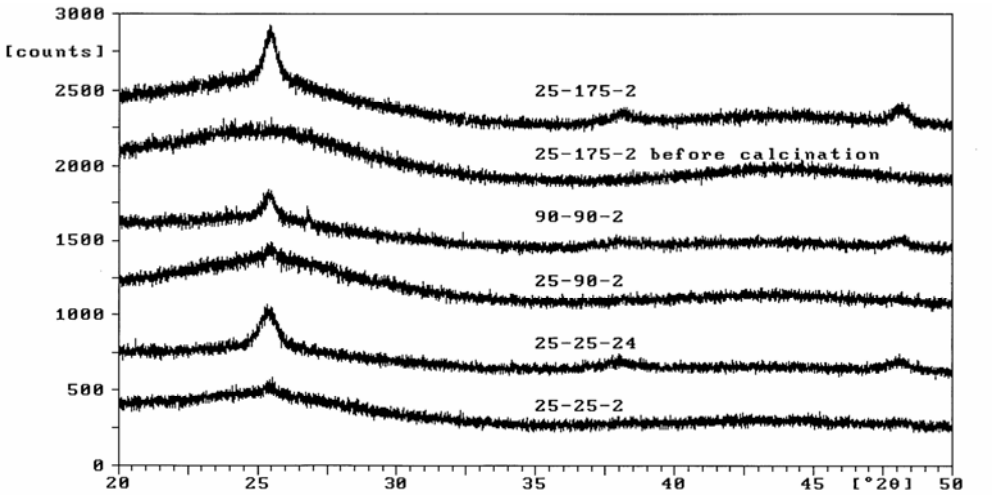

Figure 10. XRD patterns of samples prepared under different hydrolysis conditions

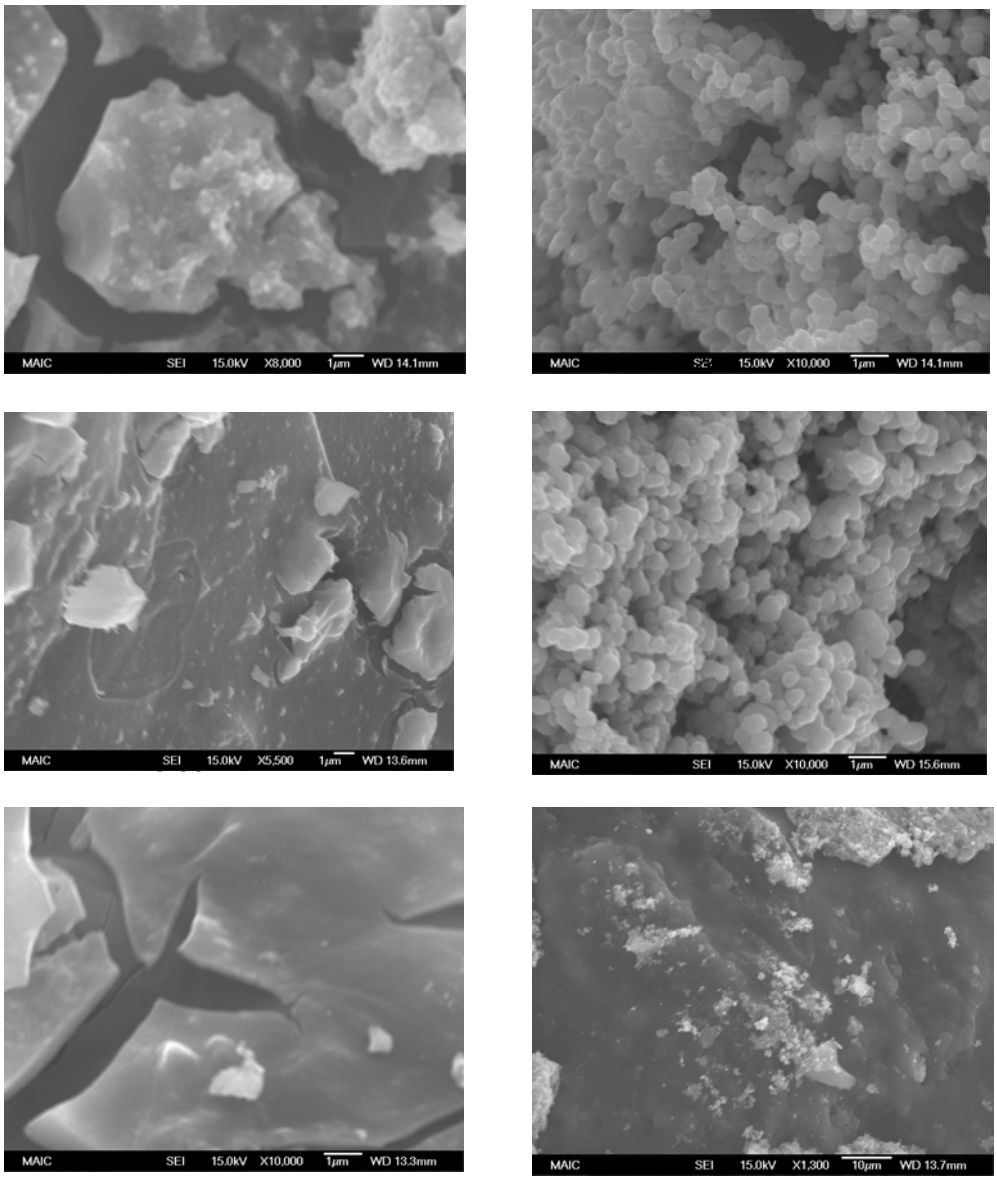

Figure 11. SEM images of TiO_2/AC composites

Figure 12 shows the SEM image and EDS spectrums of different areas of the inner surface of 25-25-24. Comparing the image in Figure 11 with the SEM image of the outer surface of 25-25-24, it can be observed that TiO_2 mostly coated on the outer surface and large pores of activated carbon. This is consistent with the results of the pore size distribution. That means the TTIP adsorbed in the carbon first desorbed and/or evaporated and subsequently hydrolyzed on the outer surface. Regarding the TiO_2 loading, the proper hydrolysis condition should meet the following criteria: 1) the TTIP evaporation rate should be equal or less than the hydrolysis rate; 2) the hydrolysis time should be long enough for complete TTIP hydrolysis. Regarding the TiO_2 morphology, high degree of hydrolysis and low TiO_2 loading result in particulate film.

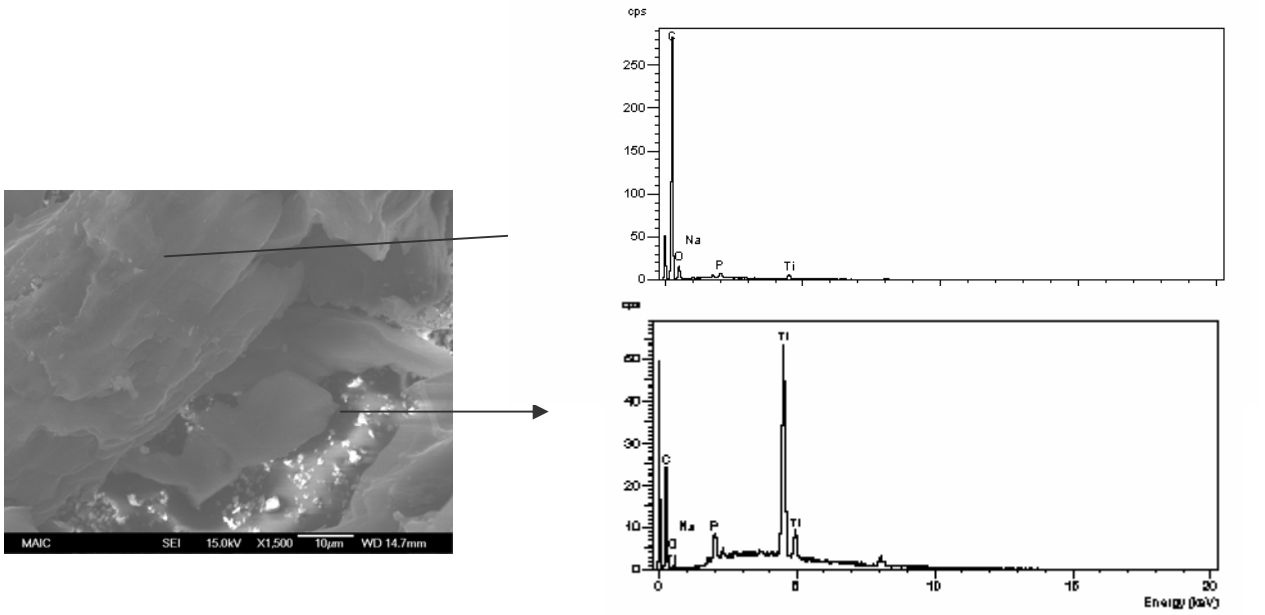

Figure 12. SEM image and EDS spectrum of 25-25-24's inner surface

In summary, the hydrolysis reaction rate positively correlates to the hydrolysis temperature and the reactant concentration. Low hydrolysis temperature and short hydrolysis time can decrease the loss of TTIP. The hydrolysis conditions also affects the morphology of TiO_2.

Evaluation of Methanol Removal Performance. The experimental setup was the same as that described in the previous section (shown in Figure 1). One gram of TiO_2/AC was placed on the frit in the reactor which was equipped with an 8-watt black light UV lamp (peak wavelength at 365 nm) at the center. The TiO_2/AC sample pre-adsorbed water vapor until saturation by passing humid air through the reactor at the rate of 0.4 L/min for 16 hours. Humid methanol laden-air was then allowed to pass through the fixed bed of TiO_2/AC with and without UV light for 6 hours. The EBCT was about 0.35 s. The photocatalytic activity of different samples was evaluated by the concentration of methanol in the effluent.

The methanol removal by the original activated carbon and various TiO_2/AC composites with and without UV light was carried out in order to compare their methanol removal ability. The effluent methanol concentration profiles are shown in Figure 13 for the AC and 25-175-2 TiO_2/AC as a representative. It is apparent from Figure 13 that methanol concentration increased and the carbon saturated quickly when treated by the activated carbon (Bionuchar) with and without UV light. When treated by 25-175-2 TiO_2/AC without UV light irradiation, a similar saturation pattern was observed, and the methanol adsorption capacities of Bionuchar carbon and 25-175-2 were similar. However, when treated by 25-175-2 TiO_2/AC with UV light irradiation, the methanol concentration did not reach saturation in 6 hours. The methanol concentration increased during the first 2 hours and then maintained around 42% removal (i.e. reaching steady state in two hours). Figure 14 shows the average methanol removal efficiency of different TiO_2/AC samples based on the measurements of the last four hours (after reaching steady state). Wherein, 9%

P25/AC was Bionuchar activated carbon coated with 9%$_{wt}$ P25 photocatalyst by boil deposition method, a commonly used method in TiO_2/AC preparation.

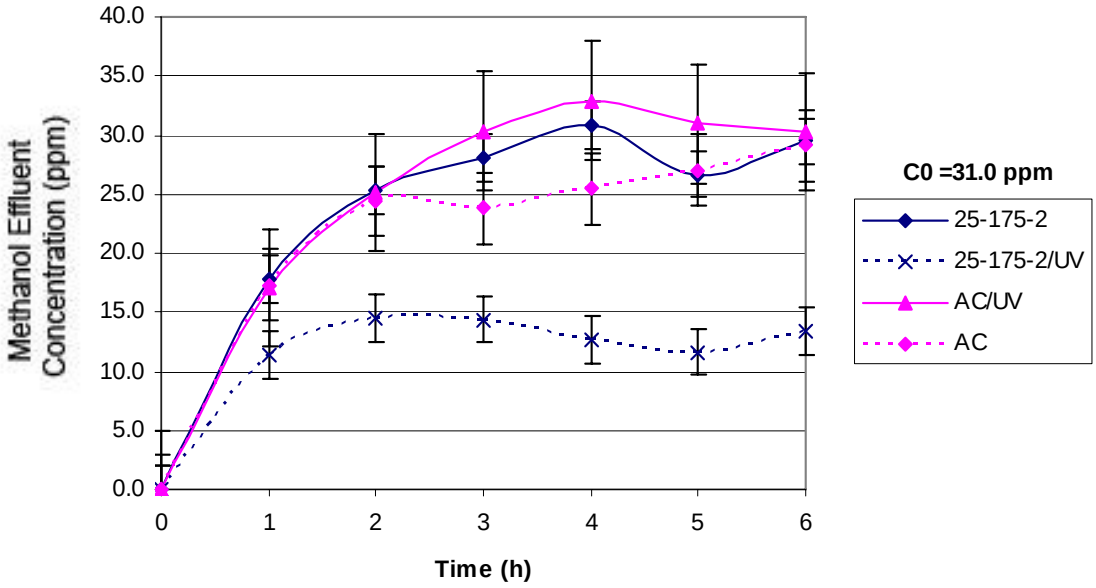

Figure 13. Methanol Effluent Concentration Profiles for Various TiO_2/AC Composites

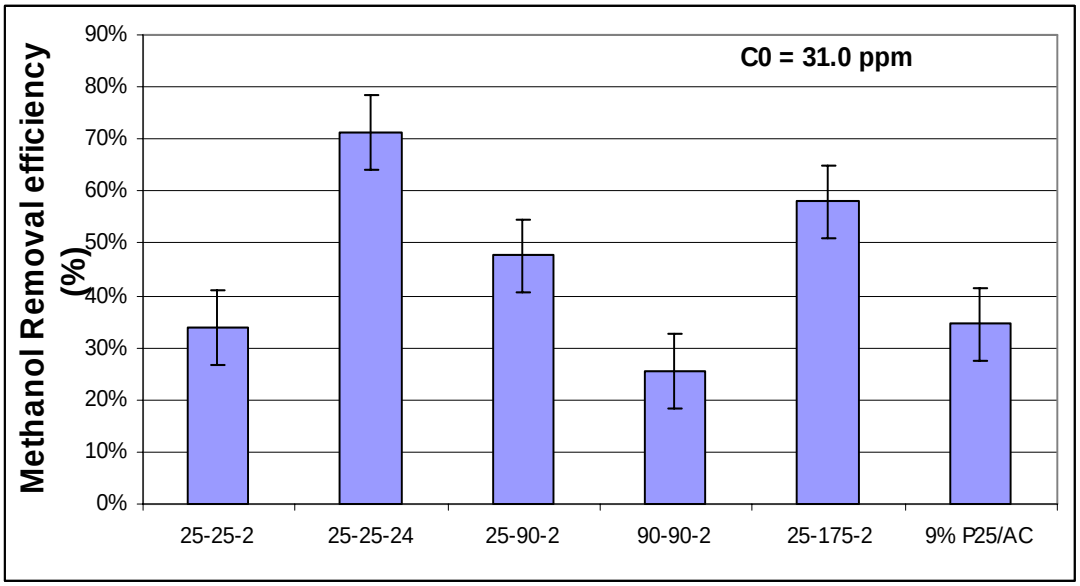

Figure 14. Average Methanol Removal Efficiency for Various TiO_2/AC Composites

Comparing methanol removal and the crystallinity of 25-25-2, 25-90-2, and 25-175-2, it is clearly demonstrated that the higher the degree of anatase crystallinity, the higher the methanol removal efficiency. However, a higher degree of crystallinity is not the only important parameter. TiO_2 morphology is also important. Because of the low surface area of solid film compared with particulate film, photocatalytic activity of 25-25-2, 25-90-2 and 90-90-2 was lower. The TiO_2 loading also plays an important role. The TiO_2 loading amount on 90-90-2 was the highest and the film thickness on 90-90-2 should be the thickest. It is well known that the photocatalytic activity decreases with the increase of particle size due to quantum size effect. Although 90-90-2 has a higher degree of anatase crystallinity than 25-25-2 and 25-90-2, its methanol removal efficiency was the lowest because of the increase of the

film thickness. Interestingly, the results are different for samples of particulate film. In this case, the particle size did not increase with the increase of the TiO_2 loading. The methanol removal efficiency of 25-25-24 was higher than that of 25-175-2 due to the higher TiO_2 loading. In comparison, the methanol removal efficiency of the base line, 9% P25/AC, was lower than those samples of particulate film even though its TiO_2 loading was higher. The better distribution of TiO_2 particles prepared by the pore volume impregnation contributes to the better performance. The results demonstrate that the pore volume impregnation method is an effective method for preparing the photocatalytic TiO_2/AC composites that have a high photocatalytic activity for methanol removal.

Microwave Assisted Impregnation of TiO_2 onto Activated Carbon

As described in the previous section, TiO_2/AC composites were successfully prepared by impregnating activated carbon with TTIP solution followed by hydrolysis and calcination. Because the major decomposition of TTIP occurs at about 230^oC, it is possible to use thermal decomposition instead of hydrolysis. Although thermal decomposition requires a higher temperature than hydrolysis does, it can combine the drying and calcination steps to simplify the preparation process.

Microwave is a dielectric heating method, wherein the applied energy is converted into heat by mutual interaction between microwave and media (Hayes, 2002). Microwave energy transfer is not dependent on thermal conduction and is very rapid. The feature properties of microwave heating are (Sutton et al., 1988):

- Volumetric heating;
- Potentially “uniform” in heat distribution;
- Quick “on and off ”of the source – no thermal lag;
- Dependent upon the material properties;
- Can achieve temperature in excess of 2000^oC in certain material.

In recent years, microwave technology has been successfully applied to a wide variety of chemical reactions and applied for the preparation of ceramic nanoparticles such as $BaTiO_3$, $BaZrO_3$. Although TTIP is a non-polar material and does not absorb microwave, activated carbon is a good microwave absorber. It is possible to use the microwave to prepare TiO_2/activated carbon.

Material and Methods. A commercial SHARP CAROUSEL II microwave oven was used as the microwave source. The capacity of the oven is 1.0 ft^3, the outage power is 800 W, and microwave frequency is 2450 MHz. Microwave heating depends on the materials properties, and two different commercially available activated carbons were examined. One is wood based chemically activated carbon, BioNuchar120 (MeadWestvaco). The other one is a coal-based thermally activated carbon, F400 (Calgon). Before experiments, activated carbon was dried at 110 ^oC for 2 hours.

A typical procedure of the preparation of TiO_2/AC by microwave assisted impregnation was as follows: activated carbon (1.00 g) was impregnated with 50%$_{vol}$ TTIP 2-propanol solution (0.80 g) in a 20 mL glass vial and then stood for overnight. A certain amount of water was added into the vial and the vial was immediately exposed to microwave irradiation. Table 6 lists the preparation conditions. After a designated period of irradiation time, it was taken out and weighed to determine mass loss.

Table 6. Preparation Conditions

	MW Power	H_2O/TTIP Mol. Ratio	Irradiation Time
Sample 1	Medium	28	20 min
Sample 2	Medium Low	28	20 min
Sample 3	Low	28	20 min
Sample 4	Medium	4	20 min

The TTIP solvent, 2-propanol is flammable. Its vapor may form an explosive mixture with air. Thus, explosion limits should be carefully examined to prevent an explosion. The lower explosion limit (LEL) is 2.0 vol % and the upper explosion limit (UEL) is 12.7 vol%. The autoignition temperature is 399 ^oC. (MSDS). In the current preparation procedure, 1 mL of 50% TTIP solution was used in each experiment,

the volume percentage of 2-propanol vapor in the oven was less than 1 vol%. Thus, it is lower than the lower explosion limit, indicating that the current preparation procedure is safe. However, this explosion limits must be considered in scale-up.

Results and Discussion. When no water was added to the activated carbon sample, most of the TTIP evaporated before thermally decomposing. Therefore, water was added to allow hydrolysis to replace thermal decomposition. Because of the high reaction rate of hydrolysis, most of the TTIP was hydrolyzed and reduced the loss of TTIP. TiO_2/AC composite photocatalysts were prepared by impregnation of TTIP solution followed by microwave assisted hydrolysis.

Figure 15 shows the carbon weight loss under different levels of microwave irradiation: medium and high. The results show that under high microwave power level, BioNuchar activated carbon kept losing weight in 10 minutes, and F400 activated carbon only lost weight in the first 2 minutes. Under medium microwave irradiation, BioNuchar activated carbon kept losing weight in 5 minutes, and F400 activated carbon only lost weight in the first 2 minutes. The weight loss of F400 activated carbon was due to desorption of volatile materials because it stopped losing weight after 2 minutes. The weight loss of BioNuchar activated carbon under medium microwave power level was also due to desorption of volatile materials. However, BioNuchar was partly oxidized under high microwave power as evidenced by the continuous weight loss. Compared with BioNuchar under high microwave power, F400 was more stable. However, the weight loss rate of F400 was much higher than that of BioNuchar, showing that F400 was a better microwave absorber than BioNuchar.

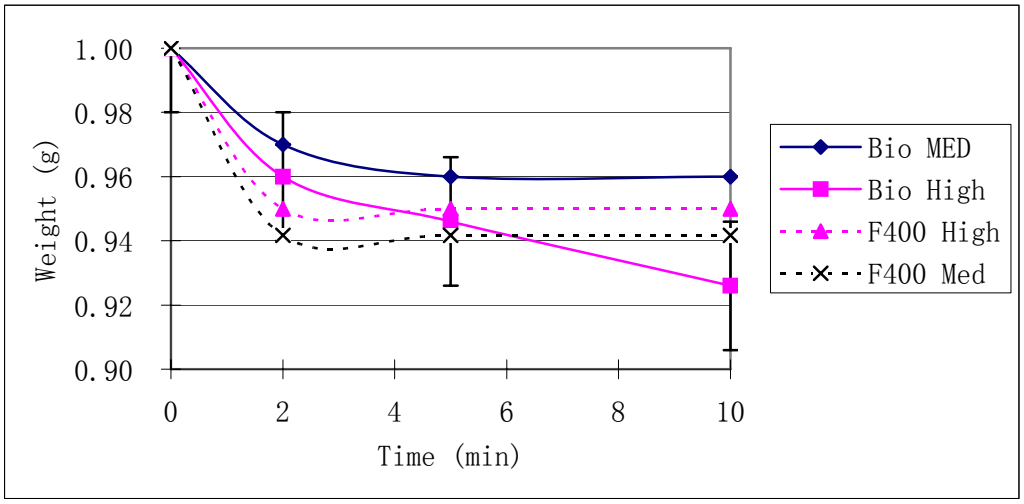

Figure 15. AC Weight Loss of AC under Microwave irradiation

Figure 16 shows the weight loss of TTIP impregnated carbon under different microwave power levels. The results showed that the higher the microwave power, the faster the weight loss occurred. Assuming that all the TTIP was converted into TiO_2, 0.125 g TiO_2 would be generated. Under med, med low, and low level microwave irradiation, the weight increases of carbon were 0.13 g, 0.13 g and 0.32 g respectively. Considering the weight loss of virgin AC under microwave irradiation, there was still volatile material (solvent, by-products, and/or unhydrolyzed TTIP) adsorbed on the carbon after 20 min irradiation. Higher microwave power and/or longer irradiation time should be used to eliminate those volatile materials. The BET surface area analysis revealed the specific surface area of sample 1 was 577.7 m^2/g. Compared with the specific surface area of virgin F400 AC (741.8 m^2/g), it decreased 22%. Figure 17 shows the SEM images of TiO_2/AC prepared by the described method. It reveals clearly that TiO_2 particles formed on the carbon surface and the particle size was around 100 nm. The effect of microwave power on TiO_2 morphology was minor when using high water/TTIP mol. ratio (28:1). When using low water/TTIP ratio, large particles were formed. Figure 18 shows the SEM image of the cross section of a sample 1 particle. Figure 19 shows the SEM images and EDS spectra of section 1 (outer surface of carbon particle) and section 2 (inner surface of carbon particle). It clearly revealed that TiO_2 was formed on both areas; however TiO_2 was much richer in area 1. The TiO_2 in the section 2 is undesired because the UV light can

not penetrate into the carbon particle. Figure 20 shows the XRD spectra of sample 4, proving the formation of anatase phase.

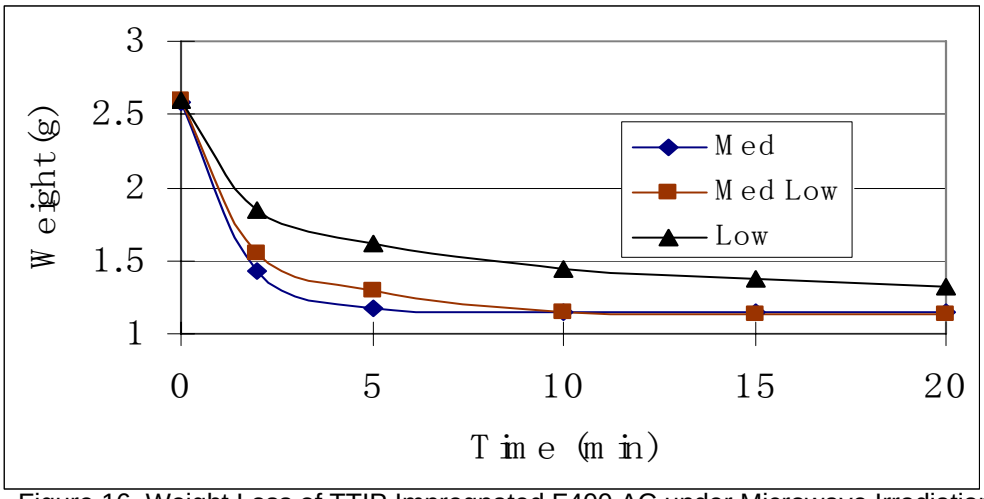

Figure 16. Weight Loss of TTIP Impregnated F400 AC under Microwave Irradiation

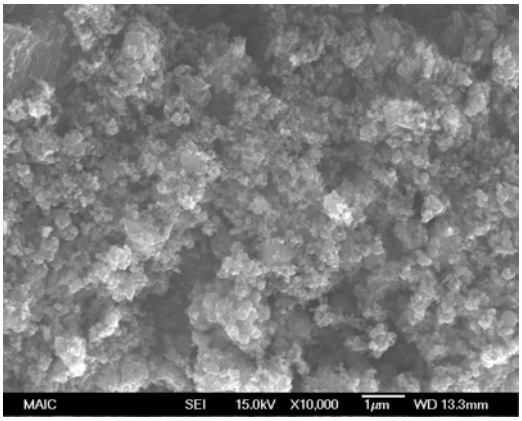

Sample 1

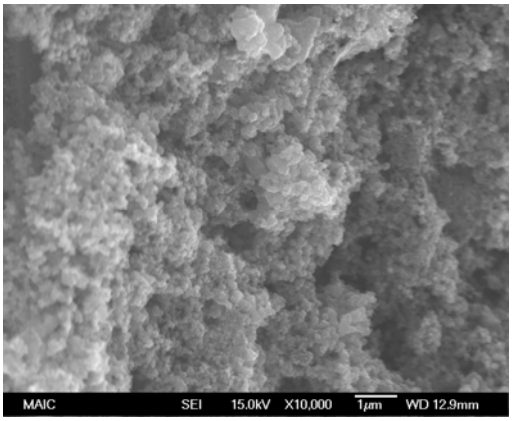

Sample 2

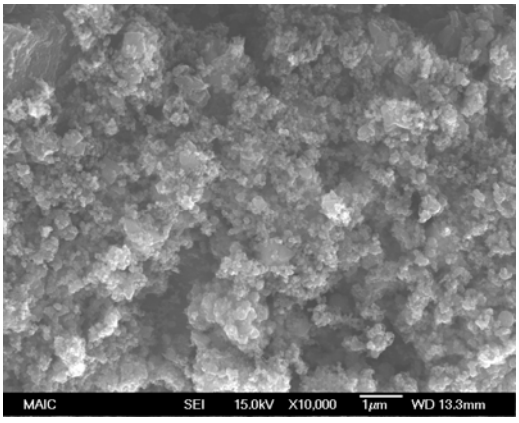

Sample 3

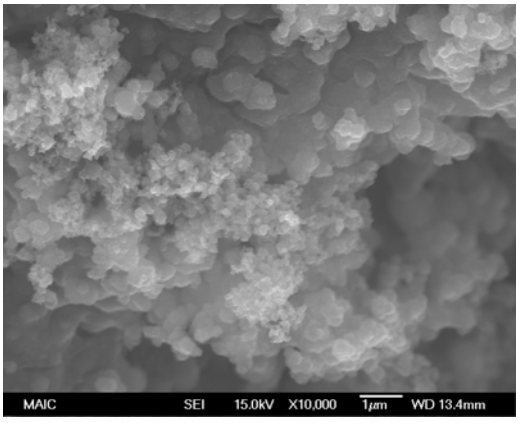

Sample 4

Figure 17. SEM Images of TiO_2/AC Synthesized using Microwave Irradiation

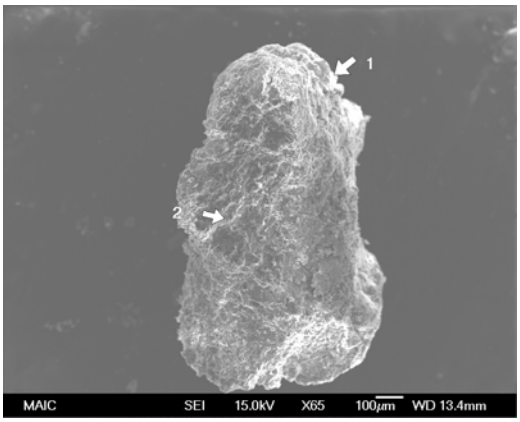

Figure 18. SEM Image of Cross-section of Sample 1 Particle

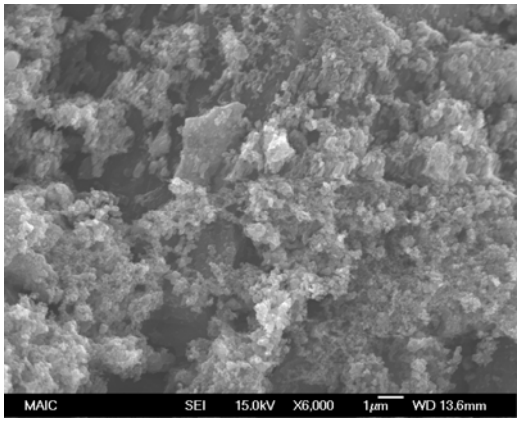

×6000

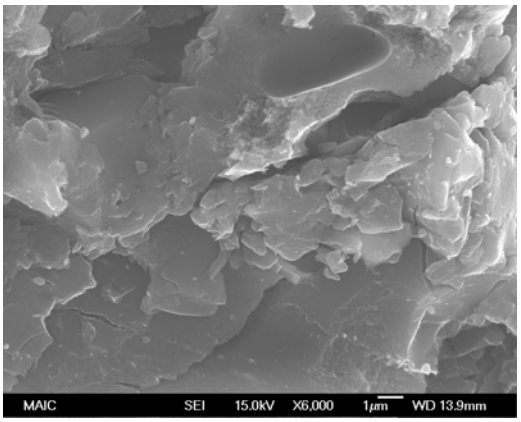

×6000

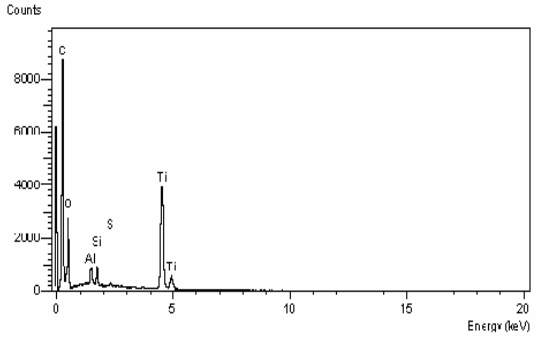

EDS Spectrum

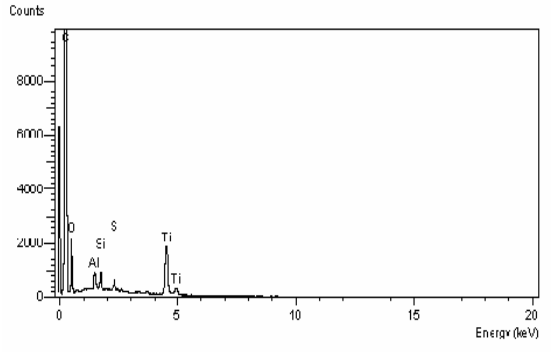

EDS Spectrum

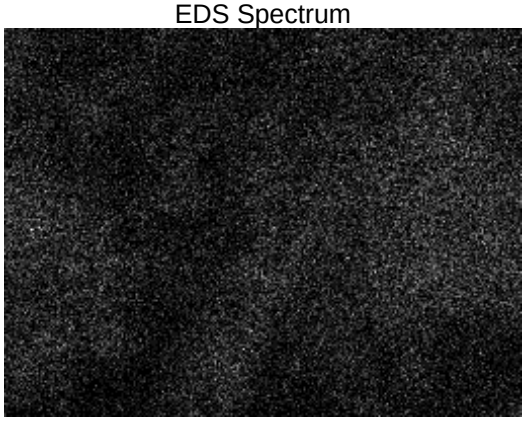

Ti EDS Mapping
Section 1

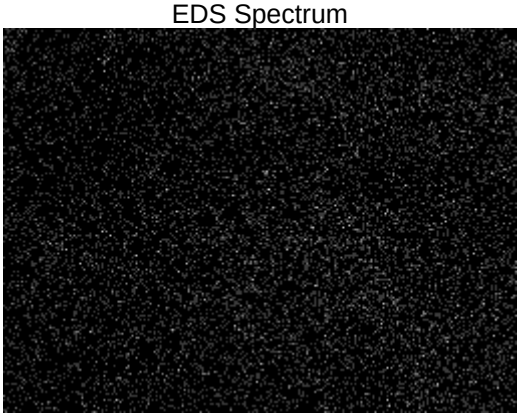

Ti EDS Mapping
Section 2

Figure 19. Comparison of Section 1 and Section 2

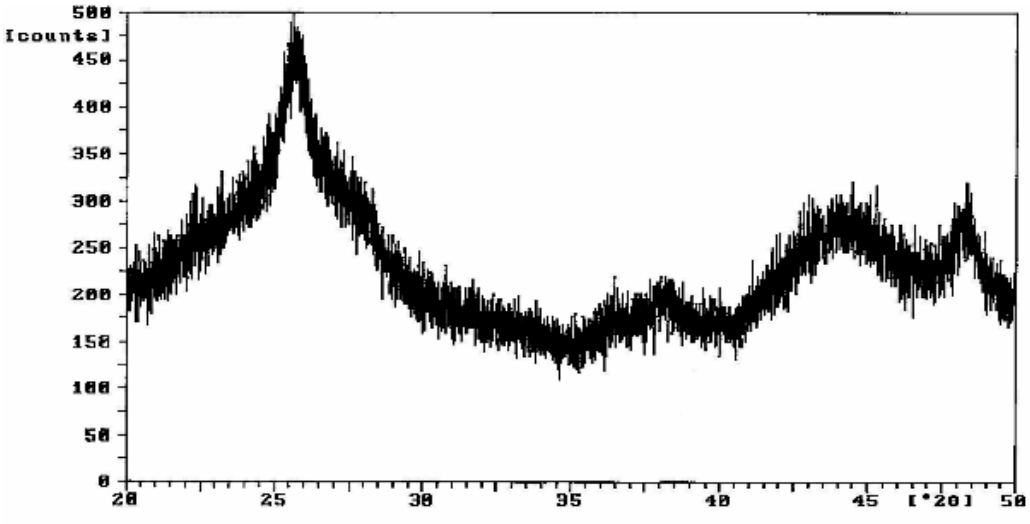

Figure 20. XRD Pattern for Sample 4

These results show that anatase phase TiO_2 was successfully formed on the activated carbon by the proposed method. The TiO_2 was concentrated on the outer layer of the carbon particles where the UV light can reach.

Evaluation of Methanol Removal Performance. The methanol removal performance of TiO_2/AC composite was carried out following similar procedures described in previous sections. Due to the density and particle size difference between F400 AC and BioNuchar AC, 2.00 g F400 AC or TiO_2 coated F400 AC was used. The empty bed contact time (EBCT) was 0.35 s, which was the same as before. The initial methanol concentration was 22.8 ppm_v, and relative humidity was around 80%. Before experiments, the adsorbent was pre-saturated by moisture. The TiO_2 loading, estimated by the weight increase after TiO_2 coating was 11.5%wt. Figure 21 shows the relative methanol effluent concentration profiles of F400 AC and sample 1 with and without UV irradiation.

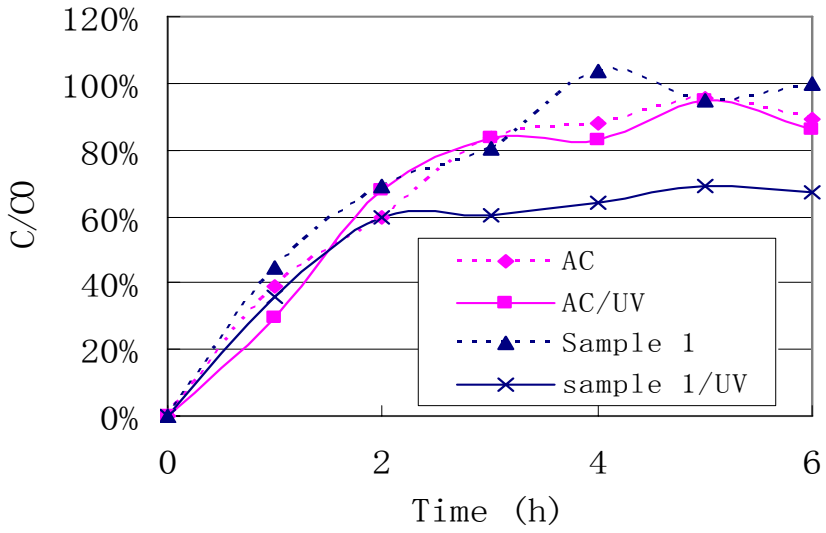

Figure 21. Methanol Effluent Concentration Profiles for F400 AC and Sample 1

The effluent methanol concentration increases quickly when treated by virgin F400 AC with and without UV light. When treated by sample 1 without UV light irradiation, a similar adsorption profile was observed, and the total methanol removal amount slightly decreased compared to virgin F400 AC. However, when treated by sample 1 with UV irradiation, the methanol effluent concentration did not reach saturation in 6 hours. The methanol concentration increased in the first 2 hours and than maintained at about 33% removal. Table 7 lists the total methanol removal amount in 6 hours.

Table 7. Summary of Methanol Removal Amounts after 6 Hours

F400 AC	F400 AC/UV	Sample 1	Sample 1/UV
0.967 mg	0.989 mg	0.694 mg	1.376 mg

Conclusions. Under medium level of 800 W microwave irradiation, anatase TiO_2 was quickly formed from TTIP precursor in a short time, at atmospheric pressure. F400 AC was stable under this energy level, and the formed submicron TiO_2 particles were rich on the external surface of carbon. When the TTIP conversion was completed, the irradiation time and water/TTIP ratio would no longer pose any significant impact on the final product. The prepared TiO_2/AC composite photocatalyst showed lower adsorption capacity for methanol than virgin carbon due to pore blockage by the newly formed TiO_2 particles. Photocatalytic oxidation of methanol from humid air was successfully accomplished by the composite, and the material did not reach saturation for the duration of the experiment.

V_2O_5 Modified TiO_2/AC Composite Photocatalyst

Doping with transition metals has been widely employed in order to enhance the photocatalytic activity of TiO_2 and extend the light absorption. Doping quantum-sized TiO_2 with Fe^{3+}, Mo^{5+}, Ru^{3+}, Os^{3+}, Re^{5+}, V^{4+}, V^{5+} and Rh^{3+} has been shown to enhance photoreactivity for both the oxidation of $CHCl_3$ and the reduction of CCl_4, while doping with Co^{3+} and Al^{3+} has been shown to decrease photoreactivity (Choi et al., 1994). Photocatalytic efficiency of TiO_2 depends, in part, upon the relative degree of branching of the reactive electron/hole pairs into interfacial charge-transfer reactions. Metal ion dopants influence the photoreactivity of TiO_2 by acting as electron (or hole) traps and by altering the e^-/h^+ pair recombination rate through the following process:

$$M^{n+} + e_{cb}^- \rightarrow M^{(n-1)+} \quad \text{Electron trap}$$

$$M^{n+} + h_{vb}^+ \rightarrow M^{(n+1)+} \quad \text{Hole trap}$$

where the energy level for $M^{n+}/M^{(n-1)+}$ lies below the conduction band edge (E_{cb}) and the energy of $M^{n+}/M^{(n+1)+}$ above the valence band edge (E_{vb}) of TiO_2 (Choi et al., 1994). Doping with V^{5+} at 0.1- 0.5 $\%_{wt}$ significantly increases photoreactivity for both oxidation and reduction (Choi et al., 1994).

On the other hand, supported V_2O_5 catalysts are used in various oxidation reactions concerning mostly the oxidation of hydrocarbons and selective catalytic reduction (SCR) of nitrogen oxides by ammonia in the gas from stationary sources. It was demonstrated that V_2O_5 supported on TiO_2 is a better catalyst than V_2O_5 supported on Al_2O_3 or SiO_2 and methanol was oxidized by both vanadia and titania when using V_2O_5/TiO_2 catalyst at 230°C (Herrmann et al., 1997).

The objective of V_2O_5 modified TiO_2/AC composite is to improve the photoreactivity of TiO_2/AC by doping V^{5+} and to improve the methanol removal efficiency by V_2O_5 oxidation. In this section, several V_2O_5 modified TiO_2/AC composites were prepared, characterized, and tested for methanol removal efficiency.

Materials and Methods. Several V_2O_5 modified TiO_2/AC composites were prepared by pore volume impregnation of vanadium triisopropoxide (VTIPO) and TTIP solution in 2-propanol. The hydrolysis and calcination condition was the optimal condition used in the TiO_2/AC preparation: hydrolyzed at 25°C for 24 hours; the humidifier temperature is 25°C; then dried at 105°C for 4 hours; at last calcined at 300°C for 2 hours in air. Table 8 lists the preparation conditions.

Table 8. Preparation Conditions for V_2O_5 Modified TiO_2/AC

	TTIP Concentration	V/Ti Ratio
Sample 1	20%	1%
Sample 2	10%	1%
Sample 3	20%	2%
Sample 4	20%	0.2%

Results and Discussion. Figure 22 shows the SEM images and the EDS mappings for sample 1. The SEM images show that V-doped TiO_2 formed uniform solid film on the carbon surface, and the film cracked during the heat treatment. The EDS mappings show that the V and Ti were homogeneously mixed. Figure 23 shows the XRD spectrum of sample 1. There was no clear peak for the anatase phase of titanium dioxide. The peak around 35° may belong to V_2O_5 or $V_3Ti_5O_{17}$.

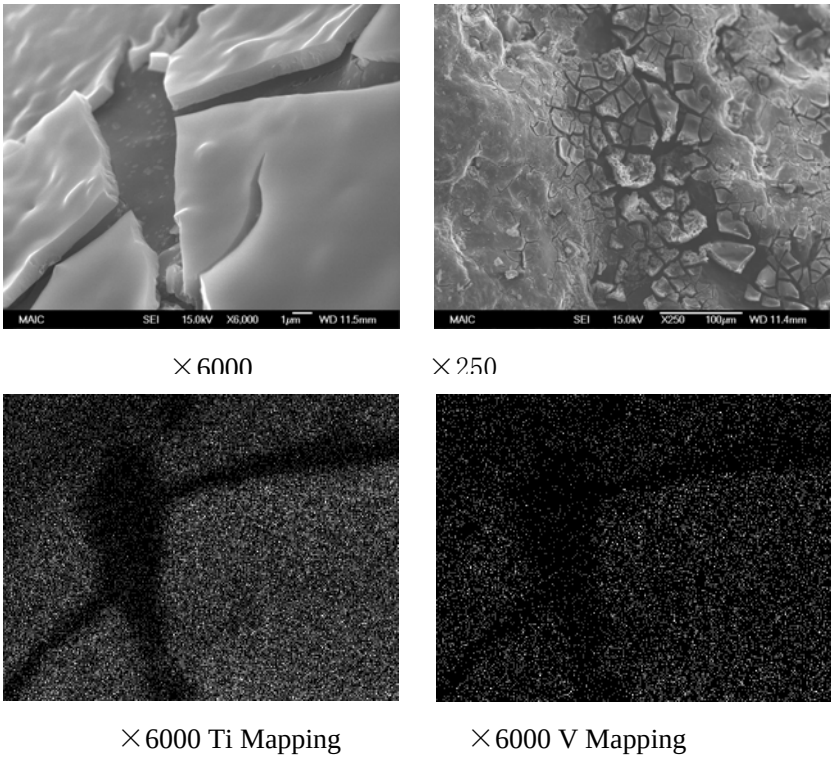

Figure 22. SEM Image and EDS Mapping for Sample 1

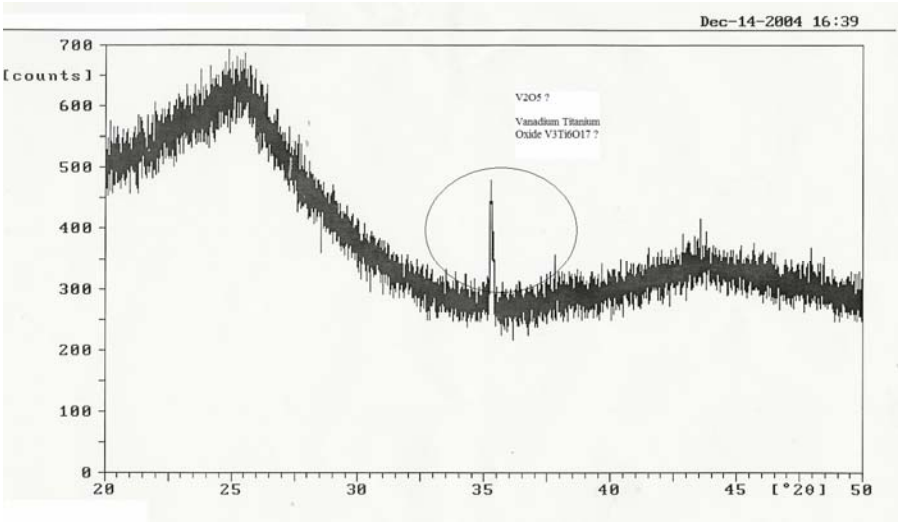

Figure 23. XRD Spectrum for Sample 1

Figure 24 shows the SEM images for sample 2, 3 and 4. Compared with the SEM images of sample 1, decreasing the TTIP concentration did not significantly change the structure of surface. A particulate film was formed on the surface of sample 3 and sample 4. However, the particle size was bigger than the TiO_2/AC without doping, which means that the hydrolysis of TTIP was strongly affected by the hydrolysis of VTIPO.

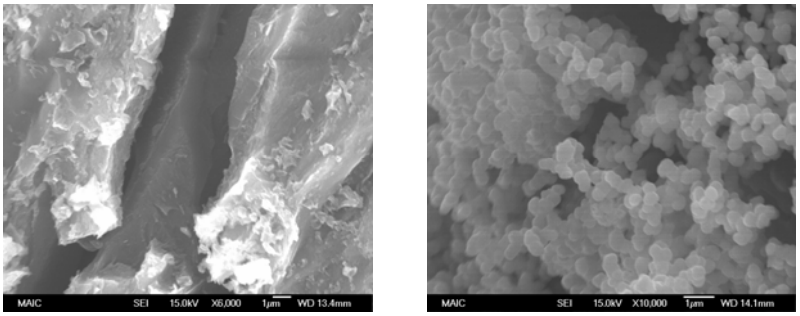

Sample 2 ×6000 TiO_2/AC (25-25-24)

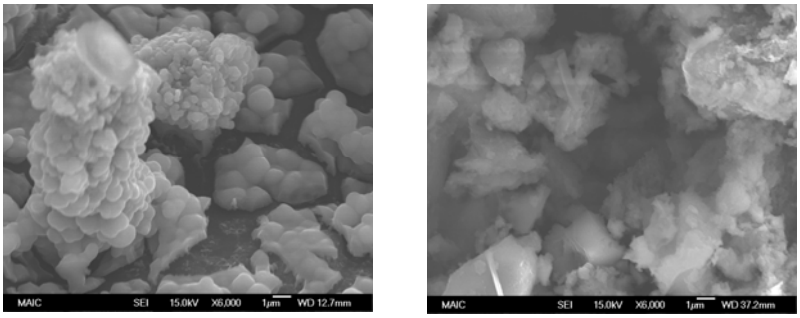

Sample 4 ×6000 Sample 3 ×6000

Figure 24. SEM Images for Various TiO_2/AC Samples

Evaluation of Methanol Removal Performance. According to the previous experimental results, high photocatalytic activity prefers high surface area (particulate film) and the anatase phase of titania. Therefore, the photocatalytic activity of sample 1 should be low. The methanol removal performance of sample 1 was evaluated by the same method used in previous experiments. Figure 25 shows the methanol effluent concentration profiles for sample 1. Figure 26 shows the methanol effluent concentration profiles for sample 2.

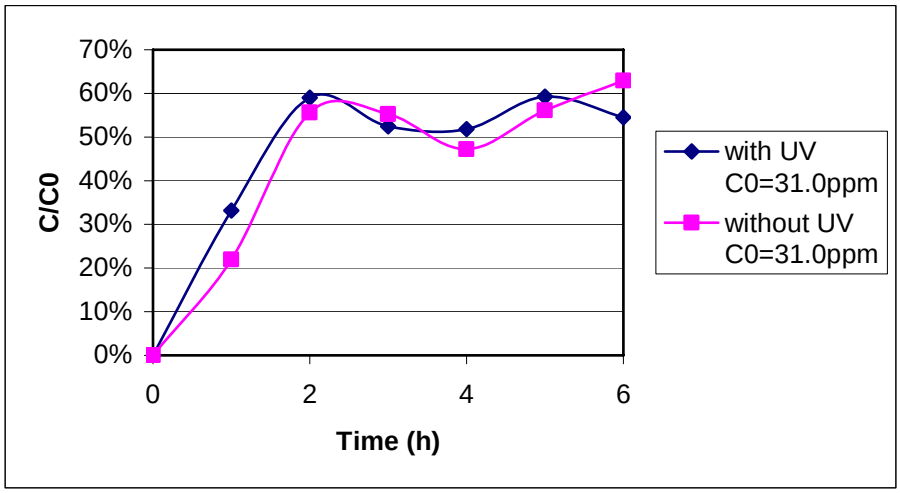

Figure 25. Methanol Effluent Profiles for Sample 1

For sample 1, with or without UV light, the methanol outlet concentration maintained around 60% of the inlet concentration in either case. This illustrates that sample 1 has no photocatalytic activity. The methanol removal is due to adsorption and V_2O_5 oxidation. For sample 2, with UV light, the methanol outlet concentration maintained around 40% of the inlet concentration; without UV light, the methanol outlet concentration maintained around 70% of the inlet concentration. This shows sample 2 has photocatalytic activity. Compared with sample 1, the photocatalytic activity of sample 2 increased due to the decrease of the TTIP/VTIPO precursor concentration which resulted in the decrease in TiO_2/V_2O_5 loading and film thickness.

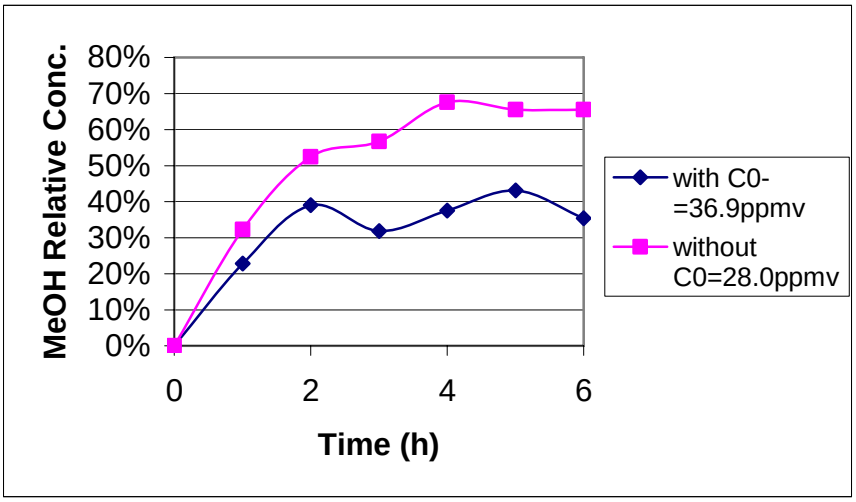

Figure 26. Methanol Effluent Concentration Profiles for Sample 2

Removal of H_2S Using Activated Carbon

Total reduced sulfur species, such as hydrogen sulfide, methyl mercaptan, dimethyl sulfide, and dimethyl disulfide, are major pollutants from pulp and paper mills. In this section, the removal performance of the TiO_2/AC composites for hydrogen sulfide, which was chosen as the representative TRS gas, is examined.

Materials and Methods. A schematic diagram of the experimental system is shown in Figure 27. The reactor was the same as described previously. The H_2S (1000 ppm_v in air) from a cylinder was mixed with air and diluted to around 40 ppm_v. The temperature of the reactor was measured by the thermal couple inserted in the reactor. Each time 1.00 g adsorbent was used. Virgin and TiO_2-coated Bionuchar 120 activated carbon was used as the adsorbent. The TiO_2/AC was synthesized using a dry impregnation technique with TTIP as the TiO_2 precursor. The flow rate was 0.42 L/min and the EBCT was 0.35 s. The H_2S removal was tested with and without UV light (at room temperature). Because the reactor had no cooling system, the temperature rose to 328 ± 2 K when the UV light is turned on. The H_2S removal by AC at 328 K was also carried out to investigate the effect of temperature (the UV lamp was covered by aluminum foil and turned on so that there was no UV light in the reactor but the temperature was the same as the run with UV light). For convenience, the labels RT (at room temperature, without UV), 328 K (at 328 K, without UV), and UV (under UV Light irradiation) were used to indicate the experimental conditions. No photolysis (i.e., oxidation by UV light alone) of hydrogen sulfide with UVA light (peak wavelength = 365 nm) was observed. A Jerome 631-X H_2S analyzer (Arizona Instrument LLC) was used to measure H_2S concentrations in the sample gas. The detection range of the analyzer was 0.003 to 50 ppm_v and the precision was 5% relative standard deviation. H_2S concentration at the inlet of the reactor was measured when the H_2S laden gas bypassed the reactor. By comparing the outlet H_2S concentration with the inlet level, the H_2S removal efficiency was obtained. Finally, the gas stream passed through an alkaline trap before it was exhausted into the fume hood.

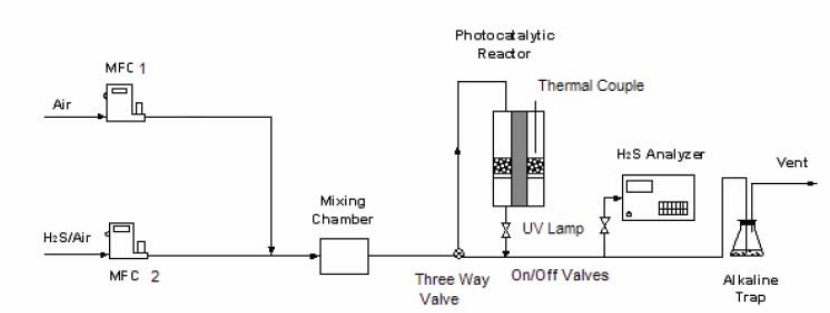

Figure 27. Schematic Diagram of the Experimental Setup

Figure 28 shows the outlet concentration profiles of virgin BioNuchar AC and TiO2/AC in dry condition. In all cases, the outlet H_2S concentration increased with time and was lower than the inlet concentration during the entire operation period (120 min), indicating that the adsorbents were not saturated. The outlet concentrations of TiO_2/AC were higher than that of AC in all three conditions. For AC, the removal efficiencies were 91.40 ± 1.84 % (RT), 96.84 ± 0.65 % (328 K), and 97.97 ± 0.10 % (UV); the sulfate conversion efficiencies were 15.01 ± 1.93 % (RT), 12.57 ± 1.66 % (328 K), and 14.10 ± 2.15 % (UV). For TiO_2/AC, the removal efficiencies were 45.70 ± 5.64 % (RT), 53.78 ± 0.32 % (328 K), and 86.62 ± 1.93 % (UV); the sulfate conversion efficiencies were 13.45 ± 4.37 % (RT), 12.11 ± 0.39 % (328 K), and 18.73 ± 1.24 % (UV). Details of the effect of each parameter are discussed below.

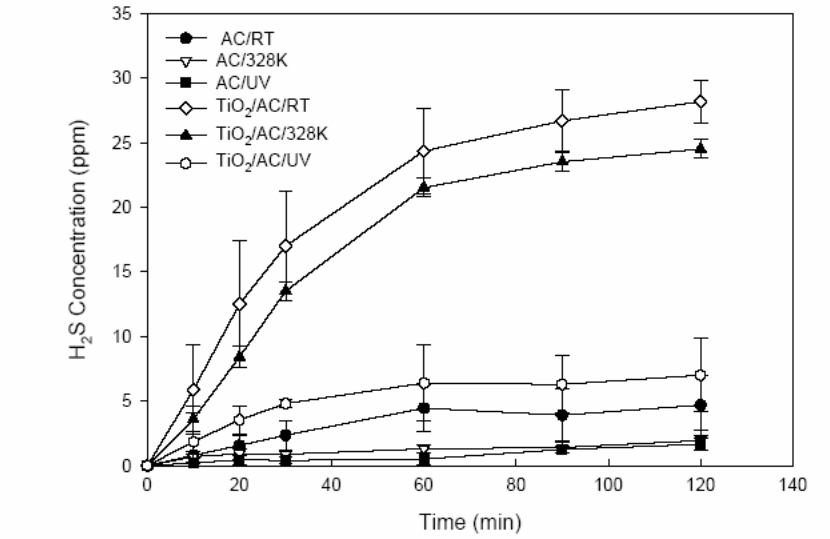

Figure 28. Outlet H_2S Concentration Profiles (inlet concentration was 40.5 ppm, RH = 0%)

As shown in Table 9, the virgin BioNuchar AC has a moderate pH, which is good for both high capacity and sulfuric acid formation (Bandosz, 2002). After coating TiO_2, the surface pH was decreased to acidic range which is not desired for H_2S removal.

Table 9. Surface pH of AC and TiO_2/AC

Sample	Surface pH
BioNuchar AC	6.84 ± 0.13
TiO_2/AC	4.19 ± 0.36

High temperature improved the H_2S removal on AC and TiO_2/AC. Generally, a chemical reaction proceeds faster at higher temperature. The oxidation of H_2S on AC was faster at 328 K than at room temperature. Therefore the removal efficiency increased. The sulfate conversion efficiencies at 328 K decreased compared to at room temperature. Elemental sulfur is the main product of H_2S oxidation on unmodified AC at elevated temperature (Bandosz, 2002). At the same temperature (at 328 K), UV light

irradiation improved the H2S removal on TiO_2/AC from 53.78 % to 86.62%. Furthermore, sulfate conversion efficiency, which is important for regeneration using water wash, was also increased. This proved that H_2S was photocatalytically degraded on TiO_2/AC composite. UV light also improved the removal of H_2S on AC. The outlet H_2S concentration of AC/UV was lower than that of AC (328 K).

The difference between AC/UV and AC (328 K), however, was not clear because the removal efficiencies in both cases were high. To clarify the effect of UV light, the H_2S inlet concentration was increased to 59 ppm_v. With the increase of inlet H_2S concentration to 59 ppm, the removal efficiencies decreased to 85.03 ± 5.07 % (RT), 88.77 ± 3.78 % (328 K), and 94.75 ± 1.96 % (UV) respectively. The difference between AC at 328 K and under UV irradiation was increased. This proved that UV light improved the AC performance. The sulfate conversion efficiencies were 15.72 ± 1.87 % (RT), 20.03 ± 1.19 % (328 K), and 15.14 ± 0.12 % (UV). Except at 328 K without UV irradiation, the sulfate conversion efficiencies were almost the same as the case of 40.5 ppm_v inlet concentration.

Conclusions. BioNuchar AC itself is a good H_2S remover. Without UV irradiation, a fraction of adsorbed H_2S was already oxidized to sulfate. The presence of UV light improved H_2S removal efficiency in dry airstreams. After coating TiO_2, the H_2S removal efficiency of TiO_2/AC decreased due to the surface change. Under UV light irradiation, H_2S removal efficiency and sulfate conversion efficiency of TiO_2/AC composite increased. The sulfate conversion efficiency of TiO_2/AC composite was higher than that of AC which is preferred for water regeneration.

FEASIBILITY STUDY FOR AIR-PHASE BIOFILTRATION OF METHANOL

Overview

The primary objective of this portion of the DOE project was to develop and characterize a laboratory-scale biofiltration system for removal of methanol from air streams typically produced in pulp-and-paper mill environments. A secondary objective of this work was to prepare a life cycle assessment of the technology developed by all sub-groups in this initiative in order to quantify relevant environmental and health impacts. This final progress report outlines the status of the remaining activities in both objectives.

Development and Characterization of a Biofiltration System

Recent work on a biological activated carbon (BAC) system has focused on analysis and interpretation of results stemming from a 138-day trial to demonstrate feasibility of a lab-scale activated carbon biofilter for removal of methanol in an air stream. Subsequently, assessments have been completed for the genetic diversity of bacteria colonizing the biofilter and of bacterial cultures for potential use as biofilter inocula.

Feasibility Study for Methanol Removal using a Granular Activated Carbon Biofilter. The laboratory-scale, air phase granular activated carbon (GAC) biologically inoculated biofilter (BB) was constructed of a 24-inch long by 2-inch diameter clear PVC column, containing a mixed packing with Westvaco Bionuchar GAC, perlite, Osmocote slow-release ammonium nitrate pellets, and Agrasoke water crystals in a 4:2:1:1 ratio by volume (on an air-dry basis). The biofilter was inoculated with a well-characterized bacterial culture collected from a Florida paper and paperboard plant. This culture had previously been tested and reported to demonstrate degradation of methanol up to 10,000 mg/L in liquid, rapid growth, and morphological diversity. A non-inoculated biofilter (NB) column was also prepared in the same manner as the biofilter but without bacterial inoculum. Both columns were maintained at ambient temperature and fed methanol at loading rates ranging from 1-18 g/m^3 packing/hr in an upflow air stream with 90-95% humidity. Residence time in both columns was 5 minutes during initial high loading and startup, but reduced to 60-80 seconds during normal operation and lower methanol concentrations. A schematic of this experimental system is shown in Figure 29.

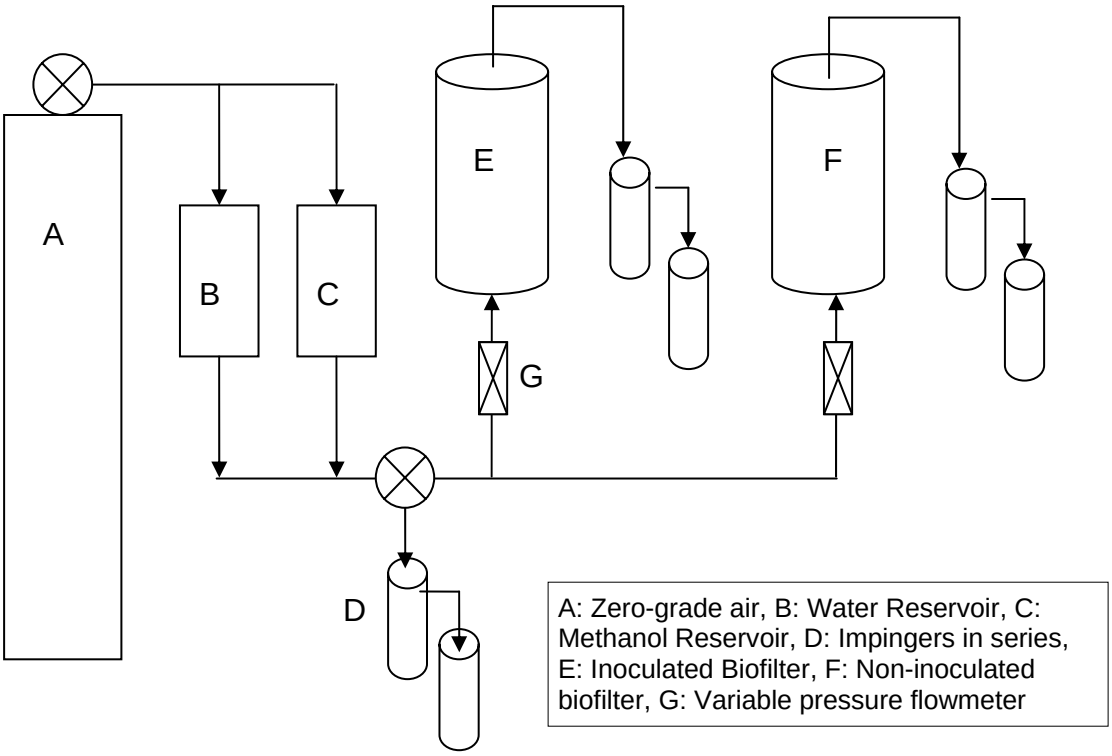

Figure 29. Schematic of the Biofilter Design

The performance of the biofilter for methanol removal is shown in Figure 30, where removal efficiency (%) of both the biologically inoculated biofilter (BB) and non-inoculated biofilter (NB) is plotted as a function of time, along with the methanol loading rate to the biofilters. Each of the points plotted in Figure 2 represents samples collected in duplicate, over the 138-day operation of the biofilters. During the startup period, both biofilters showed excellent removal of methanol and a lag time of about four days to achieve 100% methanol removal. However, the BB showed much lower removal over those first four days, likely a result of pre-saturation of the packing material with methanol-laden medium during the inoculation period. When the methanol loading rate was rapidly decreased on day 50, the performance of the NB also fell dramatically, with an almost 10-day period before it returned to 100% removal. When the methanol loading rate was increased to 5 g/m^3 packing/hr at day 110, both biofilters continued to perform well. However, the NB experienced another decrease in methanol removal at the conclusion of the trial, between days 133 and 138.

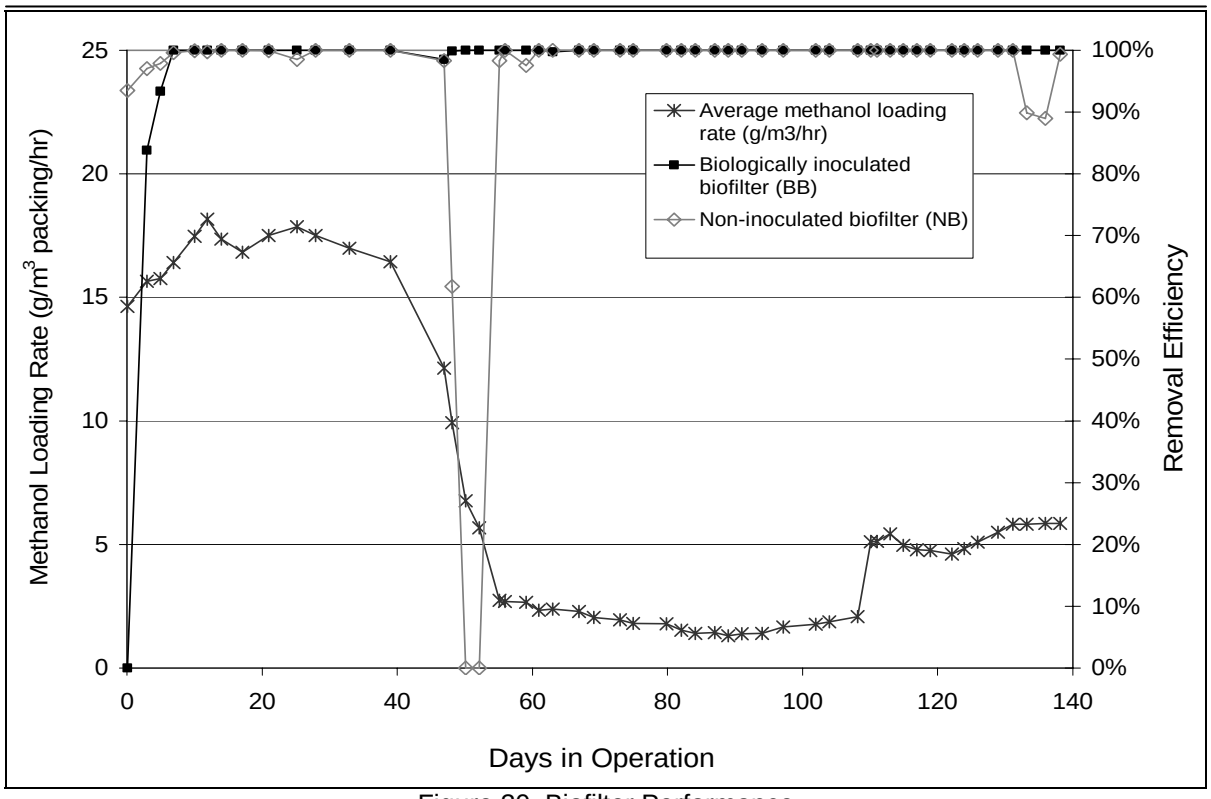

Figure 30. Biofilter Performance

Interestingly, an easily visible biofilm was observed on the BB after only about six days of operation, whereas no biofilm could be readily detected on the NB until after about 25 days of operation. These results would suggest a “stabilizing” effect of the presence of biofilm enriched for growth of methanol-degrading organisms. These results also show that the column design, particularly use of packing material that not only provides adsorptive capacity but also contributes to nutrient availability and moisture regulation, contributes to the ability to support biological methanol removal.

Bacterial Abundance over the Length of the Biofilters. At the conclusion of the experiment, packing material samples were collected from the inlet, middle, and outlet of the column. The packing sample (about 2 grams) was first rinsed gently with sterile distilled water to remove particles and non-attached bacteria. Then the sample was mixed with 5 mL of sterile phosphate-buffered saline (PBS) and vortexed in 10-second pulses at 2500 rpm for a total of two minutes to transfer biomass from the packing surface to liquid suspension. To determine bacterial abundance as a function of length along the column, the liquid suspension from these samples was serially diluted eight-fold, and 100 uL aliquots were spread on agar plates. Three types of agar plates were used: nitrate mineral salts and ammonium mineral salts with

methanol added in the vapor phase and nutrient agar with mixed N- and C-sources and no methanol added. These different types of agar media were used to determine if cultivable bacteria in different regions of the biofilters could be differentiated based on their nitrogen and carbon requirements. All plates were incubated at 30°C for 72 hours, and then visible colonies were counted and averaged for three replicates of each plate type.

Bacterial abundance at the inlet, middle, and outlet of both biofilters was compared for the three types of media, with results presented as colony forming units (CFU) per gram of packing (with standard error for measurement in triplicate). These results (Fig. 31) show a 1-2 order of magnitude greater colonization of the BB inlet than any other region of the BB or NB. Regardless of medium type, the bacterial counts in the BB decreased significantly in the middle region of the column and maintained similar counts in the outlet region of the column. The counts were observed to increase in the middle region of the NB columns, with no significant change in counts in the outlet regions. Interestingly, despite the higher counts in inlet samples taken from the BB compared to those removed from the NB, counts on AMS and NMS media observed in the middle and outlet regions were higher in the NB samples.

With the exception of the BB inlet and NB outlet, a significantly higher number of bacteria were enumerated on nutrient medium. It is possible that these results are due to the acclimatization of the specific inoculum used in the BB to a much wider range of substrate and nutrient concentration, both in their original mill source and in the batch enrichment, as compared to the NB colonizers. The variation in distribution of abundance could also connect the observation that the NB performance dropped shortly before the end of the trial, suggesting that superior colonization of the inlet by an acclimatized bacterial consortium could possibly contribute to greater reliability and performance.

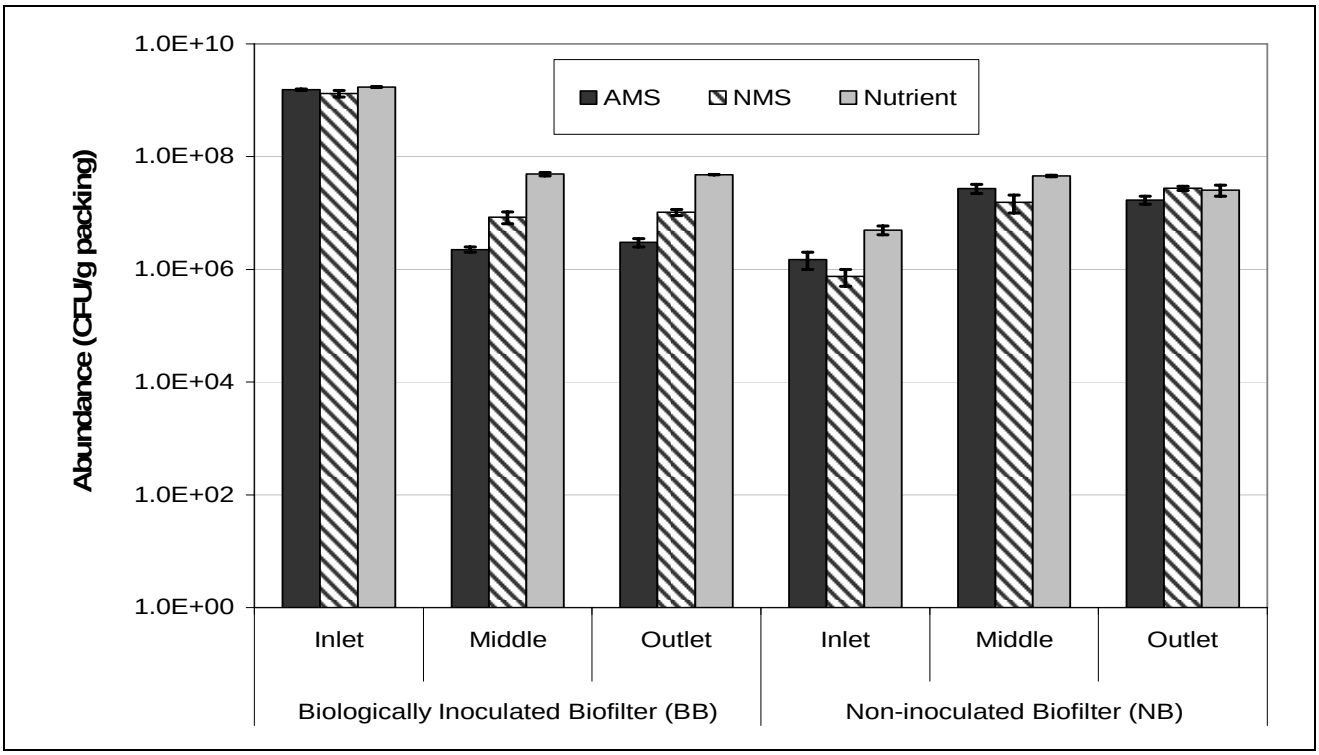

Figure 31. Abundance of Cultivable Bacteria in Three Spatial Regions of the Biofilters

Bacterial Diversity of the Biofilter under Varied Operating Conditions. Throughout the operation of the biofilter and control column, packing material was removed from the inlet portion of the columns twice during each operating condition and analyzed for genetic diversity using optimized molecular techniques. The packing material was taken from the inoculated and non-inoculated columns at six times, days 22, 46, 77, 102, 125, and 138, which provided two samples during each of the three operating conditions described previously (1: 18 g/m^3 and 5 min residence time; 2: 1 g/m^3 and 80 seconds residence time; 3: 5 g/m^3 and 80 seconds residence time). The non-inoculated column was not sampled on day 22, as it was not known to be colonized by a microbial population at that point. At the conclusion of the experiment packing material samples were also collected from the inlet and outlet of the column as well. The packing

sample was first rinsed gently with sterile distilled water to remove particles and non-attached bacteria. Then the sample was mixed with 5 mL of sterile phosphate-buffered saline (PBS) and vortexed in 10-second pulses at 2500 rpm for a total of two minutes to transfer biomass from the packing surface to liquid suspension. DNA was extracted from this mixture using MoBio UltraClean Microbial DNA extraction kits and amplified by polymerase chain reaction (PCR) using primers designed to amplify a highly conserved region of the gene coding for methanol dehydrogenase, the enzyme responsible for methanol degradation in all known Gram negative methylotrophs. The PCR reaction mixture contains 1X $MgCl_2$-free PCR buffer, 1.5 mM $MgCl_2$, 100 M of each dNTP,1U *Taq* polymerase (all from Invitrogen), 0.5 M of each primer (Integrated DNA Technologies, Inc.), 2 L of template DNA, and sterile water to a final volume of 50 L. Reactions were conducted with an initial denaturation at 94^{o}C for 3 minutes, 30 subsequent cycles of 30 second denaturation at 94 deg. C, 30 second annealing using a touchdown program from 60-50^{o}C for the first 20 cycles and 50 ^{o}C for the final 10 cycles, and 45 second extension at 72 ^{o}C; with a final extension of five minutes at 72^{o}C. The PCR mixture and reaction program were optimized for specificity and yield. The same reaction setup was used for the 16s rRNA primers, but with an annealing touchdown temperature profile of the first 10 cycles from 55 to 50 ^{o}C at -0.5 deg/cycle and the last 20 cycles at 50 ^{o}C. The touchdown program was used because it increased yield and number of bands observed on subsequent DGGE gels, over a set annealing temperature. PCR products were checked on a 1.2% agarose gel, photographed, and their yield estimated using ImageJ software (Rasband, 2006) calibrated with a low DNA marker (50-2,000 bp, BioNexus, Inc.).

DNA fragments were separated using denaturing gel gradient electrophoresis (DGGE), with a 16x16 cm, 1 mm thick gel containing 6% acrylamide, 1X TAE, and a linear gradient of 35-65% denaturant (100% denaturant is equivalent to 7 M urea and 40% formamide), cast for 90 minutes. Approximately 500 ng of PCR product was mixed with 10-20 uL of 2X gel loading dye (70% glycerol, 0.05% Bromophenol Blue, 2mM EDTA), loaded on the gel, and electrophoresed at 60 deg C for 5 hours at 150V in 1X TAE, using a DCode Universal Mutation Detection System Model 475 Gradient Delivery System (Bio-Rad Laboratories.). Gels were stained with 50 ug/mL ethidium bromide in 1X TAE for 15 minutes and destained in 1X TAE for 10 minutes. Bands were visualized and photographed using a Fisher Biotech Model 88A variable UV intensity Transilluminator and DCode DocIt software system (Bio-Rad Laboratories).

The digitized gel images were analyzed using ImageJ (Rasband, 2006). The background was subtracted using a rolling ball radius of 50. Bands in each lane were automatically detected and plotted. Peak area and relative intensity of each band was measured, and bands contributing less than 1% to the total intensity within one lane were omitted from subsequent analysis. No comparisons were made between different gels, because an internal standard was not used. A distance matrix for pairwise comparisons between lanes was generated by the unweighted Gower's distance,

$$D = \frac{1}{P}\sum_{j=1}^{P}\frac{\left|y_{1,j} - y_{2,j}\right|}{R_j},$$

where P is the total number of bands being compared, y1 and y2 are the band intensities for the two lanes being compared, and R is the largest difference found across all bands in that gel (Legendre and Legendre, 1998). This matrix, generated with Mathcad 13 (Mathsoft, Parametric Technologies Corporation), was used for hierarchical clustering with the unweighted pair group method with arithmetic mean (UPGMA), constructed using MEGA version 3.1 (Kumar et al., 2004), and results are shown in Figures 4 and 5.

Figure 32A shows the change in bacterial diversity in both biofilters from the initial inoculum through the six sampling times in each of the three operating conditions. When considering methylotrophs specifically, only a single band was observed in common among the inoculum, BB, and NB, suggesting that the bacterial community that was observed to rapidly colonize and be maintained in both biofilters was not derived solely from the inoculum culture. This observation also suggests that the biofilter methanol-removal performance could be attributed to opportunistic methanol degraders and a favorable biofilter and packing environment (rather than to targeted inoculum), consistent with the previously shown results (Fig. 30) that the NB performed almost equally as well as the BB. Banding patterns generated by amplifying 16s rRNA genes from both biofilters were much more varied and numerous than the mxaF gene, which is likely due to the presence of non-methylotrophic bacteria in the biofilters, but could also be related to high specificity in the functional gene primer. However, similar trends were observed in that

both biofilters appear to be colonized by bacterial communities not amplified from the inoculum and that these communities persist over time and under varied operating conditions.

Cluster analyses in Figure 32B expand visual observations by taking into account the relative intensity of each band. The UPGMA clustering results can be interpreted as showing the relatedness of two samples based on similarities in their banding patterns, but no phylogeny should be inferred. The clustering patterns in the UPGMA dendogram provide quantitative comparisons of bacterial diversity among the all of the different samples collected from the BB and the NB, based on the similarities in migration distance and relative intensity of the DNA bands in the DGGE gel image. Samples that cluster together have higher similarity in banding patterns to each other than to samples that are on more distant branches. Clustering patterns can potentially support the hypothesis that samples collected from the same biofilter or during sequential sampling periods would have very similar genetic diversity profiles.

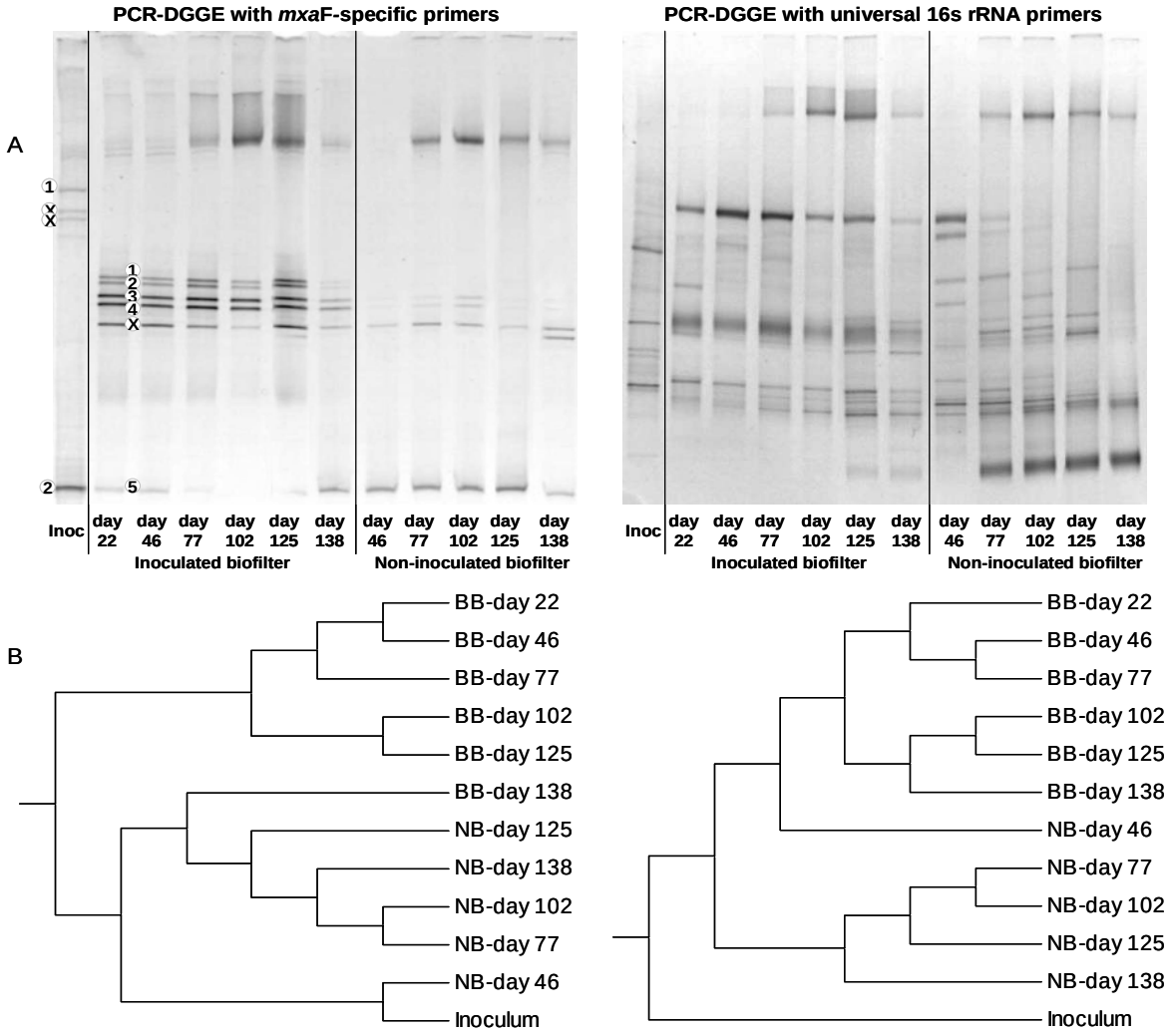

Figure 32. Diversity and Cluster Analysis of Bacterial Populations in the Biofilters over Time

The samples from the BB using both primer sets are shown to be highly similar. Although there is greater difference between the two amplification methods when considering the NB, both approaches indicate a greater similarity in the populations within each of the biofilters than in comparison to populations within each time period or under each operating condition. Although the role of the specifically enriched inoculum plays in the BB performance is not clear, it is likely that addition of this culture did influence the diversity and community structure of the consortium of bacteria that ultimately colonized and were maintained in the BB.

Figure 33A shows the bacterial diversity over three spatial regions in both biofilters and the comparisons in relatedness among these regions. For the inoculated biofilter, the results show opposing trends in diversity over length when examining methylotrophs versus all bacteria present. The methylotrophic population appears to be most diverse at the BB outlet, possibly where methanol concentration is the lowest, whereas populations are more diverse at the inlet when assessed with the 16s rRNA universal primer. No such trend is clearly evident for the NB system. It is also interesting to compare these results with measurements of cultivable bacterial abundance. For methylotrophs and all bacteria, highest abundance was observed at the BB inlet (Fig. 31), but highest methylotroph diversity was at the BB outlet (Fig. 33A). Although these results cannot be compared directly, it is important to note that the molecular comparisons add a level of information and detail about this system that is not possible with traditional culture-dependent tests alone.

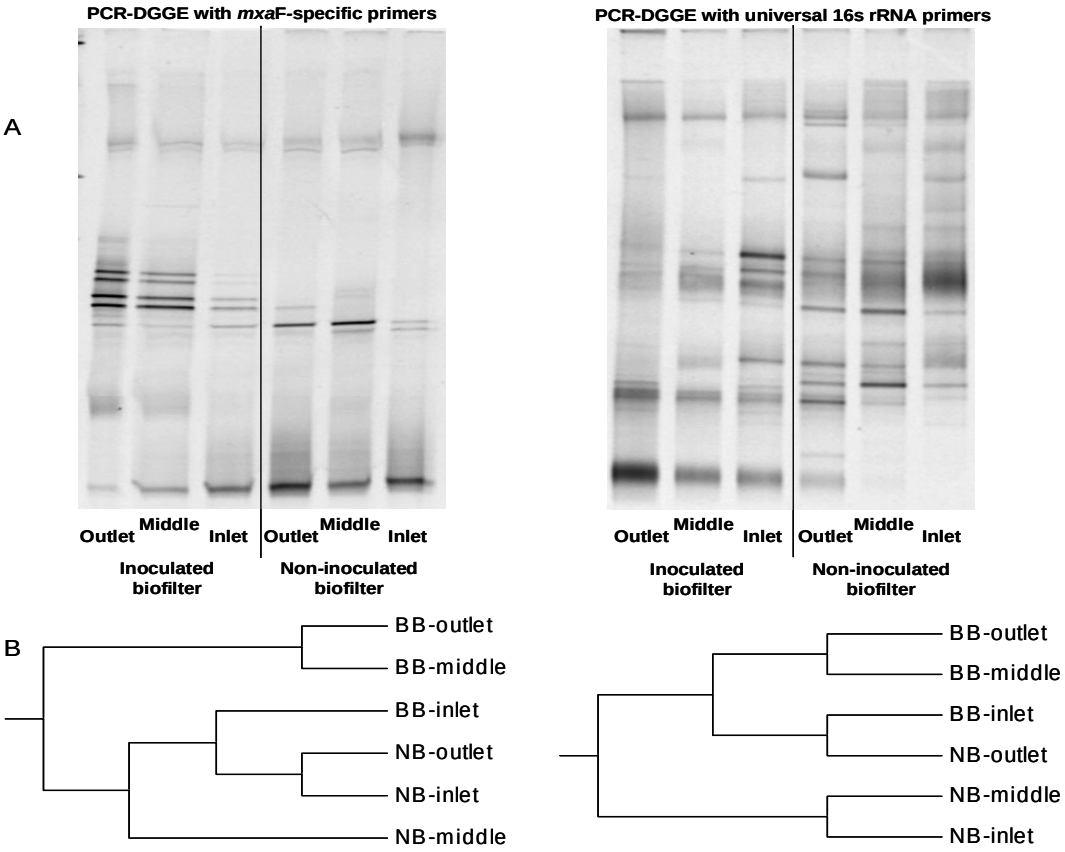

Figure 33. Diversity and Cluster Analysis of Bacterial Populations in Three Spatial Regions in the Biofilters

Figure 33B also shows hierarchical cluster analysis for the spatial comparisons within each reactor and indicates that the outlet and middle sections of the BB are very similar in composition, regardless of the amplification protocol used. Relative similarity among the regions within each biofilter and between the two biofilters was less clear when using the two approaches. These results suggest that growth and activity within each column may vary based on the type of bacteria present and the means in which they are introduced to the biofilter.

Phylogenetic Analysis of Methylotrophic Bacteria. To further examine the community of methanol-degrading bacteria present during biofilter operation and in the original inoculum, selected bands from mxaF-specific DGGE gels were excised for sequencing. The bands selected for study are identified and numbered for the inoculum and the BB in Figure 32B, with bands marked with an X corresponding to those unable to be reamplified or purified. Bands were chosen from mxaF-amplified DNA that showed the highest intensity when visualized on the UV transilluminator, and excised using a sterile pipet tip and scalpel. Gel fragments were eluted overnight at 30^{o}C at 250 rpm in 30 µL of an elution buffer containing 10mM Tris-Cl (pH 7.5), 50 mM NaCl, and 1 mM EDTA (pH 8.0) (Voytas, 2000). Gel fragments were

removed, and DNA was precipitated from the liquid by adding 50 uL of 95% cold ethanol, chilling 30 minutes at -40 ^{o}C, and pelleting the DNA by centrifuging 10 minutes at 10,000 *x g*. After pouring off the ethanol supernatant, the pellet was dried at 40 ^{o}C for 4-5 hours and resuspended in 30 µL of TE buffer (Voytas, 2000). This template was reamplified using the same methods as described previously and checked on a DGGE gel for purity and for migration to the same gradient position as in the original sample. Sequencing was performed at the University of Florida Interdisciplinary Center for Biotechnology Research using the flourescent dideoxy terminator method of cycle sequencing on either a Perkin Elmer, Applied Biosystems Division (PE/ABd) 373A or 377 automated DNA sequencer, following ABd protocols, with consensus sequences generated using the Sequencher Software from Gene Codes.

Published sequences with high similarity to sample sequences were obtained by performing a nucleotide-nucleotide BLAST (NCBI) search. The 10 most similar sequences of known species with E scores lower than 1E-20 were chosen for each sample, and duplicates were removed. All sequences were aligned using ClustalW, with default gap penalties, and manual inspection and refinement of alignments. A phylogenetic tree was constructed using the Neighbor Joining method and bootstrapped with 1,000 replicates. Because all known gamma-proteobacteria clustered into a distinct branch, this group was selected as the out-group. All phylogenetic and molecular evolution analyses were conducted using MEGA version 3.1 (Kumar et al., 2004.

Figure 34 shows that species obtained from both the inoculum and the biofilter are widely distributed across known types of methylotrophs. Inoculum 1 and BB1 appear to be closely related to species within the genera of *Methylophilus*, *Methylovorus*, and *Methylobacillus*. These genera are known to follow the ribulose monophosphate (RuMP) pathway and are non-N_2 fixing, restrictive facultative methylotrophs classified as beta-Proteobacteria (Doronina et al., 2005; Lidstrom, 2001). BB2 is grouped with several *Hyphomicrobium* species, which are also classified as non-N_2 fixing, restrictive facultative methylotrophs, but which use the serine pathway and are members of the alpha-Proteobacteria (Lidstrom, 2006; Rainey et al., 1998).

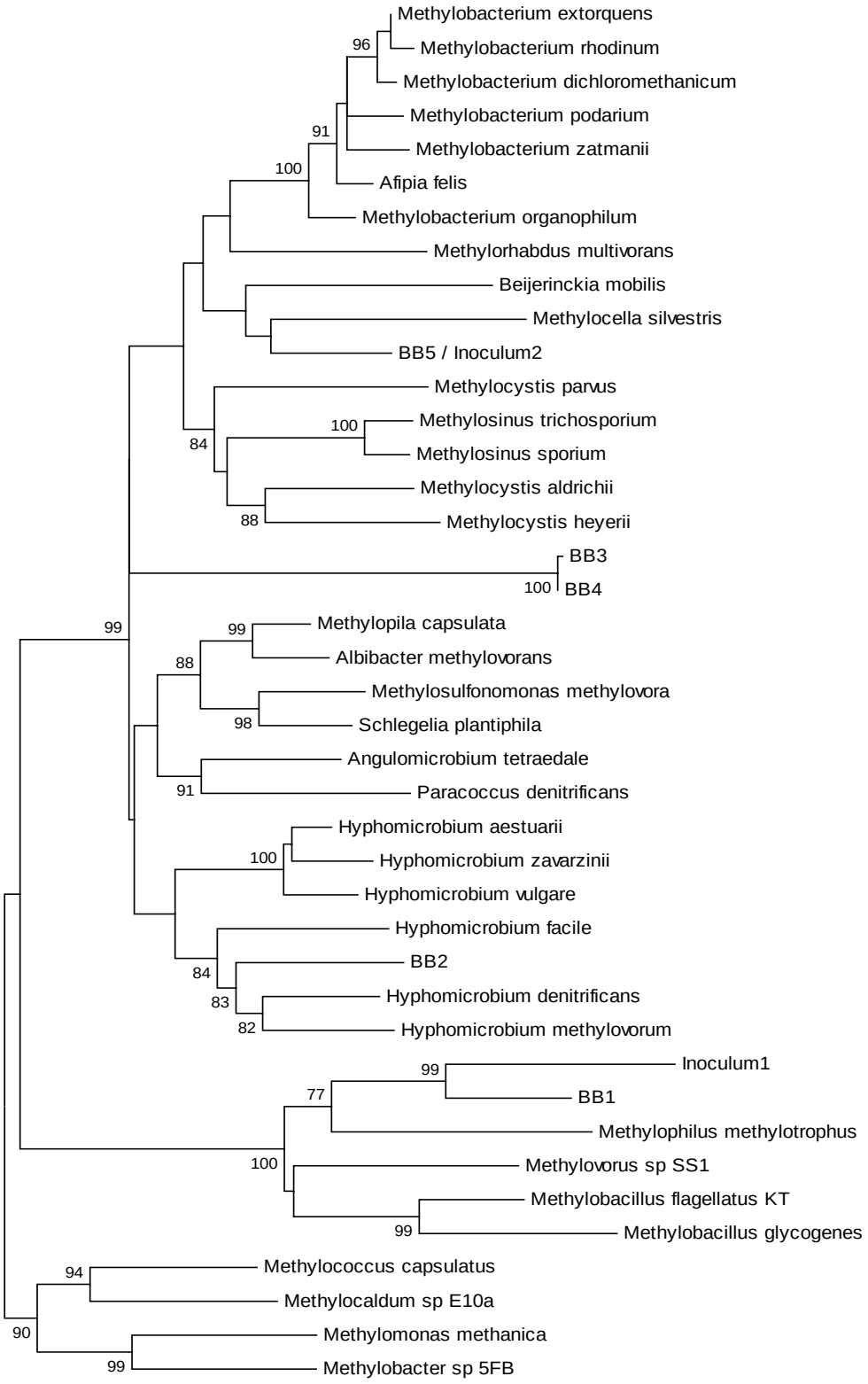

Figure 34. Phylogenetic Reconstruction of Known Methylotrophic Bacteria and Unknown Biofilter and Inoculum Strains

BB3 and BB4 are also classified with the alpha-Proteobacteria, but not clustered closely with specific known sequences. However, BB5, which was identical in species to Inoculum 2, appears to be closely related to *Beijerinckia mobilis* and *Methylocella silvestris*, both alpha-Proteobacteria. *B. mobilis* is known to be heterotrophic, N_2 fixing, and use the ribulose bisphosphate (RuBP) pathway for formaldehyde assimilation (Dedysh et al., 2005a), while *M. silvestris* is known to be facultatively methanotrophic, moderately N_2 fixing, and use the serine pathway (Dedysh et al., 2005b). Interestingly, both of these species are acidophilic and grow in environments as low as pH 3 (Dedysh et al., 2005; Dunfield et al., 2003), and, as observed in Figures 4A and 5A, the band correlating to this species increases in relative intensity over operation time and at the inlet of the BB, a region potentially growing more acidic due to operation in upflow mode and drainage of liquid in the biofilter, although this possibility cannot be corroborated with actual biofilter pH measurements.

In addition to specific characteristics about the inoculum and BB bacterial species that are hypothesized based on this phylogenetic reconstruction, a more important observation may be that the BB is colonized by a genetically (and likely phenotypically) diverse population of bacteria, expected to thrive in varied C- and N-usage niches. This diversity, which is higher than observed in the NB (although both reactor types share some of the same species), may enable the increased performance and reliability of the BB over time and under varied operating conditions.

Extended Study of Potential Biofilter Inocula. Because of the trends observed in biofilter performance and bacterial diversity between the inoculated and non-inoculated columns, it was of interest to study these mixed cultures in greater detail. Selection and enrichment of an appropriate inoculum for the biofilter systems may be greatly improved with additional knowledge of optimum nutrient requirements and concentrations. Therefore, this work sought to determine the effect of the form and concentration of nitrogen in batch enrichment cultures on the methanol removal potential and the genetic diversity of methylotrophic cultures derived from biofilm samples from a Kraft pulp mill that would potentially be used as biofilter inoculum.

Seven grab samples of biofilm samples collected from the biological treatment system at a Kraft pulp mill in the Southeast United States were collected during June 2004, from locations believed by mill staff to be representative of methanol-degrading consortia or having a high number of bacteria present. The samples were stored on ice in sterilized Teflon collection vessels until they could be processed in the lab or stored over a longer term at 4 deg. C. Initial culture-dependent growth and isolation techniques demonstrated that two of the seven samples could be good candidates for inoculum in a methanol treatment system, based on fast growth rates in varied methanol concentrations and high number of potentially distinct isolates (possibly indicating high diversity; results not shown). These samples, A and B, were named “SA” and “SB” and described as follows. The SA biofilm was obtained directly from the vent tubes of a pure oxygen activated sludge “UNOX” reactor, where the conditions would be expected to include temperatures between 32-36 deg C, methanol concentrations between 1,000-5,000 mg/L, and nitrogen as ammonium in concentrations between 20-140 mg/L (ammonium is added to the reactor to improve performance). SB biofilm was collected from the return activated sludge system, with conditions expected to include ambient outdoor temperatures (26-30 deg C), and low methanol (<10-100 mg/L) concentrations.

Subsamples (10mL each) from SA and SB were first homogenized in 90mL of sterile phosphate-buffered solution for one hour on a rotary shaker at 30 deg C at 250 rpm, then this mixture was used to inoculate batch cultures in both modified nitrate mineral salts (NMS) and ammonium mineral salts (AMS) media, containing 0.1% methanol (vol/vol) as recommended by Hanson (1998).

To compare methanol degradation by batch mixed methylotrophic cultures with two potential nitrogen sources, a factorial (32) design was used. This design included either nitrate added as KNO3 at levels of 0, 1.0, and 2.0 g/L or ammonium added as NH_4Cl at levels of 0, 0.5, and 1.0 g/L (these represent 0, 0.13, and 0.26 g N/L), and methanol added at 10, 100, and 1000 mg/L in the liquid phase. These nitrogen levels reflect common ranges used in both batch and in biofilter applications (Yang et al., 2002; Gribbins and Loehr, 1998). Concentrations of 0 g N/L were also included to assess whether the cultures could degrade methanol with only soluble cell nitrogen or atmospheric N_2 present, as such a condition might be expected if nutrients become exhausted in a biofilter or even in a batch culture. The cultures were incubated for 48 hours on a rotary shaker at 250 rpm and 30deg C. Every 4-6 hours during this incubation, growth, assayed by optical density, was measured using a spectrophotometer at 600nm,

directly from the sample in the glass vial. At 48 hours, the cells were pelleted using the floor centrifuge, and 2 mL of the liquid supernatant was collected and analyzed for final methanol concentration. Aqueous methanol concentrations were analyzed by GC/FID using a PerkinElmer Clarus 500, with helium at 31.3 psig as the carrier gas, and hydrogen and air at 45 mL/min and 450 mL/min, respectively, as combustion gases. Cyclohexanol was used as the internal standard. Results for methanol removal and growth rates are shown in Figures 35 and 36, below.

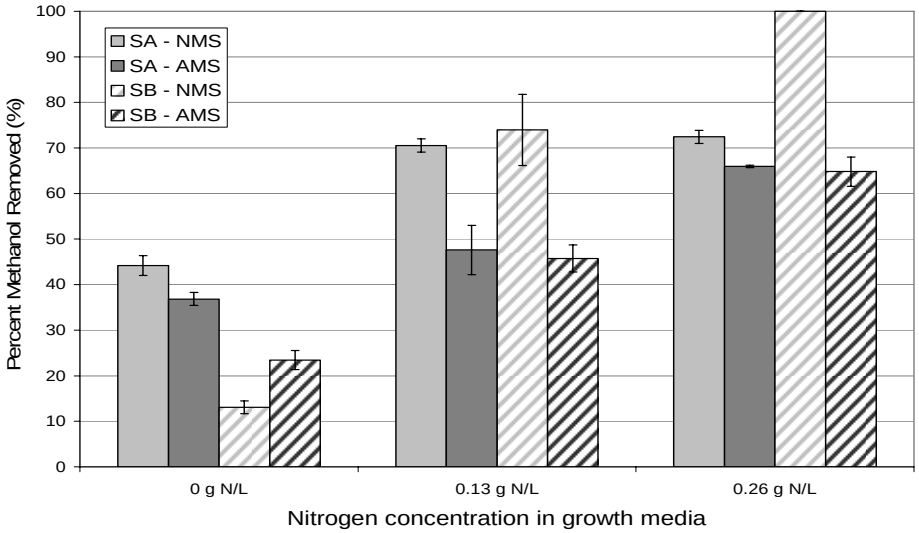

Figure 35. Comparison of Methanol Removal by SA and SB Cultures in Both AMS and NMS Media

Both samples, regardless of nitrogen source or concentration, showed 100% methanol removal for initial methanol concentrations of 10 and 100 mg/L. Differences among the cultures became apparent for methanol concentrations of 1,000 mg/L (Figure 7). These results indicate that for all of these cultures, percentage of methanol removed from the liquid phase increased with increasing nitrogen concentration. In addition, for all of the cultures assessed in media with added nitrogen, a higher methanol removal was achieved when nitrate was used as the nitrogen source during. In fact, the SB culture enriched in NMS showed 100% removal when grown in media with the highest concentration of nitrate. On the other hand, both SA cultures showed significantly higher methanol removal than SB, regardless of the enrichment N-source, when they were transferred to media with no nitrogen, perhaps because of the presence of nitrogen fixing bacteria enriched from the original SA biofilm sample. An additional possibility might be that because the SA biofilm was collected directly from the aerobic reactor, where the microbial community would be acclimated to degrading high concentrations of methanol (>>1,000 mg/L), the mixed culture could be more well acclimated to high methanol and occasional nitrogen-limiting environments.

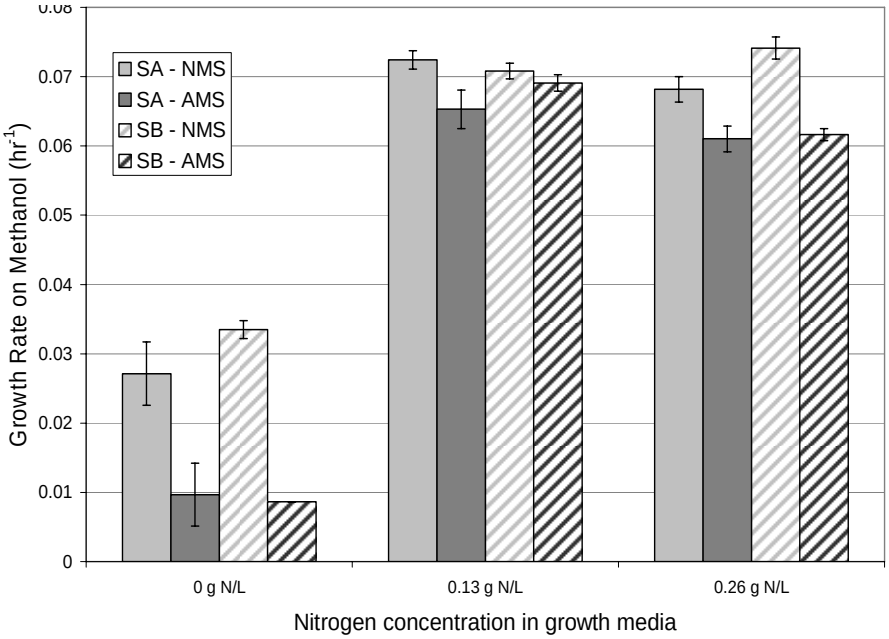

Figure 36. Comparison of Batch Growth Rates in SA and SB Cultures in Both AMS and NMS Media

A slightly different trend is observed when comparing growth rate on 1,000 mg/L methanol and varied nitrogen sources and concentrations (Figure 36). These results show that the mixed cultures grow almost equally as fast with either ammonium or nitrate present at high or medium concentrations. There is a slight increase in growth rate when NMS is used, but the trends are not as dramatic as when comparing methanol removal. However, Figure 30 also shows that the growth rate is significantly lower when the cultures are transferred into media with no added nitrogen in either form. This result is not surprising, as the nitrogen added to media would likely be necessary to support biosynthesis and faster growth rates.

Genetic Diversity in Batch Inocula Cultures. The PCR-DGGE approach described above for the biofilter studies was also used to assess genetic diversity in the batch cultures, with DNA extraction, amplification, and separation performed with the methods described above for *mxa*F and 16s rRNA. In addition, Diversity in each sample was estimated using measurements of species richness (S), diversity (H), and evenness (E), determined graphically from band intensities in the resulting DGGE images. S was determined by simply counting the bands in each lane, with the assumption that a single species would migrate to each unique location. Shannon's H (Hayek and Buzas, 1997) was used as a diversity index, as follows

$$H = -\sum_i p_i \ln(p_i)$$

where p_i is the relative intensity of the ith band compared to the total intensity of all bands in that lane. E was calculated from Pielou's evenness (Hayek and Buzas, 1997) as follows

$$E = \frac{H}{\ln(S)}.$$

Results from this analysis are shown in Table 10.

Table 10. Bacterial Species, Diversity, and Evenness for SA and SB Cultures in Both AMS and NMS Media

	Methylotrophs (*mxa*-F)			Universal (16s rRNA)		
Sample	S	H	E	S	H	E
SA	4	1.04	0.75	9	2.02	0.92
SA-AMS	1	0	0	3	1.06	0.96
SA-NMS	1	0	0	7	1.74	0.89
SB	5	1.56	0.97	10	2.09	0.91
SB-AMS	2	0.34	0.49	8	1.48	0.71
SB-NMS	6	1.39	0.78	9	1.90	0.87

Results in Table 10 show consistent trends among the different enrichment and molecular methods, except for methylotrophs enriched from SA. In this case, regardless of nitrogen source used the diversity of this type of bacteria drops to zero, with potentially only one dominant methylotrophic species present. When comparing methylotrophs in SB and all bacteria in SA, species richness, diversity, and evenness generally show a smaller decrease in the enriched culture, as compared to the original biofilm sample. It is interesting to note that in all the cases, the diversity metrics are greater for the mixed cultures enriched using nitrate, as compared to ammonium, as the nitrogen source. This result could potentially correspond to the observation that cultures enriched in nitrate also showed higher methanol removal and growth rate.

Conclusions

Based on results of this study, it is likely that a GAC biofilter would be feasible as a final step in an innovative HAP/methanol treatment train for pulp and paper mills, or other industries faced with VOC control requirements. Some of the specific conclusions are detailed below.

- Use of a biological inoculum enriched from biofilm in the pulp and paper process has the potential to enhance the performance of a GAC biofilter.
- A biofilter inoculated with specifically-enhanced inoculum showed higher bacterial diversity for methylotrophs and all bacteria, as compared to a non-inoculated biofilter.
- Mixed methylotrophic cultures, selected as potential biofilter inocula, show increased methanol removal with highest concentrations of nitrogen provided as nitrate.
- The PCR-DGGE approach added valuable insight into the diversity and community structure of bacteria colonizing the biofilters and present in batch cultures under different conditions.
- Performance of a biofilter is better understood when it is coupled with observations on the microbial activity, diversity, and abundance throughout the biofilter and over time.
- Further study would be recommended to assess the biofilter performance for other HAPs as substrate, the change in bacterial population as a function of pH or other process variables, and the use of a functional gene primer in PCR-DGGE to assess diversity of specific bacterial systems of interest.

Currently, all laboratory studies have been completed, and the collected data have been analyzed and are in preparation for publication in two manuscripts; the first on the topic of the performance and bacterial abundance and diversity of the biofilter, and the second on the role of nitrogen concentration and form on methanol removal and bacterial diversity in mixed methylotrophic cultures.

BENCH-SCALE STUDIES USING SILICA-TITANIA COMPOSITES (STC)

Synthesis and Characterization of the Silica-Titania Composites (STC)

The STC pellets were prepared using a sol-gel technique in which nitric acid and hydrofluoric acid (HF) were used to catalyze hydrolysis and condensation reactions, thereby decreasing the time to gelation. Tetraethyl orthosilicate (TEOS) was used as the silica precursor. The pore size of the STC was dependent on the concentration of HF in solution since HF causes the etching of pores within the silica gel matrix. For bench-scale studies, STC pellets with three different pore sizes (ca. 40 Å, 120 Å, and 260 Å) and various titania loadings (between 1 and 60%) were synthesized. A known mass of Degussa P25 titania (Majemac Enterprises) was mixed into a solution of TEOS, ethanol, water, and acids. The quantity of titania in the STC is expressed as a ratio based on the weight of titania (in grams) to the volume of TEOS (in mL). For example, STC with a 12% titania loading contained 0.12 g of titania per 1 mL of TEOS. The ingredients were allowed to mix via a magnetic stir plate before being transferred into 96-well assay plates, forming the STC into cylindrical pellets upon gelation. After aging and drying, each pellet was approximately 3 mm by 5 mm.

The STC pellets were analyzed for BET surface area, total pore volume, and average pore size (results shown in Table 11) using a Quantachrome NOVA 2200e (Boynton Beach, FL). Each type of STC synthesized was identified based on its approximate pore size and titania loading (e.g., 40 Å 12%). As shown in Table 13, an inverse relationship exists between average pore size and surface area (i.e., as the pore size decreases the surface area increases) when gels with the same titania loading (i.e., 12%) are compared. An inverse relationship also exists between titania loading and surface area for the 40 Å STC. This is likely due to the low surface area of the titania, which is about 50 m^2/g. Since the STC pellets were made in a series of batches, the error shown in Table 13 is the standard deviation of measurements from at least three different batches of pellets synthesized from the same recipe.

Table 11. BET surface area, pore volume, and average pore size of STC pellets

STC	Surface Area (m^2/g)	Total Pore Volume (cc/g)	Actual Pore Size (Å)
40 Å 1%	636	0.88	55
40 Å 4%	616 ±19	0.79 ± 0.03	52 ± 2
40 Å 12%	532 ± 43	0.60 ± 0.06	46 ± 4
40 Å 36%	383	0.55	57
40 Å 60%	297	0.48	65
120 Å 12%	274 ± 23	0.77 ± 0.11	124 ± 7
270 Å 12%	154 ± 18	0.99 ± 0.11	259 ± 11

Bench-Scale Reactor for Methanol Removal using STC

The photocatalytic oxidation of methanol was tested using a bench-scale annular reactor with an eight-watt UV bulb surrounded by a quartz sleeve (25 mm outside diameter) in the center. UV lamps (Spectronics Corporation) with peak wavelengths of 365 nm (UVA) and 254 nm (UVC) were used in the experiments. The UV intensity was measured at the peak wavelength of the bulb using a UVP radiometer (Upland, CA). Measurements were taken at the surface of the quartz sleeve that housed the lamp. The annulus of the reactor, which was approximately 8 mm, was packed with 30 mL of STC pellets. Compressed air containing 1000 ppm_v of methanol was diluted with humid air, which was first passed through a water bubbler, to obtain an influent gas stream containing high humidity (about 95%) and between 50 and 250 ppm_v of methanol. The reactor set-up is shown in Figure 37. The residence time (or empty bed contact time) was varied between about 1 and 4.3 seconds by changing the flow rate of the air entering the reactor. Initial studies performed with an empty reactor showed no photolysis of methanol in the presence of UVA or UVC light. Similarly, adsorption of methanol to the reactor and its appurtenances was negligible.

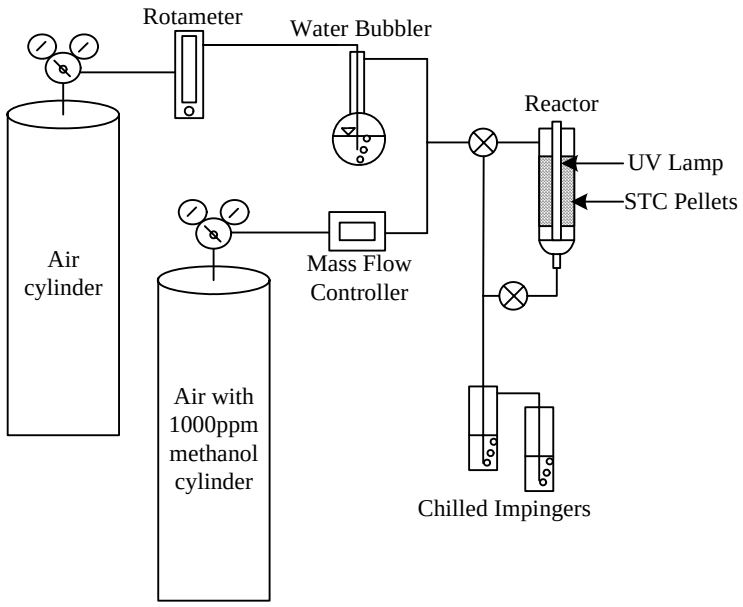

Figure 37. Bench-scale Photocatalytic Reactor Set-up for Testing of STC

Both influent and effluent methanol concentrations were tested using the NCASI (National Council for Air and Stream Improvement) Chilled Impinger Method (NCASI, 1998). Methanol concentrations were quantified using a PerkinElmer GC/FID (Wellesly, MA). The variation between actual air-phase methanol concentrations and that measured via the NCASI chilled impinger method was less than ± 12%. Effluent formaldehyde concentrations were quantified colorimetrically using a Hach DR/4000U spectrophotometer (Loveland, CO) as described in the NCASI Chilled Impinger Method (NCASI, 1998). In order to quantify total byproduct formation, total organic carbon concentrations of the impinger samples were determined using a Tekmar Dohrmann Apollo 9000 total organic carbon analyzer (Mason, Ohio). Error bars in the graphs represent the standard deviation of at least triplicate measurements.

Adsorption of Methanol

STC pellets were tested in the dark to determine methanol adsorption capacity using an influent methanol concentration of 50 ppm_v and residence time of 4.3 seconds. As shown in Figure 38, the time required to reach exhaustion was dependent on the pore size of the STC pellets, with the smallest pore size (i.e., 40 Å) having the greatest methanol adsorption capacity. These adsorption breakthrough curves suggest that methanol adsorption occurred via monolayer coverage versus pore filling since the adsorption trends correlated with the BET surface area data, but not with the total pore volume.

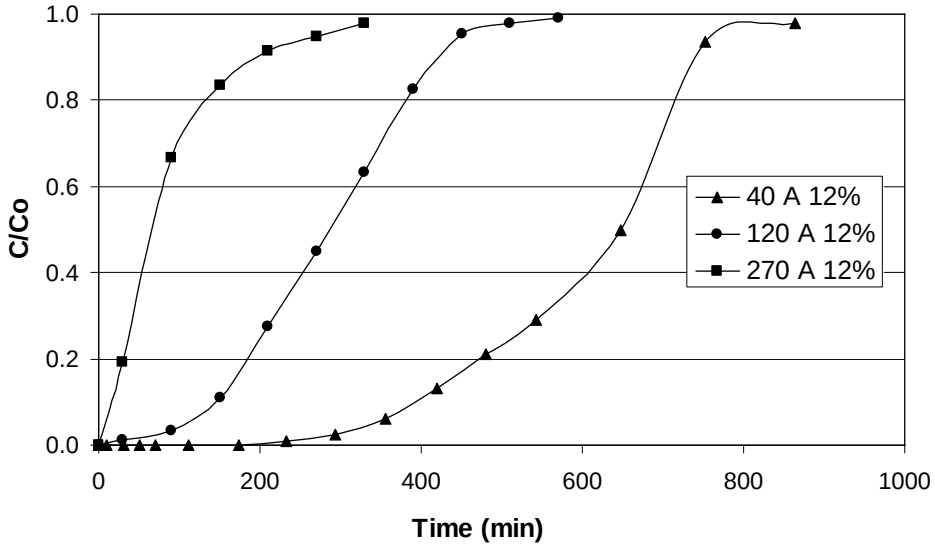

Figure 38. Methanol adsorption breakthrough curves (Co = 50 ppm_v) for STC pellets of varying pore sizes (40 Å, 120 Å, and 270 Å) at a residence time of 4.3 seconds

Simultaneous Adsorption and Oxidation of Methanol

The photocatalytic oxidation of methanol was tested by repeating the experiments described above in the presence of UVA light. Figure 39 shows the methanol removal capabilities of the ca. 40 Å, 120 Å, and 270 Å STC pellets. Initially, the breakthrough curves for the pellets in the presence of UV light followed those in the dark. After a period of time (e.g., approximately 400 minutes for the 40 Å STC pellets), the system appeared to reach a pseudo-steady state (i.e., the effluent concentration is relatively constant). Before the system reached a steady state, the rate of oxidation was less than the rate of adsorption. Otherwise, the first portions of the breakthrough curves in Figure 39a would be different (i.e., lower C/Co values) than those in Figure 38. The oxidation rate may initially be low due to the lack of surface coverage of methanol on the catalyst surface. This is according to the Langmuir-Hinshelwood model, which states that the reaction rate is proportional to the surface coverage of the compound on the catalyst surface. Alternatively, if methanol is primarily oxidized via hydroxyl radicals (rather than directly oxidized via the electron hole), then the oxidation rate would initially be low due to the lack of adsorbed water vapor.

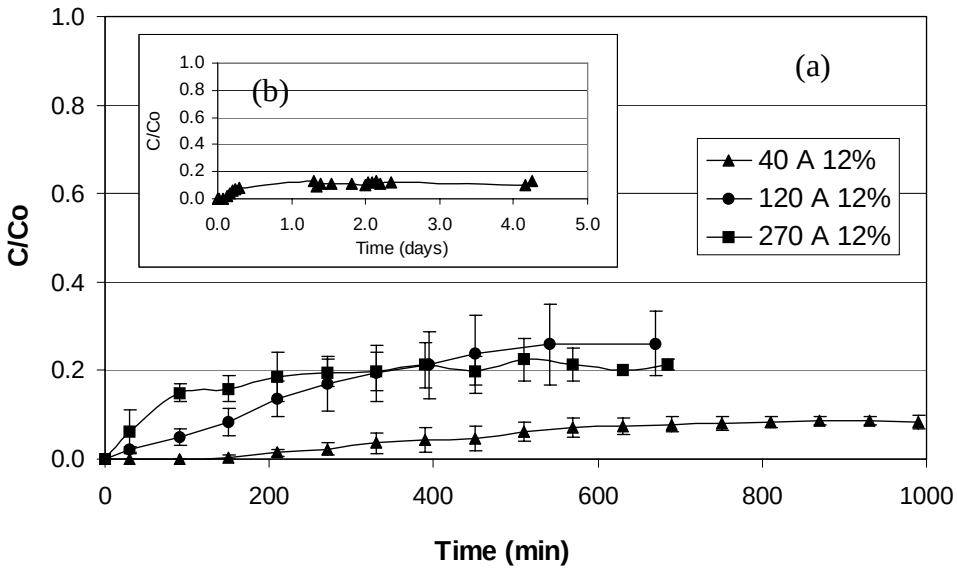

Figure 39. (a) Methanol removal (Co = 50 ppm_v) using STC pellets of varying pore sizes (40 Å, 120 Å, and 260 Å) in the presence of UVA light (b) Extended study using 40 Å STC pellets (RT = 4.3 s)

The removal efficiency of the 120 Å and 270 Å pellets at steady state was similar (about 80%). The 40 Å pellets removed greater than 90% of the methanol at steady state. The enhanced performance of the 40 Å pellets shown in Figure 39a is probably a result of the high internal surface area of these pellets. Although the UV probably does not reach the very center of each STC pellet due to the opacity of the titania, these results suggest that photons do make it past the external surfaces of the pellets; otherwise, the performance of the pellets at steady state would be similar regardless of internal surface area.

To assess whether the system in Figure 39a was truly at steady state, an extended study was conducted over a period of four days using the 40 Å pellets. This study (results shown in Figure 39b) confirmed that the system was at steady state, achieving approximately 90% methanol removal for the duration of the experiment.

Formaldehyde, a byproduct of the photocatalytic oxidation of methanol, was identified in the effluent of all studies conducted in the presence of UV light. The concentration was dependent on the pore size of the pellets, as shown in Figure 40. The effluent formaldehyde concentration produced by the 270 Å, 120 Å, and 40 Å pellets was approximately 7, 4, and 2 ppm_v, respectively. STC pellets with a higher surface area would produce a higher concentration of hydroxyl radicals per gram of composite and possess a greater number of active sites for adsorption and subsequent photocatalytic oxidation to occur. In addition, diffusion of formaldehyde out of the pellets would be dependent on the pore volume of the composite (i.e., a composite with a smaller pore volume would result in less pore diffusion). Thus, the higher surface area and restrained desorption of formaldehyde in the 40 Å STC aided in the more complete oxidation of methanol to carbon dioxide.

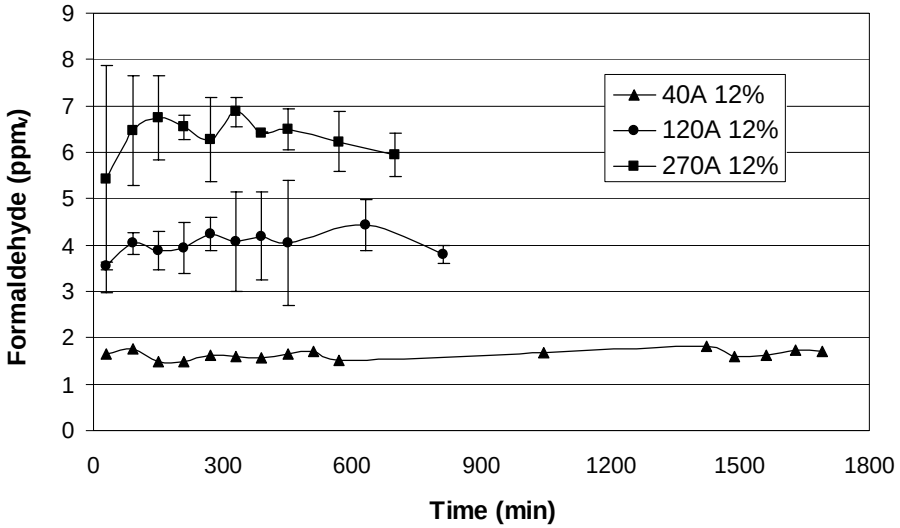

Figure 40. Effluent formaldehyde concentrations from STC pellets of varying pore sizes (40 Å, 120 Å, and 270 Å) in the presence of UVA light (Co Methanol = 50 ppm_v, RT = 4.3 seconds)

In addition to testing effluent streams for methanol and formaldehyde, TOC analysis was performed in order to identify additional organic byproducts. For all studies, TOC analysis proved that other organic byproducts were not measurable regardless of the test parameters. For example, when 40 Å STC pellets were irradiated with UVA light, methanol and formaldehyde were released in the effluent at a rate of about 0.003 mg of methanol (as carbon) per minute and about 0.004 mg of formaldehyde (as carbon) per minute at steady state. The results of TOC analysis showed the total rate of carbon released in the effluent was 0.007 mg/min. This mass balance shows that the TOC present in the effluent (0.007 mg C/min) was accounted for by the methanol (0.004 mg C/min) and formaldehyde (0.003 mg C/min). The lack of the presence of measurable amounts of formic acid in the effluent can be attributed to the fact that only one electron hole is necessary for the total degradation of formic acid, which, according to other literature values, results in a high apparent quantum yield (0.45) compared to other compounds (0.06-0.001) (Dijkstra et al. 2002). Since formic acid is degraded directly to carbon dioxide and water, the balance of the effluent carbon should be present as carbon dioxide (Dijkstra et al. 2002).

Table 12 shows a summary of the influent methanol concentrations and effluent methanol and formaldehyde concentrations for each of the three pore sizes studied. The effluent formaldehyde and methanol concentrations are those present after steady state methanol removal was obtained. Since the only intermediate byproduct was determined to be formaldehyde, the quantity of methanol that was completely oxidized (i.e., mineralized) was calculated and is shown in Table 12. The 40 Å 12% STC, which performed the best, achieved 88% mineralization of methanol. In other words 88% of the influent methanol concentration was completely oxidized while the remaining 12% was present in the effluent as either methanol or formaldehyde.

Table 12. Summary of Methanol Removal Performance of STC with Various Pore Sizes at Steady State in the Presence of UVA light (RT = 4.3 seconds)

STC	Influent Methanol (ppm_v)	Effluent Methanol (ppm_v)	Effluent Formaldehyde (ppm_v)	% Mineralized
40 A 12%	50	4.5	1.7	88
120 A 12%	50	10	4	72
270 A 12%	50	10	7	66

Effect of Residence Time on Methanol Removal

The effect of residence time on methanol removal was studied to evaluate the effect of residence time of methanol removal and byproduct formation. In addition, the residence time will directly affect the size, energy consumption, and economics of the system. Adsorption and adsorption/destruction tests were also conducted using shorter residence times of 1.1 and 2.1 seconds.

The methanol adsorption capacity of STC with pore sizes of 40, 120, and 270 Å were tested with a shorter residence time of 2.1 s, which was obtained by increasing the flow rate of the gas through the packed bed. All other test parameters were identical to that of Figure 38. As shown in Figure 41, the methanol exhaustion times were again dependent on the pore size of the gel, with the smaller gels having the greatest methanol adsorption capacity. The total adsorption capacity of each gel was similar to that achieved with the 4.3 second residence time, indicating that the increase in flow rate did not affect mass transfer.

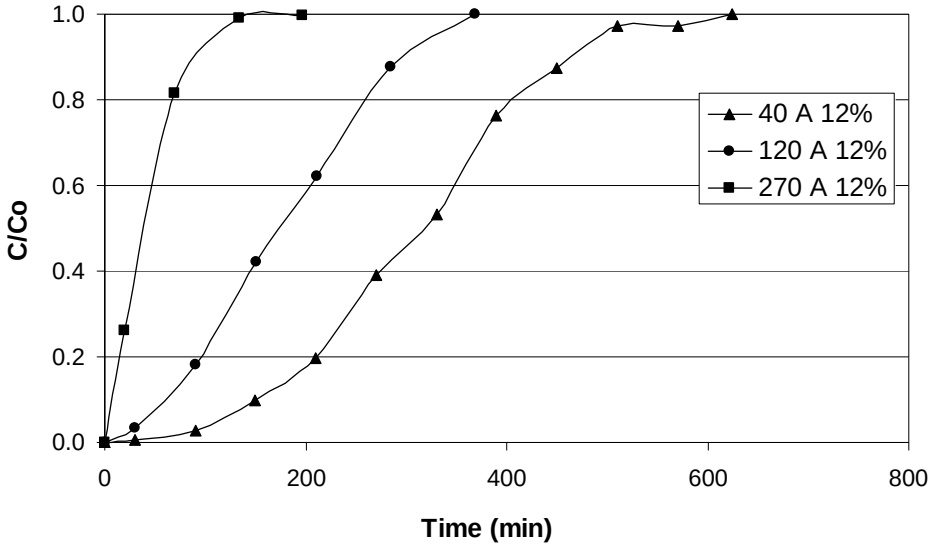

Figure 41. Methanol adsorption breakthrough curves (Co = 50 ppm_v) for STC pellets of varying pore sizes (40 Å, 120 Å, and 270 Å) at a residence time of 4.3 seconds

In the presence of UVA light, the 40 Å and 120 Å gel performed similarly (as shown in Figure 42). These gels removed greater than 60% of the influent methanol at steady state. The 270 Å gel removed about 50% of the methanol at steady state. Effluent formaldehyde concentrations are shown in Figure 43 and are dependent on the pore size of the STC. This is similar to the trend for the 4.3 second residence time. The effluent formaldehyde concentration for all STC pore sizes is higher than the 4.3 second residence time, indicating that there was not sufficient residence time for complete oxidation to occur.

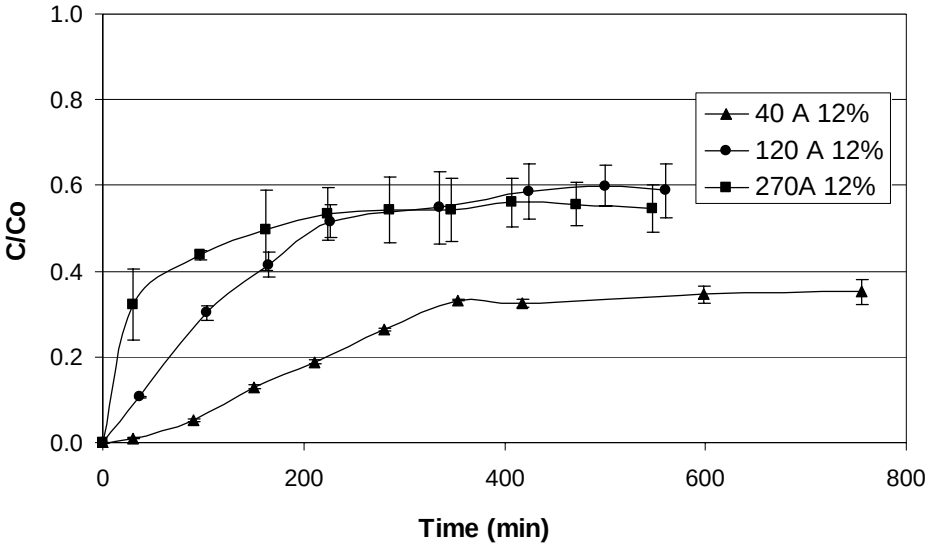

Figure 42. Methanol removal (Co = 50 ppm_v) using STC pellets of varying pore sizes (40 Å, 120 Å, and 270 Å) in the presence of UVA light (RT = 2.1 seconds)

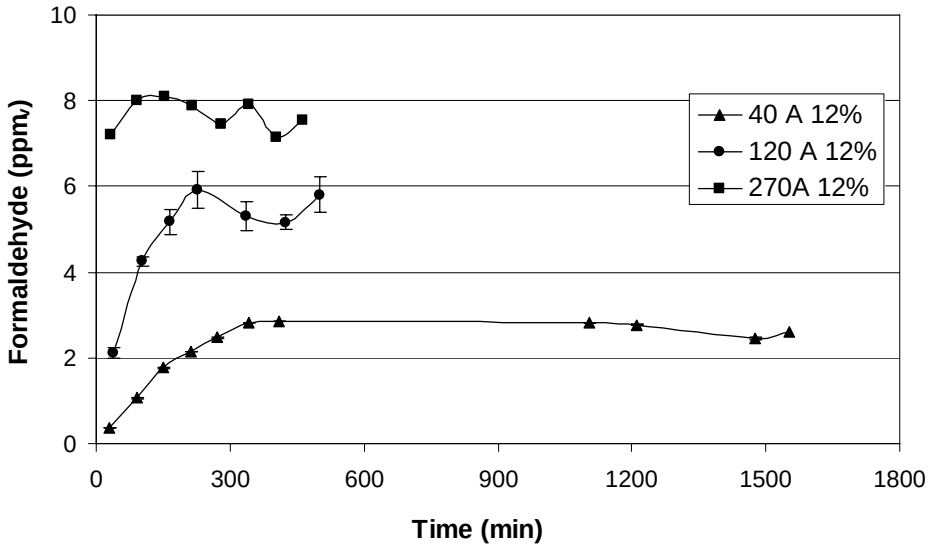

Figure 43. Effluent formaldehyde concentrations from STC pellets of varying pore sizes (40 Å, 120 Å, and 270 Å) in the presence of UVA light (Co Methanol = 50 ppm_v, RT = 2.1 seconds)

As shown in Table 13, the steady state mineralization efficiency of the STC was about 62% for the 40 Å 12% STC and 30% for the 120 Å 12% and 270 Å 12% STC. As in the case of the 4.3 second residence time, the 40 Å 12% gel performed the best. However, the 270 Å 12% and 120 Å 12% STC performed similarly with respect to overall oxidation efficiency.

Table 13. Summary of Methanol Removal Performance of STC with Various Pore Sizes at Steady State in the Presence of UVA light (RT = 2.1 seconds)

STC	Influent Methanol (ppm_v)	Effluent Methanol (ppm_v)	Effluent Formaldehyde (ppm_v)	% Mineralized
40 A 12%	60	20	2.7	62
120 A 12%	47	27	5.6	30
270 A 12%	50.5	28	7.7	30

The previous experiment was repeated with a shorter residence time (1.1s) in the presence of UVA light. As shown in Figure 44, the 40 Å 12% STC removes about 50% of the methanol at steady state, while the 120 Å 12% and 270 Å 12% STC both removed slightly less than 40% of the methanol at steady state.

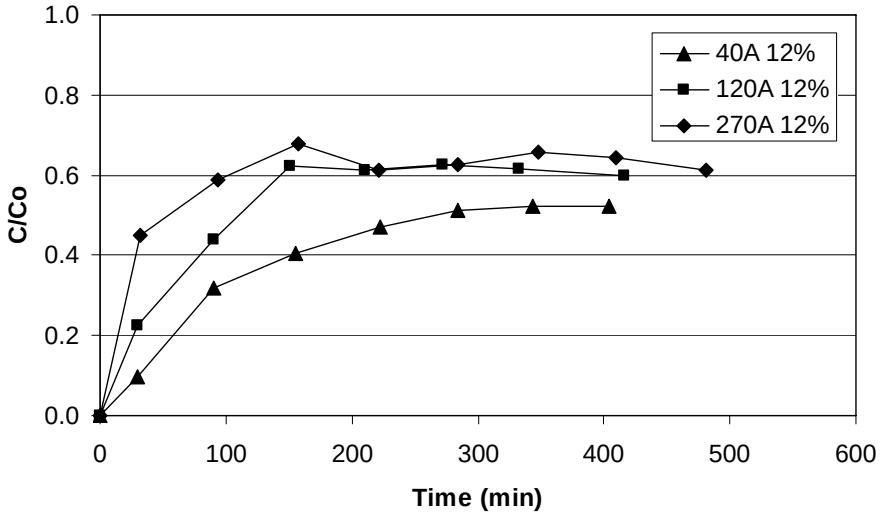

Figure 44. Methanol removal (Co = 50 ppm_v) using STC pellets of varying pore sizes (40 Å, 120 Å, and 260 Å) in the presence of UVA light (RT = 1.1 seconds)

Formaldehyde analysis was performed on the test described above. As shown in Figure 45, the formaldehyde production was dependent on the pore size of the gel, with the smallest pore size producing the least amount of formaldehyde. This trend is similar to that of the 2.1 s and 4.3 s residence times.

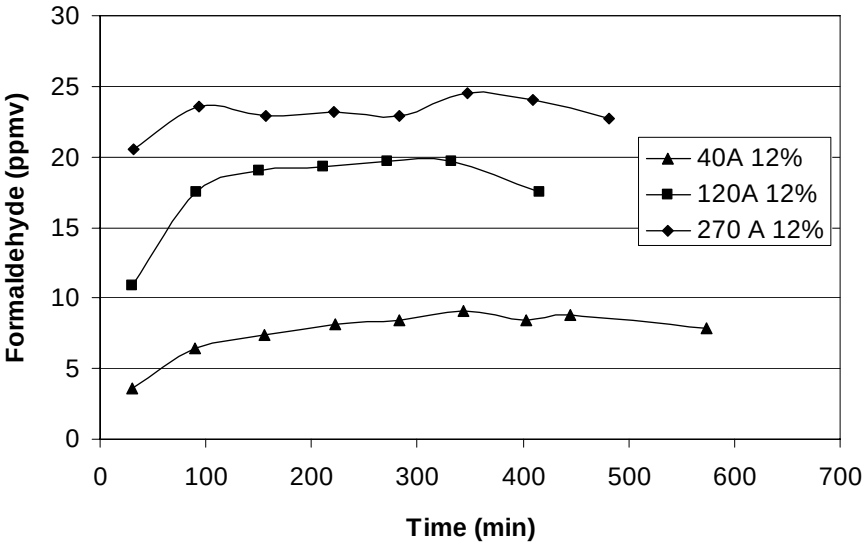

Figure 45. Effluent formaldehyde concentrations from STC pellets of varying pore sizes (40 Å, 120 Å, and 270 Å) in the presence of UVA light (Co Methanol = 50 ppm_v, RT = 1.1 seconds)

Table 14 shows a summary of the steady state performance of the STC of varying pore sizes at the residence time of 1.1 seconds. The 270 Å 12% STC did not mineralize any of the methanol. The 23 ppm_v of methanol that was removed was converted to formaldehyde. The 120 Å 12% STC mineralized only about 4% of the influent methanol. The 40 Å 12% STC mineralized about 34% of the influent methanol.

Table 14. Summary of Methanol Removal Performance of STC with Various Pore Sizes at Steady State in the Presence of UVA Light (RT = 1.1 seconds)

STC	Influent Methanol (ppm_v)	Effluent Methanol (ppm_v)	Effluent Formaldehyde (ppm_v)	% Mineralized
40 A 12%	50	25	8	34
120 A 12%	52	30	20	4
270 A 12%	53	30	23	0

At all residence times studied (i.e., 4.3 s, 2.1 s, and 1.1 s), the 40 Å 12% STC performed the best with respect to methanol removal and mineralization, achieving about 88% mineralization at a residence time of 4.3 seconds. Since the residence time of the gas through the reactor was varied by changing the flow rate through the packed bed and the influent methanol concentration in the gas remained constant, the mass of methanol entering the packed bed per time increased as the flow rate was increased (i.e., as the residence time was decreased). At the various residence times, the influent methanol loading was 0.03, 0.06, and 0.12 mg of methanol per minute (as shown in Table 15). The rate of methanol mineralization for the 40 Å 12% STC was 0.026 mg/min at RT = 4.3 s, 0.037 mg/min at RT = 2.1 s, and 0.041 mg/min for RT = 1.1 s. Therefore, although the effluent methanol concentration increased with decreasing residence time, the methanol mineralization rate (expressed in mass of methanol per time) increased with decreasing residence time. Thus, the photonic efficiency of the reactor (mass of methanol mineralized per photon generated by the UV light) increased as the residence time through the reactor decreased since the number of photons generated by the UV lamp was constant for all residence times studied.

Table 15. Rate of Methanol Mineralization by the 40 Å 12% STC at Various Residence Times in the Presence of UVA Light

Residence Time (s)	Influent Methanol Loading Rate (mg/min)	Rate of Methanol Mineralization (mg/min)
4.3	0.03	0.026
2.1	0.06	0.037
1.1	0.12	0.041

Effect of Titanium Dioxide Loading on Methanol Removal

STC with an average pore size of about 40 Å were tested with various titania loadings (i.e. 1%, 4%, 12%, 36%, 60%) in a reactor system using a UVA lamp, an initial methanol concentration of 50 ppm_v, relative humidity greater than 90%, and residence time of 4.3 s. As shown in Figure 46, all of the STC pellets, regardless of titania loading, removed similar amounts of methanol (ca. 90%) at steady state. The time to initial breakthrough (i.e., time when the effluent methanol concentration was detectable) was similar for STC pellets loaded with 1-36% titania. Initial breakthrough for the pellets loaded with 60% titania occurred immediately due to the lower specific surface area of the composite (297 m^2/g) compared to that of the STC with lower titania loadings (e.g., 616 m^2/g for the 40 Å 4% STC). Note that there is an inverse relationship between titania loading and the specific surface area of the composite as shown in Table 11.

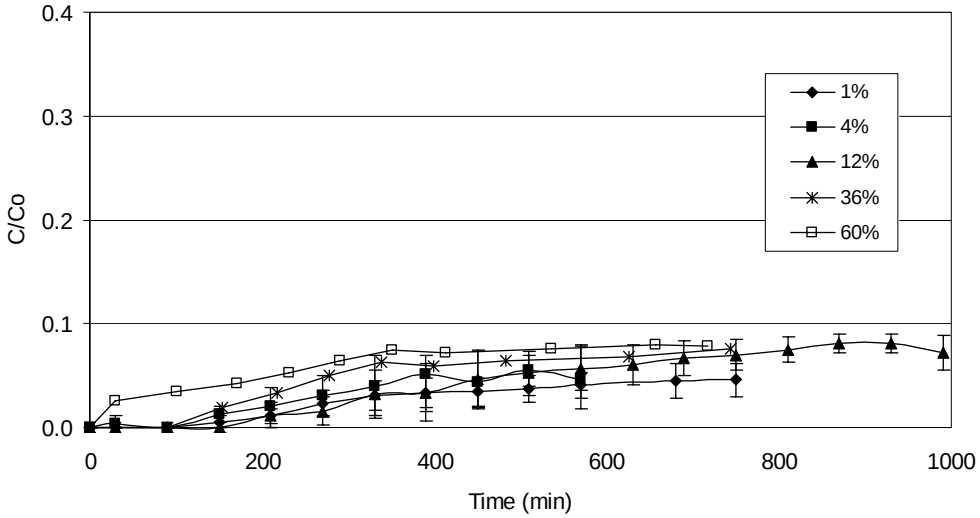

Figure 46. Effect of Titania Loading in 40 Å STC on Methanol Removal in the Presence of UVA Light

Titania loading did effect effluent formaldehyde concentration, as shown in Figure 47. This graph shows that a 4% titania loading is optimum, resulting in effluent formaldehyde concentrations below 1 ppm_v. An increase in titania loading results in increased formaldehyde production due to the decrease in specific surface area of the pellets and the formation of titania agglomerates. The 1% titania loading likely resulted in higher formaldehyde concentrations because there was an insufficient quantity of titania. Thus, a lack of hydroxyl radicals resulted in increased formaldehyde concentrations. Since methanol can be oxidized directly by electron holes or indirectly via hydroxyl radical formation, the decrease in titania loading from 4% to 1% was not sufficient to reduce methanol removal.

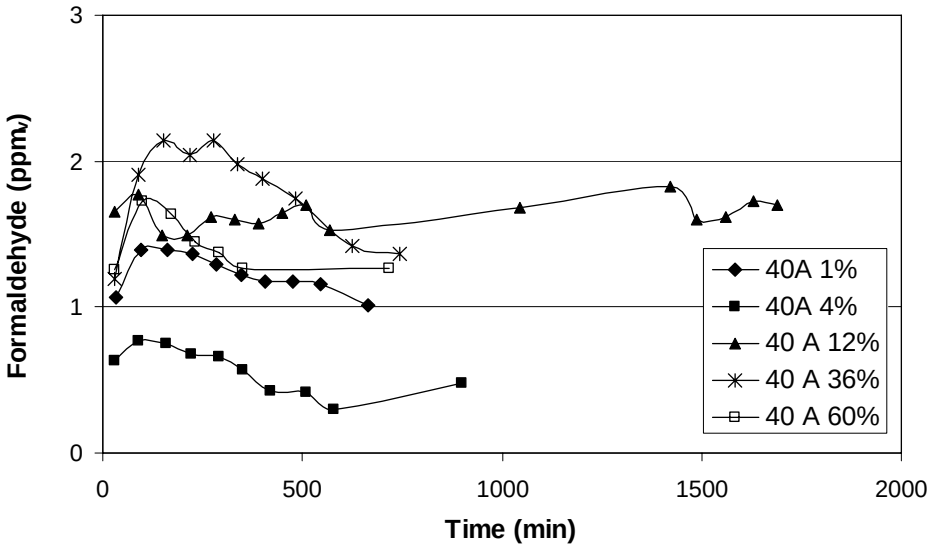

Figure 47. Effect of Titania Loading in 40 Å STC on Effluent Formaldehyde Concentration

The surface area of the 40 Å 60% STC (297 m^2/g) is similar to that of the 120 Å 12% STC (274 m^2/g). However, the methanol mineralization rate for the 40 Å 60% STC (which was about 88% at steady state) was greater than that of the 120 Å 12% STC (which was about 72% at steady state). This indicates that the pore size of the STC is more important in determining methanol mineralization efficiency that the surface area. This may be because the smaller surface area results in restrained desorption of oxidation byproducts (i.e., formaldehyde) resulting in more complete oxidation.

Effect of UV Wavelength on Methanol Removal

The effect of UV wavelength on methanol oxidation was evaluated by using UVA and UVC lamps. STC pellets with a 40 Å pore size were used for each test, which had an influent methanol concentration of 50 ppm_v and residence time of 4.3 seconds (which is similar to the previous tests described above). The initial methanol breakthrough time (i.e., the time when the effluent concentration is measurable) was about 308 ± 28 minutes when the titania was activated using the UVC lamp. This time was greater than the initial breakthrough time (135 ± 25 minutes) when the UVA lamp was used. The UVA and UVC lamps performed similarly with respect to methanol removal when the reactor reached steady state, resulting in the oxidation of about 90% of the influent methanol (data not shown). Figure 48 shows that the use of the UVC lamp resulted in lower effluent formaldehyde concentrations (i.e., more complete oxidation) compared to the UVA lamp.

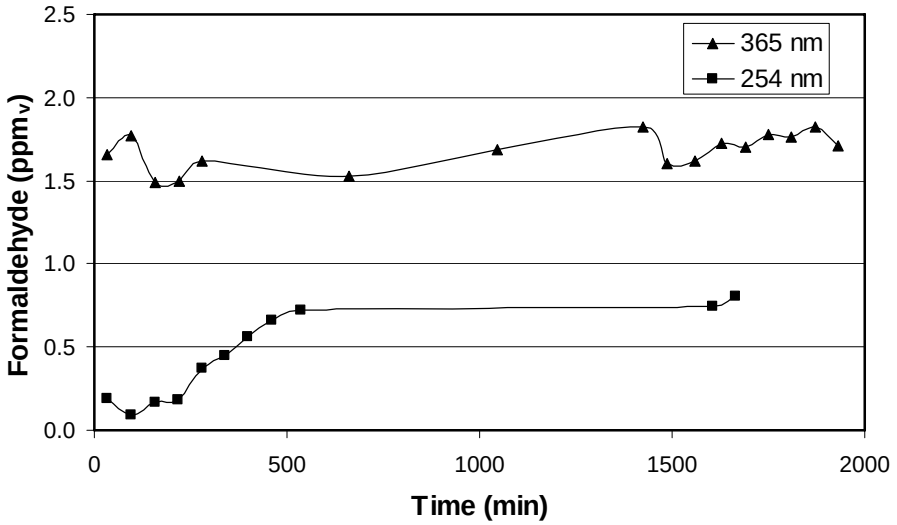

Figure 48. Effect of UV wavelength on effluent formaldehyde concentration using 40 Å STC pellets (Co Methanol = 50 ppmv, RT = 4.3 seconds)

Table 16 shows a summary of the influent methanol concentration and effluent methanol and formaldehyde concentration at steady state. In addition, the percentage of influent methanol that was mineralized is shown. In the presence of UVA light, 88% of the methanol was mineralized. The use of UVC light resulted in 90% removal, which increased the efficiency of mineralization of the STC pellets by 2%.

Table 16. Effect of UV Wavelength on Methanol Removal at Steady State

STC	Influent Methanol (ppm_v)	Effluent Methanol (ppm_v)	Effluent Formaldehyde (ppm_v)	% Mineralized
40 A 12% UVC	50	4.5	0.7	90
40 A 12% UVA	50	4.5	1.7	88

It is likely that the UVC lamp enhanced reactor performance because the photocatalytic reaction rate is proportional to the rate of generation of electrons and holes on the titania surface, which is in turn proportional to the photon flux. The intensity of the UVA and UVC lamps at the outside of the quartz tube, which housed the lamp inside the reactor, was measured to be 3.5 mW/cm^2 and 9 mW/cm^2, respectively. Since both the UVA and UVC lamps create photons with energy larger than the band gap energy of titania, the photons generated from both lamps have sufficient energy for photocatalysis to occur. Since the photon flux from the UVC lamp is greater than that from the UVA lamp, the UVC lamp should result in an increase in the oxidation rate of organic compounds. It is likely that the increased intensity of the UVC lamp resulted in an increase in the intensity of UV light penetrating through the interstitial space between STC pellets and reaching the outer layer of pellets in the reactor, thus resulting in more complete oxidation of the byproducts.

Effect of Influent Methanol Concentration

In order to further challenge the performance of the STC pellets and to potentially accelerate the impact that UV wavelength has on methanol oxidation, the influent methanol concentration was increased to 250 ppm_v. The influent relative humidity was about 85% and residence time was 4.3 s. Figure 49 shows that, in the presence UVA light, initial methanol breakthrough occurred after approximately 90 minutes. After about 700 minutes, steady state was achieved for the duration of the experiment and the system removed 64-69% of the influent methanol. When the STC pellets were irradiated with the UVC lamp and exposed to an influent methanol concentration of 250 ppm_v, the initial breakthrough time was about 90 minutes (similar to that using the UVA lamp) and steady state removal, which occurred after about 500 minutes, was about 75%. Thus, the increase in light intensity as a result of using the UVC lamp resulted in an increase in methanol oxidation rate for both the 50 ppm_v and 250 ppm_v influent concentrations. When the influent methanol concentration was 250 ppm_v, effluent formaldehyde concentrations from pellets exposed to the UVA and UVC lamp were similar. As shown in Figure 50, the formaldehyde concentration rose steadily over time and did not reach steady state during the experiment. Since methanol and water compete for adsorption sites on the STC surface and methanol can be oxidized directly via the electron hole, accumulation of methanol on the surface would result in a decrease in the concentration of hydroxyl radicals over time. Thus, at the higher methanol concentration, the concentration of hydroxyl radicals available for the oxidation of formaldehyde decreased over time causing an increase in the effluent concentration. The continuous increase in effluent formaldehyde concentration was a result of the accumulation of methanol on the STC surface over time.

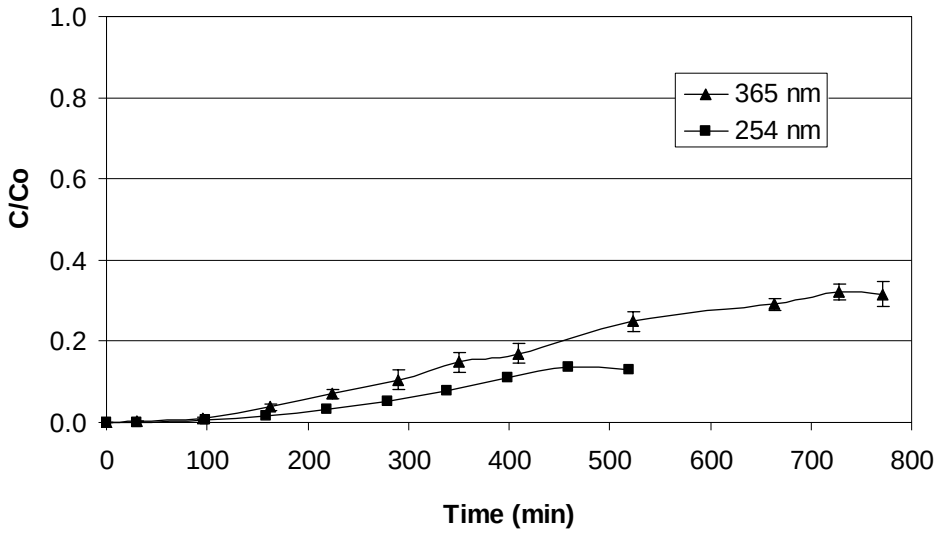

Figure 49. Methanol Removal by 40 Å 12% STC in the Presence of UVA (365 nm) and UVC (254 nm) light when Co= 250 ppm_v

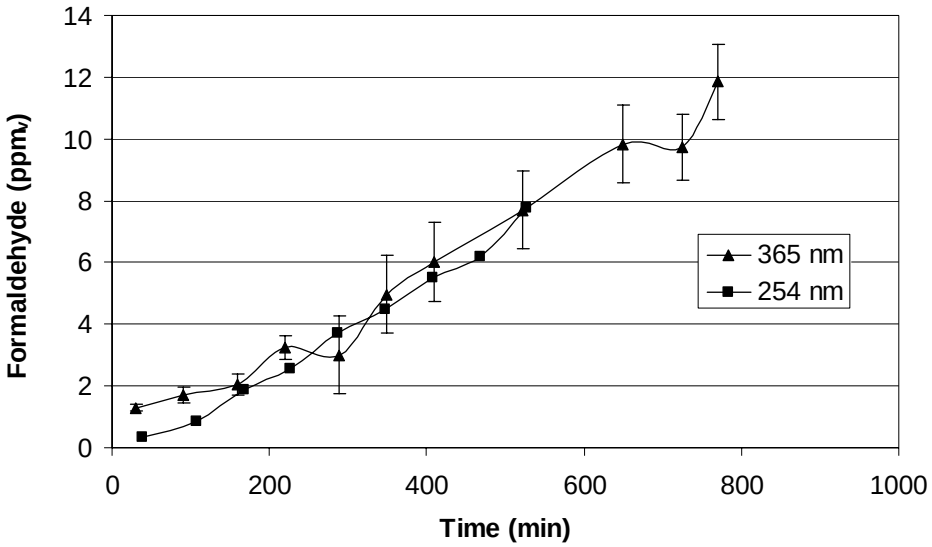

Figure 50. Effluent Formaldehyde Concentration for 40 Å 12% STC in the Presence of UVA (365 nm) and UVC (254 nm) light when Co= 250 ppm_v

Modification of STC Synthesis Procedure

The STC is synthesized using a sol-gel method with TEOS as the silica-gel precursor. A *sol* is a colloidal suspension of particles, while the term *gel* refers to the semi-rigid material formed when the colloidal particles link together in a liquid to form a network. The STC forms through a series of hydrolysis and condensation reactions. Generally speaking, hydrolysis replaces the alkoxide group of the TEOS with a hydrogen ion, while condensation produces siloxane bonding (Si-O-Si) with the products of the reaction being water or alcohol. As the number of siloxane bonds (Si-O-Si) increases, the individual molecules join together to create a silica network. After condensation reactions begin, gelation can occur. Gelation is considered the growth period for the colloidal particles, which grow by polymerization or aggregation. Eventually, as the last links are made, the viscosity of the sol increases to the point where the sol becomes a semi-rigid gel that consists of a network of pores filled with liquid. After gelation occurs, the STC is allowed to age so that terminal silanol groups (Si-OH) re-orient themselves and react with each other to form additional network linkages (Si-O-Si). This results in shrinkage of the gel and forces the removal of some liquid from the pores. The drying step involves the removal of the solvent from within the pores of the gel.

The synthesis protocol of the STC used thus far involved an aging process of four days (two days at room temperature and two days at 65 °C). By reducing this aging time, a higher production capacity can be realized and energy consumption associated with aging the pellets at 65 °C can be reduced. To evaluate if a reduction in aging time could be achieved without adversely affecting the properties of the STC, 40 Å 12% STC were synthesized and aged for various times (as shown in Table 19). It should be noted that the STC pellets did not shrink enough to be easily removed from the molds when aged less than one day. The STC were tested for BET surface area, total pore volume, average pore size, and methanol destruction efficiency. As shown in Table 17, the various aging times did not have a significant effect on the physical properties of the STC.

Table 17. The Effect of Various Aging Times on STC Properties

Room Temp (days)	65°C (days)	SSA (m^2/g)	Pore V (cc/g)	Pore Size (Å)
0	1	477	0.61	51
1	1	536	0.62	46
0	2	503	0.52	41
0	3	587	0.59	44
2	2	532 ± 43	0.60 ± 0.06	46 ± 4

The methanol destruction ability of STC aged for the various times was tested by passing methanol-laden air (50 ppm_v) through the fixed-bed reactor in the presence of UVA light. As seen in Figure 51, the destruction efficiency of each STC was similar. Therefore, using shorter aging times is feasible for full-scale production.

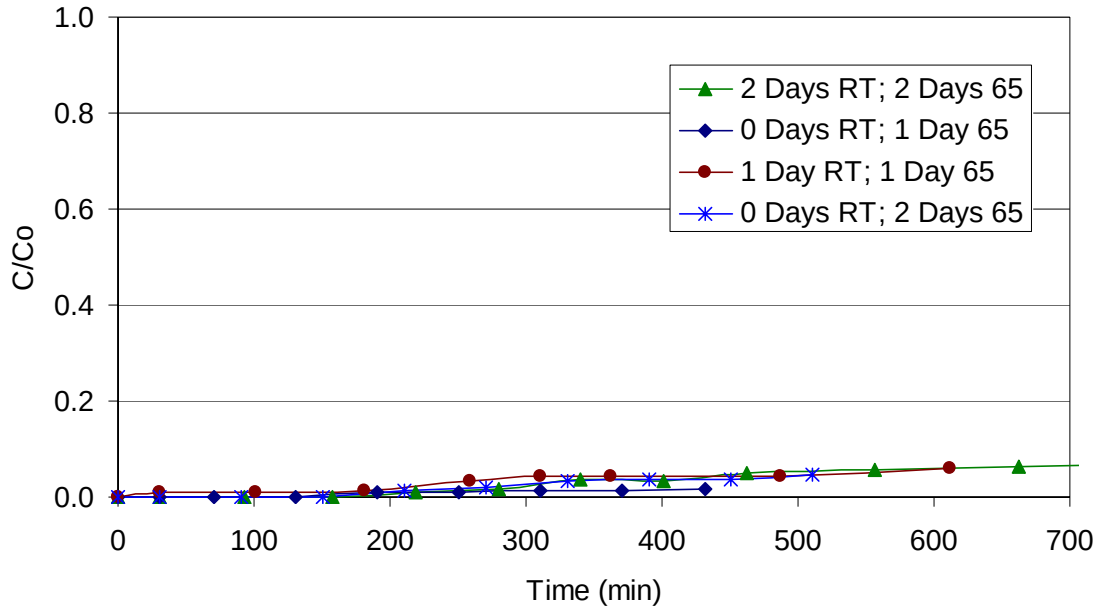

Figure 51. Destruction Efficiency of Silica Gels Aged at Various Times

COMPARISON OF CATALYST SUPPORT ON METHANOL REMOVAL

The effect of catalyst support on methanol removal was studied to compare adsorbent supports (i.e., silica gel and activated carbon) and non-porous supports (i.e., glass beads). The goal of this study was to determine if the adsorbent catalyst support provided a benefit with respect to photocatalytic oxidation efficiency compared to a thin film, which was in this case coated on glass beads. The incorporation of an adsorbent may improve mass transfer and the efficiency of the photocatalyst by allowing the contaminant to be concentrated near the photocatalyst surface, thereby increasing the rate of photocatalytic oxidation. In addition, intermediate byproducts may be retained for further oxidation thereby preventing the release of potentially hazardous contaminants into the air. Preliminary scale-up was performed at the bench-scale by increasing the annulus size of the reactor from 8 mm to 25 mm in order to evaluate the efficacy of these materials for full-scale applications.

Materials and Methods

TiO_2-Coated Activated Carbon (TiO_2/AC). Titania-coated granular activated carbon (AC) was synthesized by coating BioNuchar120 (MeadWestvaco) with Degussa P25 titanium dioxide via a boil deposition method. A titania slurry was made by adding 3 g of Degussa P25 titania to 200 mL of DI water. Next, 30 g of AC were added to the slurry and heated on a hot plate until all of the water evaporated, leaving the titania coated onto the outer surface of the AC. The actual quantity of titania deposited on the AC was determined by taking the difference of the measured ash content of the as-received and titania-coated AC. To determine the ash content of an AC sample, about 1 g of dry material was heated to 550 deg. C for 24 hours to remove the carbonaceous portion of the AC. The measured titania loading on the AC was approximately 5 ± 0.4 $\%_{wt}$.

Titania-Coated Glass Beads. Solid glass beads (5 mm diameter) were coated with a titania slurry (20$\%_{wt}$ Degussa P25 titania dispersed in water) and then dried at 110 °C. After drying, excess titania was separated from the titania-coated glass beads by gently shaking the beads on a sieve with 4 mm openings. The mass of the beads were measured before and after the titania coating was applied. The resulting mass of titania on each glass bead was 0.925 mg, which equates to 47 g of titania per m^2 of glass beads. The BET surface area of the titania (as measured by a Quantachrome NOVA 2200 e, Boynton Beach, FL) was approximately 50 m^2/g.

Characterization of Titania-Doped Adsorbents. The STC and titania-coated AC were analyzed for BET surface area and total pore volume using a Quantachrome NOVA 2200e (Boynton Beach, FL). The results of this BET analysis are shown in Table 18.

Table 18. BET Surface area and average pore size of titania-doped sorbents

Material	Surface Area (m^2/g)	Pore Volume (cc/g)
STC	616	0.79
TiO_2/AC	1424	1.06

Packed Bed Reactor System. The adsorption and photocatalytic oxidation of methanol was tested using bench-scale annular reactors with annulus sizes of 8 mm and 25 mm. The titania-coated material was packed in the annulus of the reactor, which contained an eight-watt UVC bulb (254 nm peak wavelength) surrounded by a 25 mm OD quartz tube. Compressed air containing 1000 ppm_v of methanol was diluted with air to obtain an influent gas stream containing 50 ppm_v of methanol and a relative humidity of about 95%. The reactor set-up was shown previously in Figure 37. For all the studies, the residence time (or empty bed contact time) was about 4.3 seconds and the face velocity was 1.7 ft/min. Initial studies performed with an empty reactor showed no photolysis of methanol in the presence of UVC light. Similarly, adsorption of methanol to the reactor and its appurtenances was negligible.

Methanol Adsorption and Oxidation

The adsorption breakthrough profiles for the TiO_2-doped materials are shown in Figure 52. Although the TiO_2/AC broke through faster than the STC, its adsorption capacity (1.9 mg/g) was greater than that of the STC (1.2 mg/g) due to the difference in bulk density between the two materials (i.e., 0.26 g/mL for AC and 0.53 g/mL for STC). The TiO_2-coated glass beads had very little adsorption capacity due to the low surface area of the titania (50 m^2/g).

In the presence of UV, the methanol removal efficiency of the materials decreased to about 95% for both the STC and TiO_2/AC. Initially, the breakthrough curves for the STC and TiO_2/AC in the presence of UV light followed those in the dark. After approximately 250 minutes for TiO_2/AC and 400 minutes for STC, the systems reached a pseudo-steady state (i.e. the effluent concentration is relatively constant). Before the systems reached a steady state, the rate of oxidation was less than the rate of adsorption, otherwise initial breakthrough would be extended in the presence of UV. The titania-coated glass beads immediately achieved steady-state removal efficiency, which was between 80 and 90%.

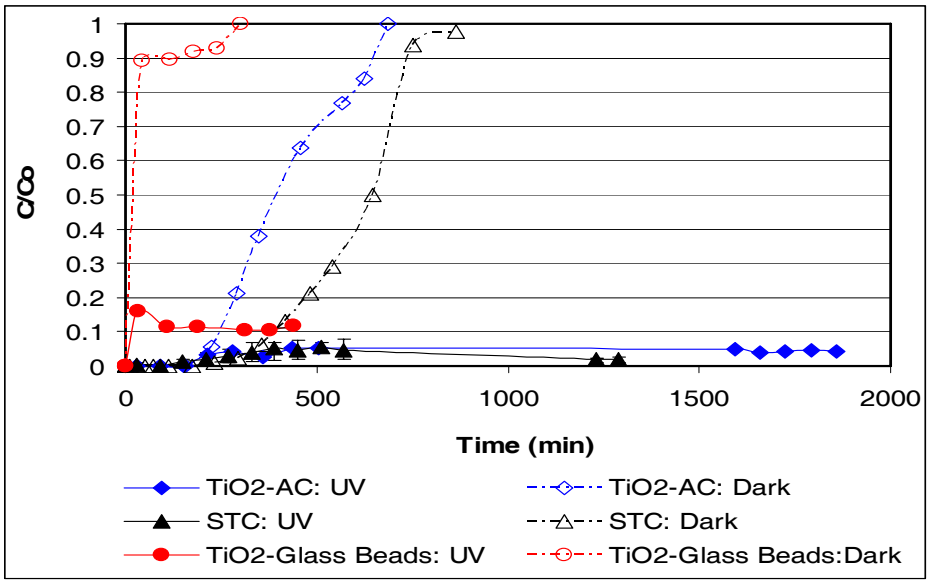

Figure 52. Normalized effluent methanol concentration for titania-doped materials used in the dark and with UV light

As shown in Figure 53, the high humidity environment resulted in an increase in effluent formaldehyde concentration for the titania-coated glass beads (about 1 ppm_v) and STC (0.4 to 0.7 ppm_v). However, the increase in humidity resulted in decreased formaldehyde production in the TiO_2/AC system (i.e., about 0.8 ppm_v at steady state). Thus, in the TiO_2/AC system, the water vapor inhibited methanol removal due to competitive adsorption; however, increased water vapor concentration resulted in more complete oxidation. This indicates that the presence of water vapor resulted in: (1) a difference in methanol oxidation mechanism (e.g., direct hole oxidation of methanol in the low humidity environment and indirect oxidation by hydroxyl radicals in the high humidity experiment) and/or (2) an inhibition of the diffusion of formaldehyde into the air stream, thus allowing time for further oxidation.

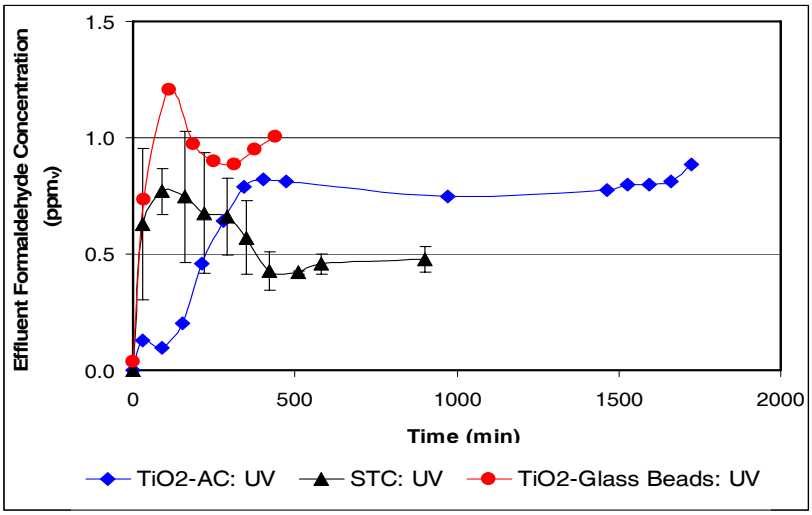

Figure 53. Intermediate byproduct (formaldehyde) formation by titania-coated materials

Laboratory Reactor Scale-up using Titania-doped Materials

The titania-doped materials were tested in a larger annulus reactor (25 mm annulus) in order to evaluate the titania-doped materials for potential use in full-scale applications. The titania-doped sorbents were tested for methanol removal in a high humidity environment. The flow rate was adjusted such that the mass transfer characteristics (i.e., residence time and face velocity) were the same as those from the smaller annulus studies. As shown in Figure 54, the titania-coated glass beads achieved 40% methanol removal for the duration of the study. The titania-coated carbon and STC initially followed the same trend

as their respective adsorption breakthrough profiles; thus, the breakthrough profile for the STC was shallower than that of the TiO_2/AC, resulting in higher removal rates for the STC between about 100 and 1300 minutes. Both titania-coated adsorbents achieved about 50% methanol removal at steady state.

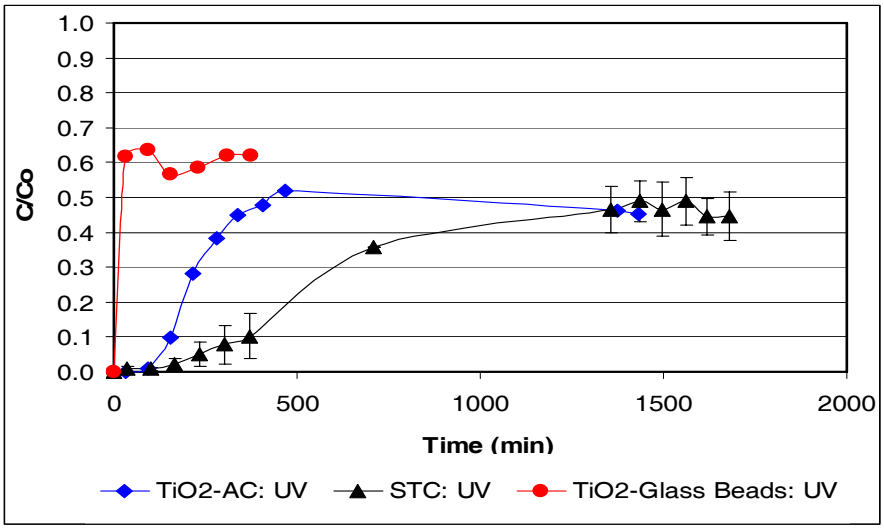

Figure 54. Normalized effluent methanol concentration for titania-doped materials used in a large annulus reactor (25 mm) with UVC light

As shown in Figure 55, the effluent formaldehyde concentration of the STC and titania-coated carbon was similar and increased steadily until reaching a steady state concentration of between 1.5 and 2.0 ppm_v. The titania-coated glass beads achieved steady state production of formaldehyde at about 1.6 ppm_v. The decrease in methanol oxidation efficiency in the large annulus reactor is likely a result of inadequate UV light exposure within the packed bed. The titania-doped adsorbents performed better than the titania-coated glass beads, indicating that adsorption of methanol onto a high surface area catalyst support results in higher oxidation rates. However, no difference in performance was discerned between the silica-gel, which is transparent, and AC, which is opaque, when used as the catalyst support.

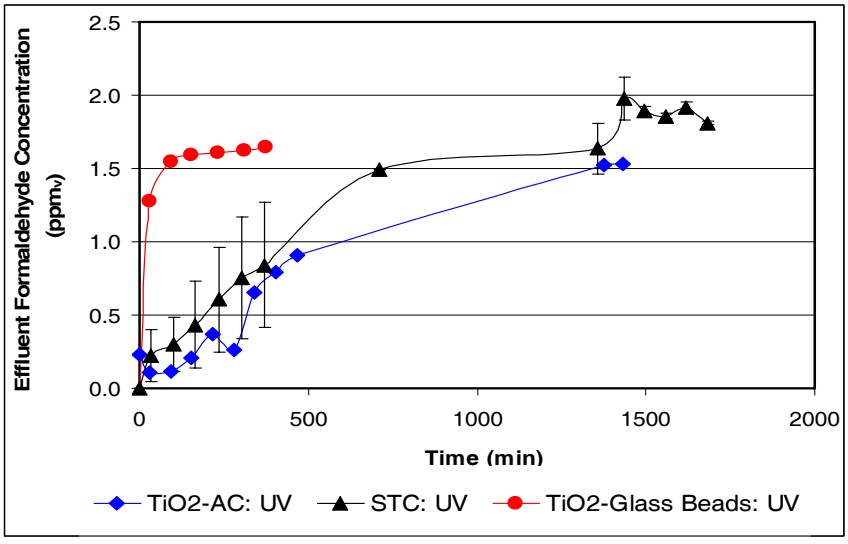

Figure 55. Intermediate byproduct (formaldehyde) formation by titania-coated materials used in a large annulus reactor

Conclusions. STC and titania-coated activated carbon were compared to titania-coated glass beads for the removal of methanol. When used in the small annulus reactor in the presence of UV light, the effluent methanol concentration for the STC and TiO_2/AC initially followed the adsorption breakthrough profile until a steady state removal of 95% was reached. When tested in the larger annulus reactor, the STC and titania-coated carbon performed similarly, achieving 50% methanol removal compared to the titania-coated glass beads, which achieved 40% methanol removal. Thus, using an adsorbent material as a catalyst support is beneficial; however, the use of silica gel, which is transparent, versus AC, which is opaque, did not result in a difference in the photocatalytic oxidation rate in the larger annulus reactor.

PILOT STUDIES

Photocatalytic Fluidized Bed Reactor

In response to laboratory results achieved at the University of Florida to develop an air pollution control system to remove VOCs (volatile organic compounds) and HAPs (hazardous air pollutants) in emissions from pulp, paper and paperboard mills, and solid wood products facilities a prototype Photocatalytic Fluidized Bed Reactor (PFBR) was designed and developed by MicroEnergy Systems, Inc. (MSI), Oakland, Maryland.

The objective was to demonstrate the efficiency of methanol recovery with activated carbon coated with TiO_2 (TiO_2/AC) in the presence of UV light. Methanol was chosen as the model pollutant due to its dominance in the gas stream from wood processing.

General Configuration. The PFBR was designed and fabricated for the evaluation of the photocatalytic activity of the TiO_2/AC. The reactor design allowed the change of flow rate, methanol concentration, humidity, and temperature to quantify their effects.

The PFBR is illustrated in Figure 56 in relation to other overall system components, including: (a). Reaction Chamber, which contains TiO_2/AC, (b). Baghouse filter, (c). Fluidizing fan, and (d). Carbon transfer and ancillary support systems. Depending on anticipated host site requirements, it was assumed that a reasonable commercial size for a PFBR was one that probably contains between 1,000 and 2,000 lb of TiO_2/AC. For orientation, relative dimensions of the prototype PFBR shown in Figure 56 are in scale compared to a 2,000 lb-carbon Reaction Chamber and a suitable sized baghouse. It was assumed that the actual size for the PFBR Reaction Chamber and baghouse would be finalized following development efforts for the PFBR and specific siting conditions for a host demonstration location.

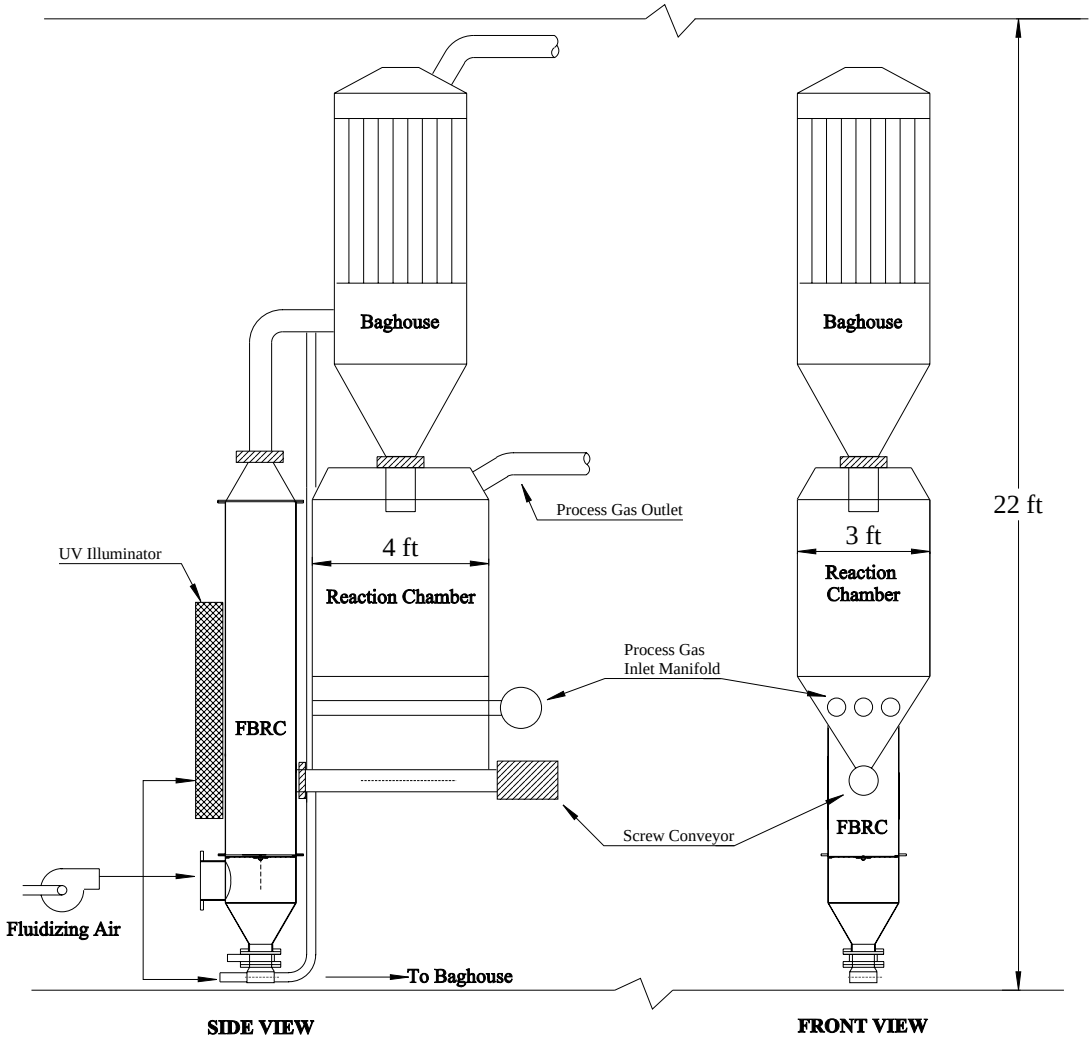

Figure 56. Conceptual Plan – Photocatalytic Fluidized Bed Reactor (PFBR)

Operation of the system was anticipated to include: (1). MeOH laden gas stream continuously passing through Reaction Chamber, (2). Approximately five to ten percent of the TiO_2/AC transferred each hour (e.g., by screw conveyor) into the PFBR for regeneration, (3). Fluidizing air introduced into the PFBR while ultraviolet (UV) lamps were simultaneously energized for approximately 10 to 20 minutes to effect regeneration of the carbon, (4). Upon completion of regeneration, the PFBR plenum bed / air diffuser component would be rotated vertically from its normal horizontal position to allow the carbon to drop into the chamber bottom; thus, facilitating its exit, (6). Fluidizing air utilized as a medium to transport the TiO_2/AC from the PFBR bottom, up into the baghouse; whereupon, (7). It would be reintroduced into the Reaction Chamber through a rotary valve.

Deign Criteria – Circular Reactor Crossection. MSI design criteria was based on information obtained from three process streams located at two different paper mills, including the following:

	Mill No.1	Mill No.1	Mill No.2
Waste gas flow (acfm):	115	750	2,500
MeOH concentration (ppm_v):	8,300	8,300	190

Preliminary sizing for the prototype PFBR was based on “averaging” this information to derive a “reasonably” sized chamber, assuming: (a). The adsorption rate of MeOH on the TiO_2- coated activated carbon could vary from 0.1 –to- 0.4 lb-MeOH per lb-carbon, and (b). Five to 10 percent of the carbon contained in the Carbon Reaction Chamber would be reactivated each hour.

Table 19 indicates results of these assumptions, which show that a PFBR with a capacity of approximately 100 lbs-carbon is a "reasonable-average" for prototype demonstration and potential commercial purposes.

Table 19. TiO2-COATED ACTIVATED CARBON REACTION CHAMBER & PHOTOCATALYTIC FLUIDIZED BED REACTOR (PFBR) - PRELIMINARY SIZING CRITERIA						Average Carbon in PFBR (lb)	
			Mill No. 1	Mill No. 1	Mill No. 2	Low	High
1	Process gas flow	ACFM	115	750	2,500		
2	MeOH Influent concentration	ppm	8,300	8,300	190		
3	MeOH loading rate	pph	4.30	28.01	2.14		
4	Carbon Adsorption rate	MeOH / lb-carbon	0.10	0.10	0.10		
5	Carbon consumption rate	pph	43	280	21		
6	Assumed Carbon Reaction Chamber capacity @ 10 cycles per 11 hours	lb	472	3,081	235		
7	Carbon in PFBR @ 10% of total	lb	47	308	24	24	308
8	Carbon in PFBR @ 5% of total	lb	2	154	1	1	154
9	Carbon adsorption rate	MeOH / lb-carbon	0.25	0.25	0.25		
10	Carbon consumption rate	pph	17	112	9		
11	Assumed carbon reaction chamber capacity @ 10 cycles per 11 hours	lb	189	1,233	94		
12	Carbon in PFBR @ 10% of total	lb	19	123	9	9	123
13	Carbon Adsorption rate	MeOH / lb-carbon	0.40	0.40	0.40		
14	Carbon consumption rate	pph	11	70	5		
15	Assumed carbon reaction chamber capacity @ 10 cycles per 11 hours	lb	118	770	59		
16	Carbon in PFBR @ 10% of total	lb	12	77	6	6	77
17				Average		10	166
18				Average of Average		88	

It was assumed that between 12 –to- 16 ultraviolet, 40 –to- 80 watt, UV lamps having standard lengths of four feet, with a peak wavelength of 365 nanometer (nm), would be utilized. These lamps would be positioned so as to circumscribe completely around the exterior sides of the PFBR chamber "looking" through a transparent housing section. With these criteria, it was assumed that an expanded bed height during fluidization of six feet would be ideal. Adding a two-foot freeboard, it was also assumed that the overall height of the PFBR chamber would ideally be eight feet.

To determine an optimal cross-section, an iterative design and test procedure was completed, which factored in the following parameters: (a). Reasonable slumped bed height based on specific volume of carbon (e.g., tests assumed virgin carbon containing 33 percent moisture, which yielded a density of 40 lbs / ft^3), (b). Desired expanded bed height of six feet, (c). Reasonable fluidizing airflow and acceptable pressure drop across the plenum air diffusers, and (d). Geometry of a suitable number of air diffusers, with properly sized air holes, to effect the desired expanded bed height.

A series of iterative air flow tests that included variations in the number of diffusers and air hole diameters were conducted, which eventually resulted in a reasonable synergy of air flow, pressure drop and expanded bed height, yielding the following criteria:

Chamber height: 8 ft.
Chamber diameter (I.D.) 19.1 inches
Number of plenum air diffusion nozzles: 31, each with four 3/8" diameter air holes

Table 20 presents a summary of key test data obtained by MSI at its research and development center in Oakland, Maryland, indicating: (a). Airflow rates (e.g., measured by pitot tube traverses on the air transport duct between fluidizing fan and PFBR plenum) to achieve a superficial vertical velocity in the PFBR chamber ranging from about five to 10 ft/second (e.g., normal range in the fluidized bed combustion industry), (b). Corresponding pressure drops (e.g., both theoretical and measured) across the plenum air diffusers, with no carbon in the bed, and (c). Similar data with 100 lbs of carbon in the bed.

Table 20. PHOTOCATALITIC FLUIDIZED BED REACTION CHAMBER (PFBR) - AIR FLOW AND PRESSURE LOSS CRITERIA								
			Calibrate Air Diffusers				Conditions During Fluidization	
1	Quantity of carbon in PFBR	lb	0	0	0		100	100
2	Measured air flow into PFBR plenum	scfm	482	770	1077		508	932
3	Measured pressure drop thru PFBR air diffusers	"w.g.	3.80	10.20	19.40		11.0	14.6
4	Superficial vertical velocity in PFBR chamber	fps	4.0	6.4	9.0		5.0	7.5
5	Air flow thru each diffuser hole	scfm	3.89	6.21	8.69		2.70	4.96
6	Air velocity thru each diffuser hole	fpm	5,068	8,096	11,321		5,098	9,354
7	Theoretic pressure drop thru PFBR air diffusers (Cd = 0.62)	"w.g.	3.79	9.84	19.71		--	--
8	Measured carbon bed height - slumped condition	in	--	--	--		14	14
9	Measured carbon bed height - fluidized condition	in	--	--	--		30	72

For reference orientation, the following photos provide visual images of the prototype PFBR.

Photo No. 1: Side view of PFBR.
Photo No. 2: Close-up of PFBR bottom discharge section.
Photo No. 3: Fluidizing air fan.
Photo No. 4: PFBR plenum with diffusers in normal horizontal bed position.
Photo No. 5: PFBR plenum with diffusers rotated in vertical position for carbon removal.
Photo No. 6: Air duct between fan and PFBR plenum, showing pitot tube airflow monitoring station.

Photo No. 1. PFBR Chamber

Photo No. 2. PFBR Discharge Section

Photo No. 3. Fluidizing Air Fan

Photo No. 4. PFBR Plenum – Horizontal Position

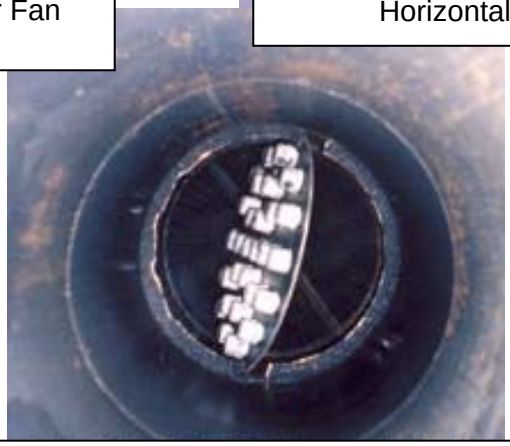

Photo No. 5. PFBR Plenum – Vertical Position

Photo No. 6. Fluidizing Airflow Monitoring Station

Design Criteria – Square Reactor Crossection. The airflow and pressure loss criteria tests provided valuable information regarding airflow rates vis-à-vis, carbon quantities, bed height, and other design parameters. However, it became problematic to procure suitable UV bulbs with sufficient radiation capacity to accommodate the program objectives. Therefore, it was decided to modify the cross-sectional area from circular to square, which allowed procurement of UV bulbs in the necessary capacity range. Installation included a total of 16 – four-foot long 40-watt UV bulbs mounted on each side, of the four-sided, PFBR chamber.

Two-step high capacity transformers allowed UV illumination at normal ("NORMAL") intensity at 40 watts and high ("HIGH") intensity at about 70 –to- 75 watts each.

Figure 57 indicates the orientation of the new chamber. Sidewalls of the chamber adjacent to the UV bulb assembly were fabricated with UVT Acrylic Polycast material, which is a clear Lucite type material that allows about 94 percent UV radiation transmission at 365 nanometer (nm) wavelength. The backside of each UV bulb assembly was lined with Alzack sheet material, which is a highly UV reflective material.

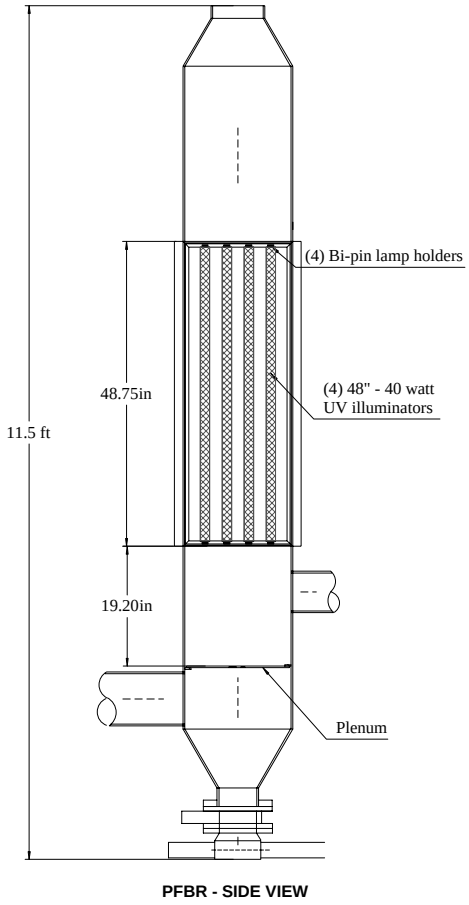

Figure 57. Sectional Side View of PFBR Showing Orientation of UV Bulbs

The following provides orientation of the UV chamber.

- Photo No. 7 shows a four (4) UV bulb array (each bulb is four (4) feet long and rated at 40 watts of <u>total</u> UV radiation). There were four (4) of these arrays (i.e., a total of 16 bulbs) which were mounted on each sidewall of the UV Illuminator Chamber.

- Photo No. 8 shows an interior view of the UV Illuminator Chamber (i.e., one UV array was removed to allow photographic visual access).

Photo No. 7. UV Bulb Array

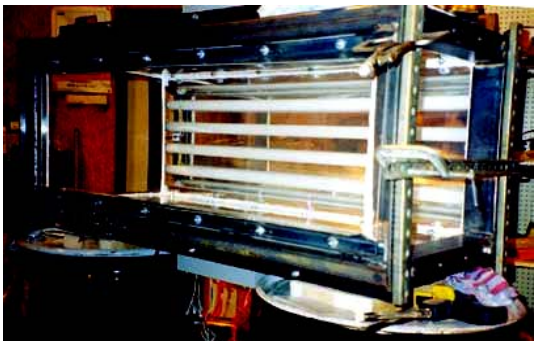

Photo No. 8. UV Section Chamber of PFBR

The following provides visual orientation of the UV Section of the PFBR:

- Photo No. 9: Side view of reactor housing.
- Photo No. 10: Rotatable plenum diffuser plate in closed position.
- Photo No. 11: Rotatable plenum diffuser plate in open position.
- Photo No. 12: UV Section close-up side view. Small silver box in middle is a two-stage transformer that allows two levels of power input to each UV bulb, referred to as: (a). NORMAL, and (b). HIGH. Note the UV radiation (bluish tint) "spilling" out the top and bottom of the reactor sidewall.
- Photo No. 13: UV Section front-view, including Dr. Mazyck conducting his inspection.
- Photo No. 14: MSI FD fan connected to inlet end of air transport pipe leading to reactor.

Photo No. 9. Reactor Section- Side View

Photo No. 10. Rotatable Plenum Diffsuer Plate - Closed

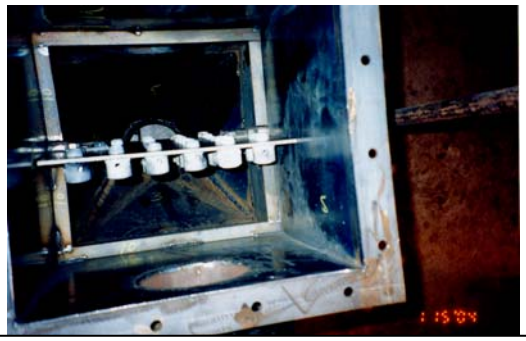

Photo No. 11. Rotatable Plenum Diffsuer Plate - Open

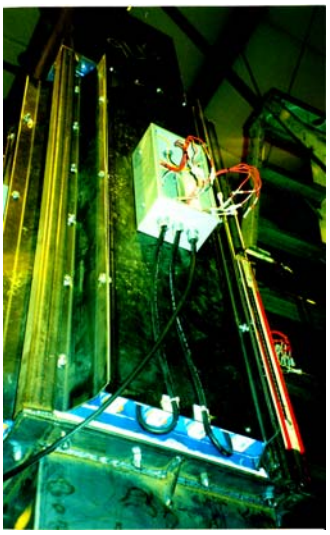

Photo No. 12. UV Section- Side View - Showing Two-Stage Transformer

Photo No. 13. PFBR – Front View – Also Dr. Mazyck Conducting Inspection

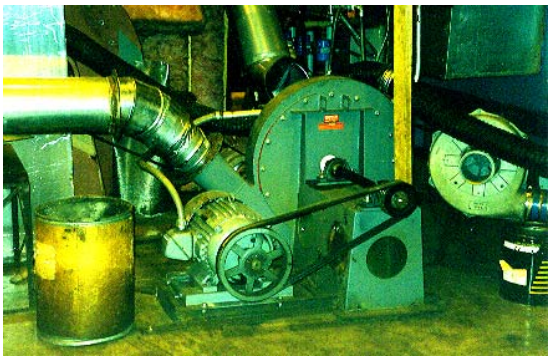

Photo No. 14. MSI FD Fan Connected to Inlet Air Transport Pipe Leading to Reactor

Airflow and UV Performance Tests. Upon completion of fabrication and installation of the PFBR and its system components, an iterative series of airflow tests were conducted with and without TiO_2/AC in the chamber.

The system was interconnected with air inlet piping and MSI's FD fan, equipped with variable speed drive. The purpose was to: (a). correlate air flows vs. pressure losses through its entire system, and (b).

optimize mass air flow that resulted in a “top” carbon bed height that reached the approximate elevation of the “upper-window-frame” of the chamber.

Following the airflow tests, a series of data acquisition performance tests were conducted, including: (a) Fine tuning of airflow patterns within the new chamber, (b). Measurement and “mapping” of UV radiation intensities at various locations within the PFBR chamber operating with varying number of UV bulbs illuminated at normal and high intensities, and (c). Preliminary reactivation testing of methanol laden TiO_2/AC.

In order to determine and calibrate the portion of UV radiation emitted by each bulb in the 365 nm range, data was gathered utilizing a single bulb.

With a single bulb illuminated, after about a ten-minute “warm-up”, a series of measurements were taken along the total length of the bulb in one-inch increments utilizing an American Ultraviolet UVX Digital-Radiometer linked with a UVX-36 sensor. The UV sensor was moved along while touching the bulb’s surface. Each reading was then allocated to its corresponding incremental surface area of the bulb, then integrated across the total bulb length, resulting in the following:

	NORMAL LEVEL	HIGH LEVEL
Rating of bulb @ total watts:	40	40
Total bulb radiation @ 365 nm (watts):	7.0	9.8
Percent of total bulb rating @ 365 nm:	18%	25%

Another test was conducted to determine the level of radiation intensity in relation to distance from the bulb’s surface, while “looking” through a piece of UVT Acrylic Polycast. The test involved measuring UV radiation at the centerline of a single bulb while incrementally moving the UVX-36 sensor away from the bulb in one-inch increments (i.e., starting at the surface of the Polycast and moving away to a distance of 18 inches at a NORMAL power level) (see Figure 58).

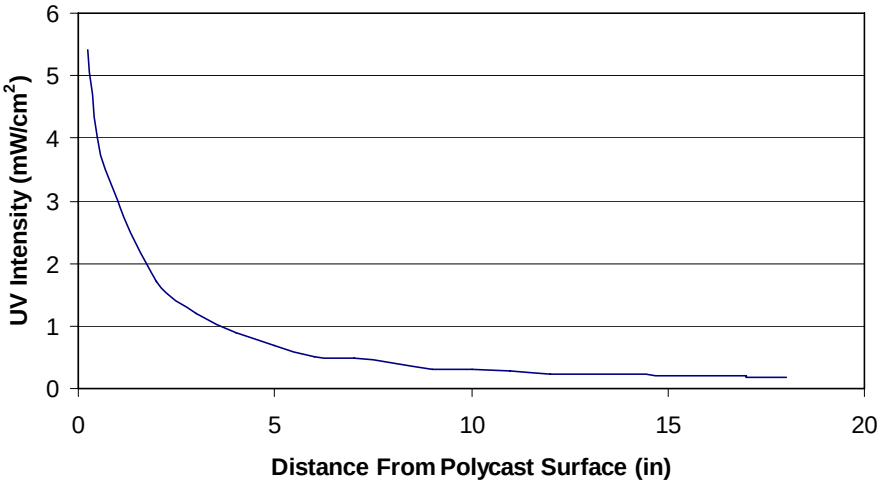

Figure 58. UV Intensity with Respect to Distance from Lamp

With all four UV bulb arrays in place, tests were conducted to obtain UV intensity levels at each node point inclusive in a 3-dimensional matrix that included the total volume of the chamber. The matrix included 3-inch increments on the vertical scale, and varying increments in the horizontal planes (i.e., distances from Polycast at 0, 1, 2, 4, 7 & 14 inches). The following test series were completed:

- Series No. 1: All 16 bulbs illuminated at NORMAL Power.
- Series No. 2: All 16 bulbs illuminated at HIGH Power.
- Series No. 3: Twelve (12) bulbs illuminated at NORMAL Power (i.e., one bulb extinguished on each wall).
- Series No. 4: Eight (8) bulbs illuminated at NORMAL Power, with two outside bulbs extinguished on each wall (i.e., Bulb Nos. 1 & 4).
- Series No. 5: Eight (8) bulbs illuminated at NORMAL Power, with two inside bulbs extinguished on each wall (i.e., Bulb Nos. 2 & 3).

The data acquired was analyzed with the intention of formulating a series of 3-dimensional maps. The maps indicated UV radiation intensities at any cartesian coordinate within the chamber, in relation to the number of illuminated bulbs and transformer power levels. This allowed quantification of total UV radiation to the chamber during the test and operational phases of the project.

PFBR Performance Tests. A series of iterative tests were conducted to determine the efficacy of reactivating TiO_2-coated activated carbon, while varying: (a). levels of UV radiation intensities, vs. (b). Differing levels of absorbed methanol.

These tests were conducted on samples of 100 lbs of TiO_2/AC that was impregnated with MeOH in varying concentrations ranging from 0.1 –to- 0.4 lb-MeOH per lb-carbon. Mass weights of the carbon before and after regeneration were utilized to quantify the degree of MeOH removal for each test, in addition to other mass flow parameters.

Westvaco Bionuchar 120 activated carbon was chosen for the tests since it was identified as one with superior methanol adsorption characteristics. Through the efforts of Dr. Mazyck, Westvaco generously contributed 150 lbs of the indicated carbon to support the project objectives.

MSI ordered quantities of TiO_2 from two different suppliers, including: (a). Spectrum Chemical Company (TI-140), and (b). Degussa (P-25).

Laboratory tests were conducted to determine if any performance differences existed between the Spectrum and Degussa TiO_2. The two samples were each dosed with equal ratios of methanol (MeOH); whereupon, each sample was then exposed to UV radiation in a water medium. Results indicated the following:

UV radiation period: 4 hours
Initial MeOH concentration: 9.8 mg/L
Final MeOH concentration & percent removal
- Degussa - P-25 6.97 mg/L (28.9%)
- Spectrum – TI-140 7.58 mg/L (22.7%)

The test results show that the Degussa P-25 was more effective.

MSI decided to use one-half (i.e., 75 lb.) of the quantity of activated carbon donated by Westvaco for its initial adsorption tests in the PFBR. The following protocol was developed to coat the TiO_2 on the activated carbon surfaces:

- A small sample of Westvaco Bionuchar 120 activated carbon, of known weight, was dosed with distilled water until it became obviously saturated, as exhibited by a “shiny - glistening” surface appearance. This test revealed that the carbon could adsorb approximately 1.5 lbs-water per 1.0 lb-carbon.

- With the intention of producing a 1% wt ratio of titania-to-carbon, a slurry was prepared containing: (a). 0.75 lbs of Degussa TiO_2 (i.e., 75 lbs-carbon x 1%), plus (b). 112 lbs of distilled water (i.e., 75 lbs-carbon x 1.5 ratio to achieve saturation). This slurry was then uniformly applied to the carbon utilizing an MSI mechanical mixing device. The result was a saturated mixture of: (a). 75 lbs-carbon, (b). 0.75 lb-titania, and (c). 112 lbs-water. This mixture theoretically should have resulted in a uniform one (1) percent, by weight, distribution of titania to carbon.

- The mixture was then distributed on a series of flat Teflon-coated trays at a carbon depth of about two-to-three carbon granules. The trays were then inserted into an oven to evaporate the water; thus, resulting in a dry titania-carbon mixture.

- Through an iterative process, it was determined the optimum drying conditions appeared to exist at 350°F temperature for 2.5 to 3 hours.

After completing the drying operation, the entire "dry-batch" of carbon-titania mixture was weighed, yielding a total weight of 76.0 lbs. This confirmed that the resulting "dry-batch" should have contained all the TiO_2, plus a small amount of residual water (i.e., 0.25 lbs-water). This sample was then sent to Dr. Mazyck's laboratory for testing, which employed the photocatalytic oxidation of organic dyes, showed that an increased loading of TiO_2 is needed to achieve good contaminant destruction.

Based on these results, a methodology of producing activated carbon coated with an optimum dose of TiO_2; in a manner, that could be replicated on a commercial scale for large quantity production.

Known quantities of Westvaco Bionuchar 120 activated carbon was dosed with slurry mixtures of distilled water and varying quantities of Degussa P-25 TiO_2 that ranged in six "steps" from one (1) percent up to nine (9) percent, by weight, based on the criteria presented in Table 21.

Table 21. Protocol for Production of GAC with Various TiO_2 Loadings

TEST NO.	PERCENT TITANIA	GAC	WATER		TiO_2
	percent	grams	Grams	oz	grams
1	1.0%	113.4	170.1	5.75	1.13
2	2.0%	113.4	170.1	5.75	2.27
3	3.0%	113.4	170.1	5.75	3.40
4	5.0%	113.4	170.1	5.75	5.67
5	7.0%	113.4	170.1	5.75	7.94
6	9.0%	113.4	170.1	5.75	10.21

Each sample was then placed in MSI's prototype external-fired test kiln to vaporize the slurry's water content; thereby, coating the activated carbon with TiO_2.

Samples from each of the six tests were sent to Dr. Mazyck for laboratory testing to determine the effect of percent TiO_2 loading on the adsorption/destruction of methanol in the presence of UV light. Results indicated that a nine (9) percent loading of yielded the best performance.

Methanol Adsorption Tests in the PFBR. With the above results and utilizing the indicated protocol, it was decided to prepare sufficient quantities of granular activated carbon (GAC) with a 9% TiO_2 loading and conduct a series of methanol adsorption tests in the PFBR at the MSI Test Facility in Oakland, Maryland.

Prior to the start of testing, samples of GAC coated with 9% TiO_2 was loaded with methanol equivalent to two (2) percent, by weight. This ratio was chosen, as an initial start point, so as to: (a). "generally" learn how the PFBR performed, vis-à-vis methanol reduction, (b). determine if methanol desorbed from the

carbon due to air flow through the chamber, (c). not exceed potential explosion limits of methanol, and (d). determine differences in methanol reduction with UV radiation.

During testing, a PerkinElmer Photovac MicroFID Portable Flame Ionization Detector was utilized to measure and monitor methanol levels at the inlet and outlet of the PFBR.

Although, levels of methanol did decrease during the duration of each test; unfortunately, results were less than satisfactory based on data obtained. It was conjectured that possibly the MicroFID instrument readings were compromised due to contamination of fine carbon dust on the instrument's inlet sampling port during testing. This is likely due to the attrition of the Westvaco Bionuchar 120 activated carbon used during testing. A possible remedy for this occurrence is the selection of a "harder" activated carbon.

Samples of the TiO_2/AC before and after testing were sent to UF for laboratory analyses. Samples were taken during testing that included TiO_2/AC that was loaded with (1) methanol and (2) methanol and water. In both cases, the TiO_2/AC was fluidized in the PFBR for about an hour in the presence of UV light. The results showed that when the TiO_2/AC was loaded with methanol only, a majority of the methanol remained in the carbon pores and, thus, was not oxidized. The TiO_2/AC loaded with methanol and water desorbed about two-third's of the methanol from its pores during fluidization. Measurements taken with the MicroFID instrument showed that only a small portion of this desorbed methanol was oxidized.

As a result of the less than satisfactory results obtained from the methanol adsorption tests utilizing TiO_2/AC, Dr. Mazyck decided that it would be prudent to investigate the use of silica gel as a catalyst support. Dr. Mazyck conducted a series of laboratory tests with silica gels impregnated with titania (STC) that showed very encouraging results, as described in previous sections. As such, it was decided to pursue a modification to the PFBR, and convert it into a fixed bed reactor capable of exposing STC pellets to UV radiation.

Photocatalytic Fixed Bed Reactor

As the previous section indicated, based on a series of laboratory tests and less than satisfactory results realized with the PFBR using TiO_2/AC, Dr. Mazyck decided to pursue a modification to the PFBR, and convert it into a fixed bed reactor capable of exposing STC pellets to UV radiation. This Section describes modifications made to the PFBR and subsequent results of its testing utilizing the STC. The objective was to: (a). Fill the PFBR with STC pellets to allow testing of a methanol-laden air stream through the reactor, when subject to UV radiation and, (b). Determine the efficacy of methanol adsorption and destruction by the STC pellets on a prototype scale.

STC Pellet Production. In order to produce a sufficient quantity of STC pellets (40 Å 4%) for the pilot studies, the bench-scale synthesis method was modified to increase production efficiency while producing composites with similar characteristics (i.e., surface area and pore size). TEOS (Silbond Condensed) was added to water, ethanol (Spectrum Chemicals), 1 N nitric acid, prepared from 15.8 N nitric acid (Fisher Scientific, certified A.C.S.), and 3% hydrofluoric acid, prepared from 48% hydrofluoric acid (Fisher Scientific, certified A.C.S.). A known mass of Degussa P25 titania (Majemac Enterprises) was mixed into the solution based on a ratio of 0.04 g of titania per 1 mL of TEOS. The ingredients were stirred using a paddle mixer. Photo No. 15 indicates an image of the mixing assembly designed by MSI for preparing the STC raw ingredients (mixing container is not shown to allow a view of the mixing paddle bars).

Photo No.15. MSI Mixer for STC Pellet Production

After mixing, the liquid STC was then transferred to molds, which were made from 2" thick polyethylene sheets drilled with 5/16" diameter holes. Each mold was approximately 16" by 24" and contained 2,750 holes. Photo No. 16 presents an image of one of the pellet trays that were prepared for manufacturing. The molds were filled by pouring the liquid sol into the molds, which were sealed on the bottom and top with sheets of solid polyethylene. The gels were aged at 65 °C for 48 hours. The lids were then loosened and the pellets dried in the molds at 103 °C in the dual thermal chambers designed by MSI. The pellets were removed from the molds, transferred to Pyrex containers, and then heated to 180 °C in the dual thermal chambers. After aging and drying, pellets were approximately 3 mm in diameter and 20 mm in length.

Photo No. 16. MSI Pellet Tray

Since the heating of the STC during drying releases ethanol, MSI investigated the availability of an explosion-proof commercially available heat transfer chamber. The investigation and subsequent analyses led to the conclusion that no heat transfer system was commercially available that was suitable for the STC preparation.

As such, MSI designed a double-chamber heat transfer system that provided a pneumatically sealed heat-generating source that was isolated from the STC materials. The system allowed the necessary temperature variations within the inner-chamber, where the pellet trays resided during their heat cycles. The inner-chamber was equipped with a vent system that allowed any volatile gases to discharge away from any source of heat or flame. Tests utilizing the new system proved successful. Its image is presented in Photo No. 17.

Photo No. 17. MSI Heat Chamber for STC Pellet Production

With a proven heat transfer chamber, MSI conducted a series of tests to prepare STC pellets by varying several criteria, including: (a). Mixing times of the gel, (b). Covering, or not covering, the mixing container during mixing, (c). Varying rotational speeds of the mixing paddles, (d). Material handling procedures of the pellets during the various heat cycles, (e). Procedures of handling the pellet trays between heat cycles, and (f). Other criteria.

After each test, samples of pellets were sent to UF for laboratory analyses. The pellets were tested for BET surface area and pore volume using a NOVA 2200e (Boynton Beach, FL). The results of this analysis are shown in Table 22. For visual orientation, Photo No. 18 shows a container of pellets produced by MSI.

Table 22. BET Surface Area, Pore Volume, and Pore Size Analysis

Silica Gel	Surface Area (m^2/g)	Total Pore Volume (cc/g)	Actual Pore Size (Å)
40 Å Pilot	723 ± 67	0.75 ± 0.12	38 ± 3

Photo No. 18. MSI-Produced STC Pellets

Modifications to PFBR. As a cost saving effort, MSI designed a means of modifying the original PFBR into a fixed bed configuration; so as, to accommodate the STC pellets and allow testing for methanol adsorption capabilities.

Criteria for modifying the original PFBR to accommodate the STC pellets and allow testing for methanol adsorption capabilities, included the following:

- Gas flow residence time in chamber: 4.3 seconds.
- Methanol concentration level in gas flow: 50 ppm_v
- Moisture content in gas flow: 95 –to- 99 percent
- Maximum distance between a UV bulb surface and most pellets: 2 inches

The modification system included a series of new UV bulbs installed in two sealed chambers composed of UVT Acrylic material, as illustrated in Figure 58. The bulb rack was capable of sliding in-and-out of the chambers for maintenance and bulb change out, if necessary.

The retrofit assembly was fabricated independent of the existing PFBR, but capable of being "dropped-into" the PFBR during tests, as illustrated in Figure 59. Other modifications to the PFBR included: (a). Perforated metal floor to serve as an air distribution plenum and support for the pellets, (b). Air distribution inlet to accommodate the designated test airflows, and (c). Other required alterations.

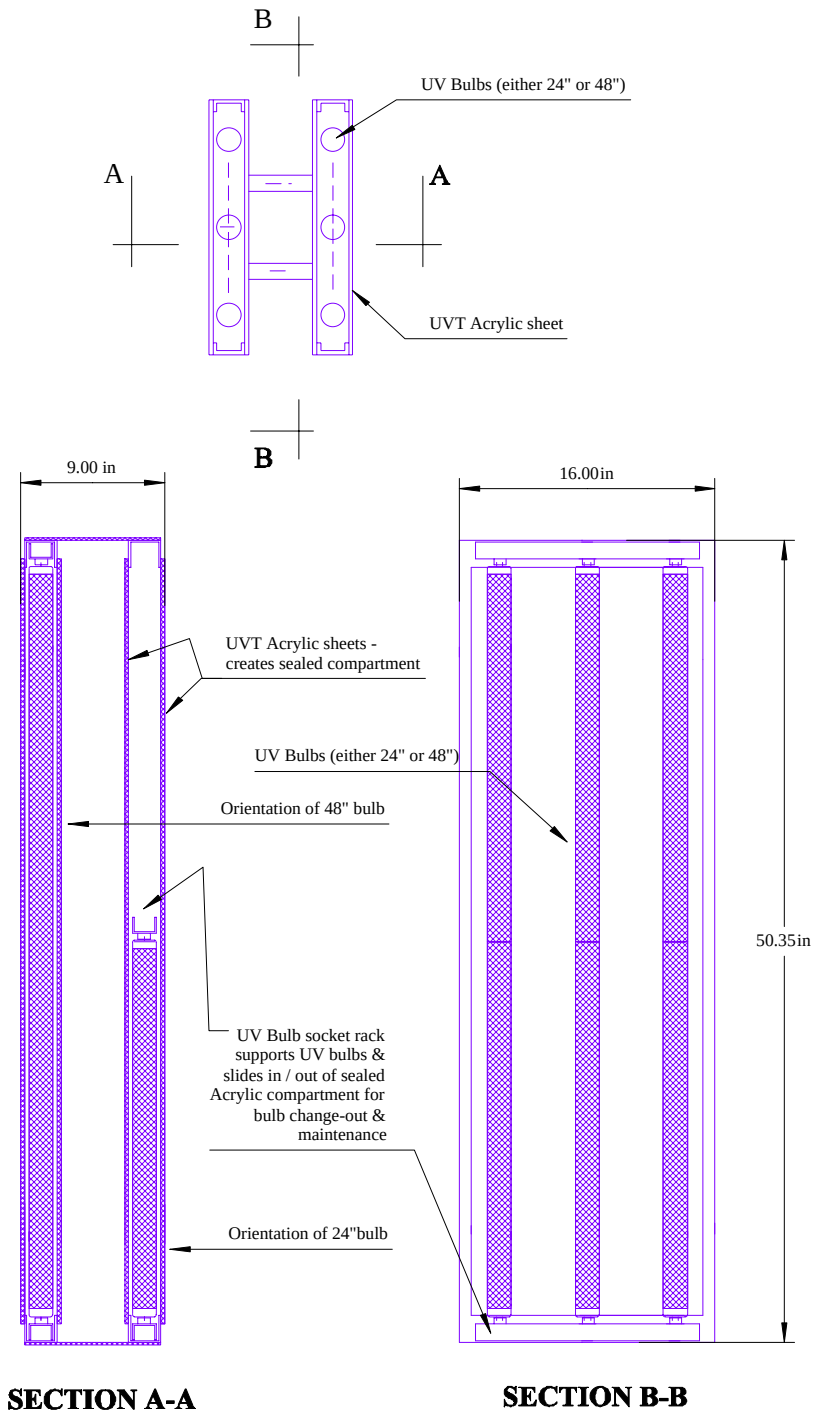

Figure 58. UV BULB RETROFIT ASSEMBLY (assembly "drops-into" existing PFBR)

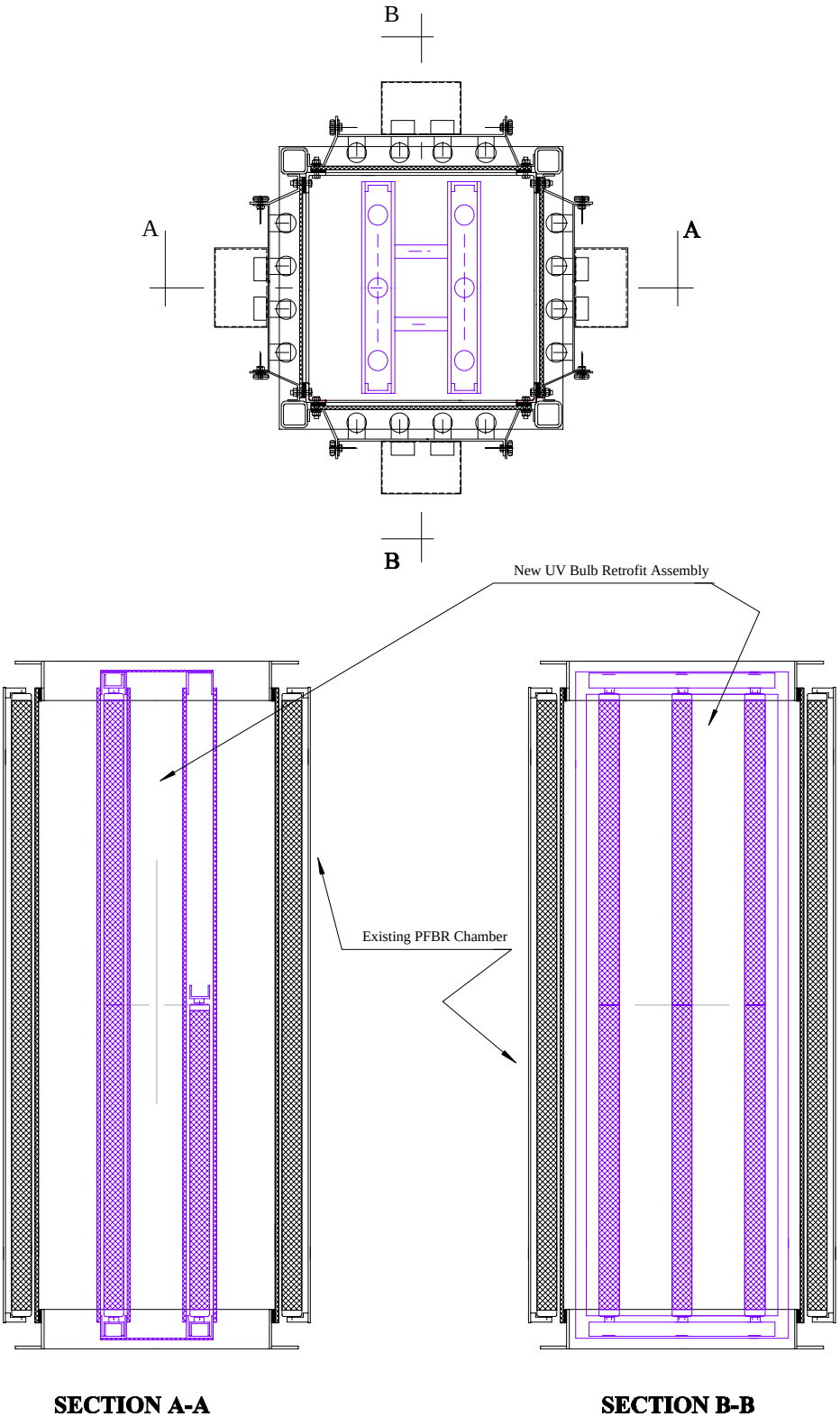

Figure 59. Existing PFBR with New UV bulb Retrofit Assembly

During initial “shake-down” testing, it became evident that a means and capability of removing the pellets after testing, while maintaining the integrity of the existing PFBR, was desirable and necessary.

The solution to this capability exists with a new trap door system illustrated in Figure 60. This design was completed by MSI and followed by fabrication. Features of the new trap door include: (a). Stainless steel perforated wire mesh floor to serve as an air distribution plenum and support, (b). Hinged to the interior frame of the existing PFBR to allow an UP and DOWN position, and (c). “Linked” to the existing PFBR plenum which could be rotated to allow trap door positioning in either the UP or DOWN location.

During testing, the trap door was in the UP position; whereupon, when testing was complete, the trap door would be moved to the DOWN position to allow pellet removal.

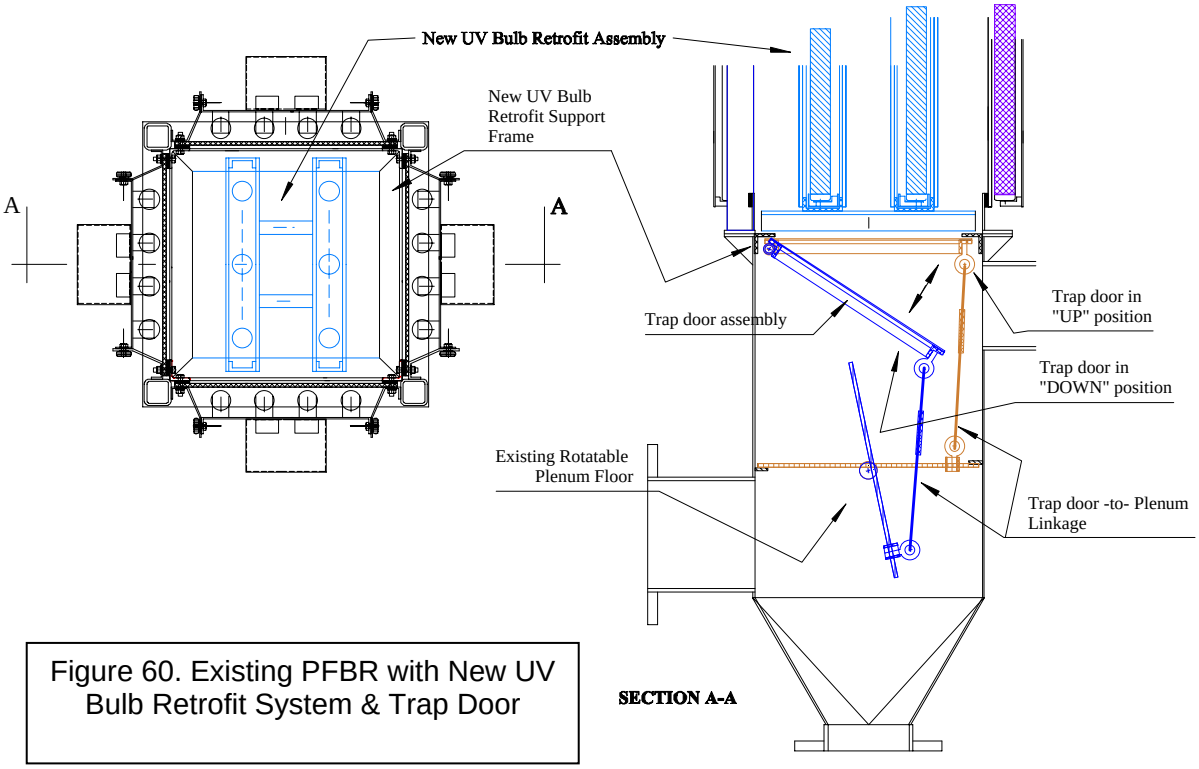

Figure 60. Existing PFBR with New UV Bulb Retrofit System & Trap Door

Thermal Heat Transfer System. MSI also designed and fabricated an electric heat exchange system capable of vaporizing a mixture of water and methanol to be used during testing; to inject and therefore produce, the desired methanol and moisture mixture contents in the test air stream. Photo No. 19 shows an image of the vaporizer’s internal heat exchange coil during fabrication and preliminary pressure and flow testing.

Photo No. 19. Methanol Vaporization System Heat Coil During Fabrication

PFBR Performance Testing with STC Pellets. Upon completion of modifications to the PFBR, fabrication of the methanol vaporization system, and the manufacture of sufficient quantities of pellets, testing was conducted to determine their efficiency while in an operating mode with the reactor.

The intent of the tests was to: (a). Simulate an airflow containing a specified concentration of methanol and moisture content approaching saturation, (b). Direct a known mass-flow of air, combined with the water/methanol mix to the reactor, (c). Monitor the methanol concentration entering and exiting the reactor, and (d). Determine the reactor's efficiency based on the measured reduction of methanol between inlet and outlet flows.

Figure 61 indicates a flow diagram of the test program.

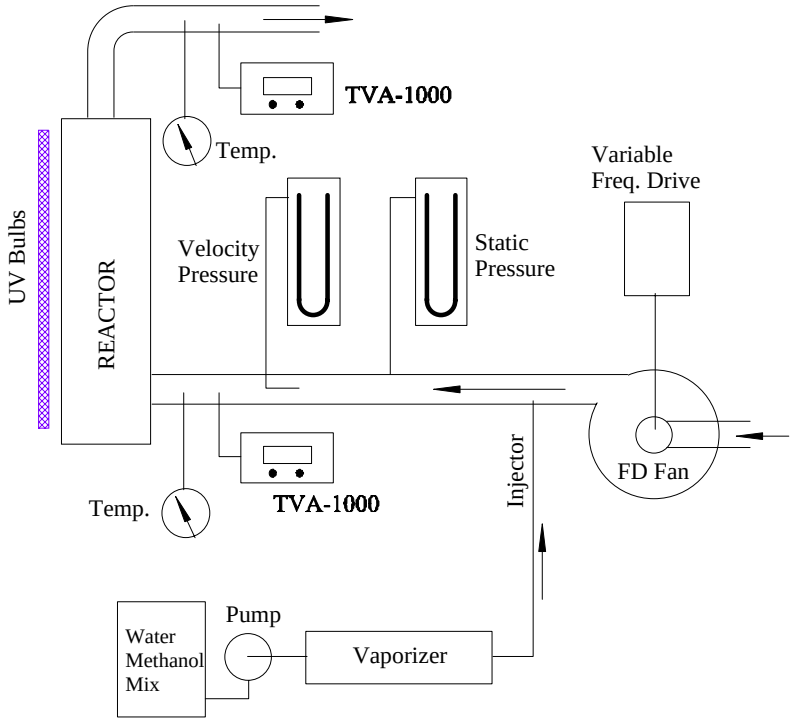

Figure 61. PFBR – STC Test Flow Diagram

To determine and quantify the correct quantities of airflow, methanol and water necessary to achieve the desired test objectives, MSI developed a computer program that considered all mass-flows in-and-out of the system, and desired criteria for testing.

Desired preliminary test criteria, as established by Dr. Mazyck during laboratory testing, included:

1. Residency time of airflow in reactor: 4.3 seconds.
2. Inlet concentration of methanol: 50 ppm_v
3. Moisture content in airflow: 95 –to- 99 percent.

Methanol concentrations at the inlet and outlet points of the reactor were measured using a ThermoElectron TVA-1000B Toxic Vapor Analyzer with flame ionization detector (FID) to measure organic compounds. Periodically, the influent and effluent was sampled using the NCASI Chilled Impinger Method (NCASI, 1998). The inlet and outlet impinger samples were analyzed for methanol and formaldehyde at UF as described previously.

Airflows were controlled and measured using MSI's in-house systems, including: (a). Variable frequency drive on the forced draft (FD) fan supplying air to the reactor, (b). pitot tubes linked with manometers to

measure static and velocity pressures in the connecting duct between the FD fan and reactor, and (c). Thermocouple to monitor temperatures on the reactor's inlet and outlet for mass flow corrections.

Based on the MSI mass-flow computer program, and designated test criteria, the mix ratio of methanol and water were determined and prepared prior to testing. A variable speed, positive displacement, pump was calibrated prior to testing to ensure the proper quantity of water/methanol mix was injected into the air stream to produce the desired methanol concentration (i.e., 50 ppmv) and moisture content (i.e., 95 – to- 99 percent).

As a double check to ensure the proper injection rate, the water/methanol mix container was located on a precision scale (accuracy capability of 1/100 pound). Periodically during testing, the rate of weight reduction of the mix was measured over a know time period to confirm that the proper injection rate was being achieved.

Photo No. 20 illustrates the inlet end of the test systems, including the vaporizer. Its exterior includes an aluminum encasement that shields insulation around heat exchanger. Photo No.21 shows the "other-end" of the test system, including the reactor.

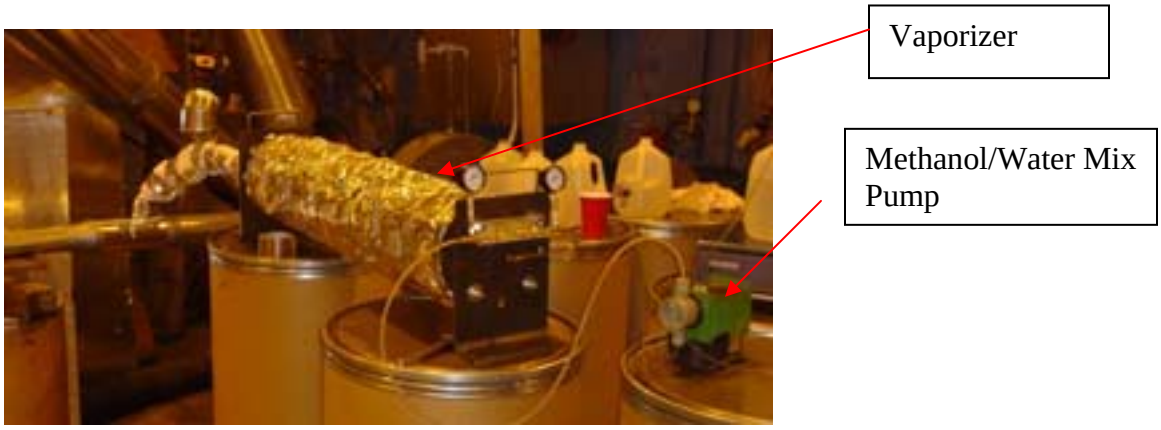

Photo No. 20. Vaporizer – Water/Methanol Mix Pump

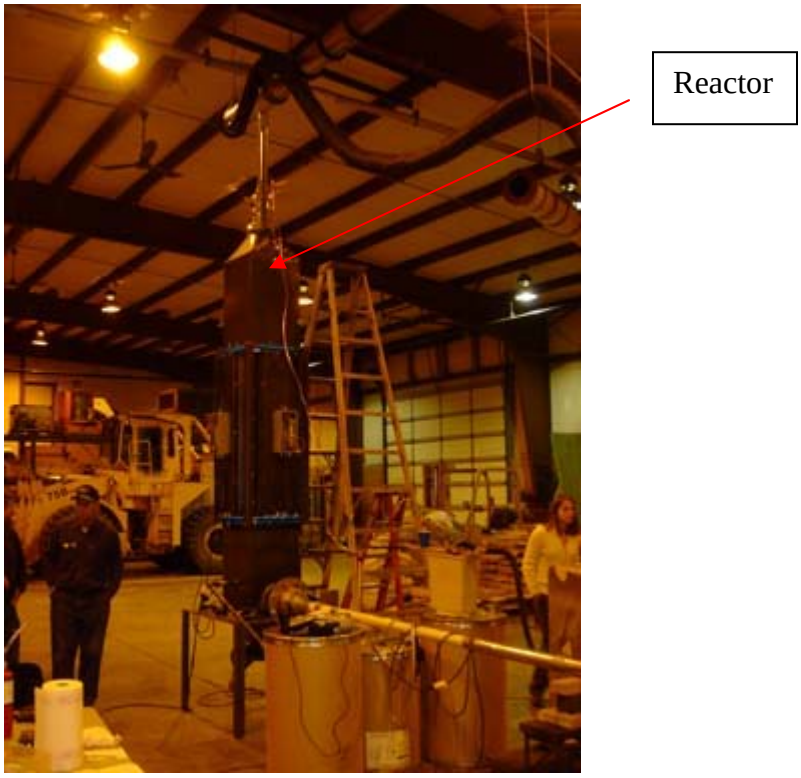

Photo No. 21. Reactor during Testing

During the first preliminary test conducted on February 8, 2005, unanticipated results were experienced on the outlet concentrations. For reasons unknown at the time, exceedingly high concentrations of hydrocarbons were present during testing. The TVA-1000 cannot distinguish between types of hydrocarbons, but only measurable totals. Laboratory analyses of the titration samples by Dr. Mazyck revealed that inordinately high concentrations of other hydrocarbons were present in the samples.

The only possible source of these stray hydrocarbons would have been residual quantities used during manufacturing and still, unexpectedly, remained in the pellets. It became obvious that the heat generated by the UV illumination caused these residual hydrocarbons to be expelled during testing.

The lesson learned from this experience was that upon completion of normal pellet manufacturing, the pellets must go through an additional heat cycle to “drive-off” any residual hydrocarbons (e.g., ethanol). In fact, this was successfully accomplished prior to the next test program, which produced a zero incidence of residual hydrocarbons.

The second preliminary test was conducted on April 14, 2005 and was successful. The same test procedures and criteria explained above were utilized.

Results were very encouraging. An arithmetic average of all input and output concentrations of methanol resulted in the following:

- Average methanol inlet concentration: 55.8 ppm_v
- Average methanol outlet concentration: 1.4 ppm_v
- Percent methanol reduction: 97.6 percent

Figure 62 presents a graph of the test results.

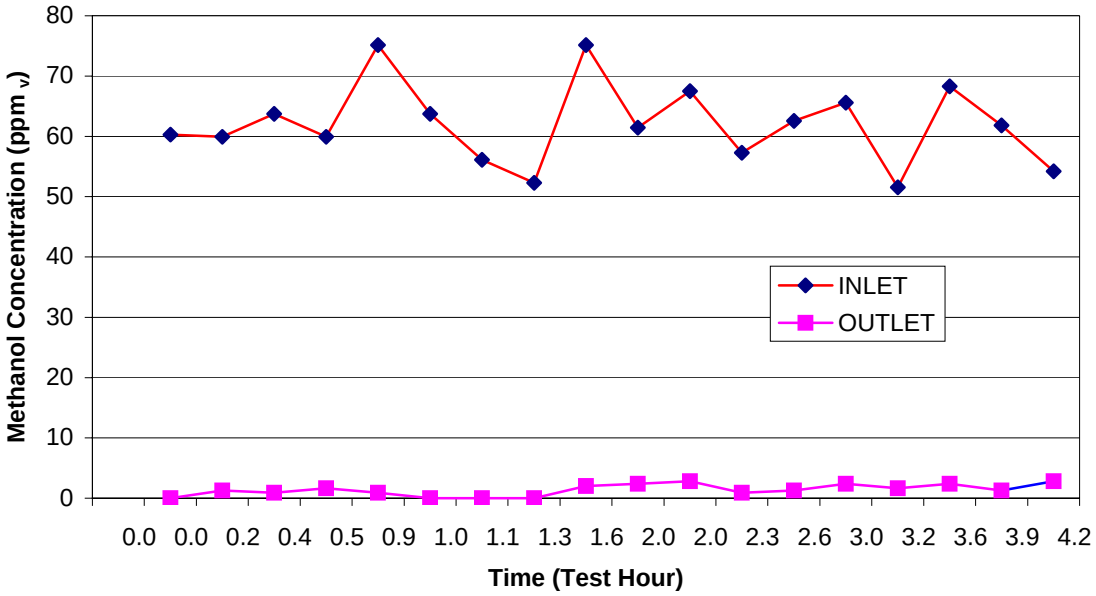

Figure 62. PFBR Test Results using STC Pellets for Methanol Capture

The next test was planned for an extended time period of at least 24 hours and was conducted on May 5-6, 2005. In addition to determining system performance efficiency, a primary objective was to determine at what time period the system reaches steady state; which is the point that the incoming methanol was oxidized by UV radiation at a rate equal to its adsorption rate on the pellets. Steady state is indicated by a constant and level methanol concentration on the reactor's outlet flow.

Test protocols were the same as previous tests.

Once the test was underway, results were initially very encouraging and replicated those experienced during the April 14, 2005 test; wherein, the outlet methanol concentrations were about 97 to 98 percent reduced from that of the inlet concentration. This phenomenon continued for about 20 hours; at which point the outlet concentration began to steadily rise until, at about the 28th hour of testing, it almost reached a level equal to that of the inlet. At this point the test was terminated.

Upon review of the test results, Dr. Mazyck concluded that the adsorption rate of methanol was much greater than the oxidation rate. Therefore, the pellets became saturated with methanol, so that no further removal was realized. To increase the rate of oxidation, the 365 nm UV bulbs that were mounted on the exterior of the of the reactor chamber were replaced with 254 nm UV bulbs, which were positioned within the packed bed. The use of 254 nm lamps in the bench-scale resulted in greater methanol oxidation rates, as described previously. Also, by positioning the 254 nm UV bulbs amidst the pellets, the distance between each bulb face and each pellet was considerably shorter; thus, intensifying the UV radiation to each pellet.

PFBR Modifications to Accommodate 254 nm UV Bulbs. Based on criteria established by Dr. Mazyck, engineering design was conducted and completed on necessary reactor modifications to accommodate the new matrix of 254 um UV bulbs, while continuing to utilize the balance of system components.

Figure 60 illustrates the system modifications and include:

- New chamber housing situated between the existing inlet plenum and outlet exhaust hood, and included: (a). One observation port located on front face, and (b). Portal on back face for passage of electrical wires to each UV bulb.

- Forty-six 254 um UV bulbs housed in protective quartz tubes, each of which included electrical connectors and wires, the latter of which passed through sealed stoppers.

- Top and bottom support racks designed to support each UV bulb assembly, and interface with the existing inlet plenum and outlet exhaust hood (Figure 61 – shows the top support rack matrix layout).

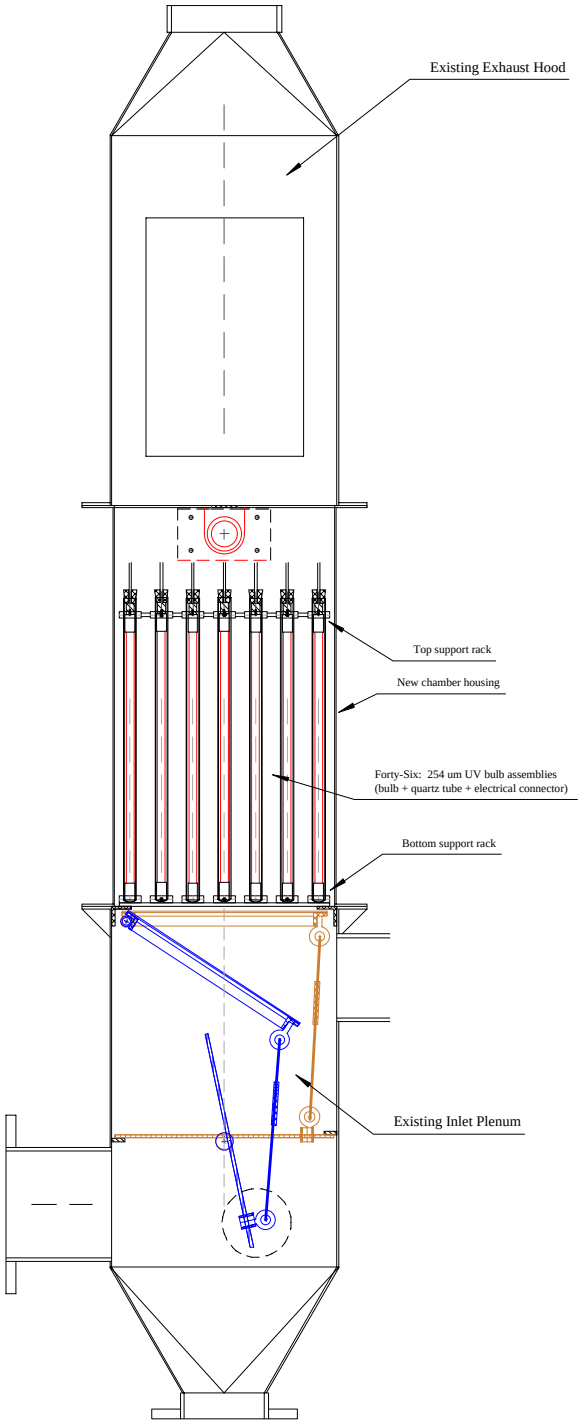

Figure 63. PFBR Modification to Accommodate 254 um UV Bulbs

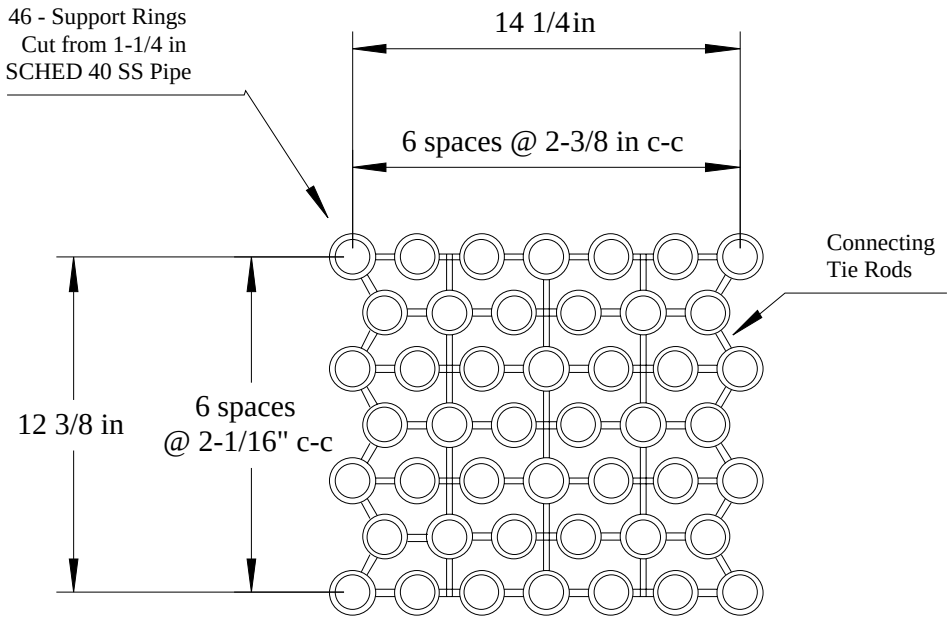

Figure 64. Top Support Rack

A UV-Technik Electronic Ballast Power Center was installed in conjunction with the 46 UV bulbs; thus, giving the capability to vary UV radiation in response to a variable voltage power input.

The following photos present images of the various system modifications, and include:

- Photo No. 22: 254 um UV Bulb – Quartz Tube Assembly
- Photo No. 23: Top Support Rack – Showing One UV Bulb Assembly with its Connecting Electrical Wires
- Photo No. 24: New Chamber Housing
- Photo No. 25: Reactor housing
- Photo No. 26: Wiring harness between UV-Technik Electronic Ballast Power Center and individual UV bulbs within the reactor chamber

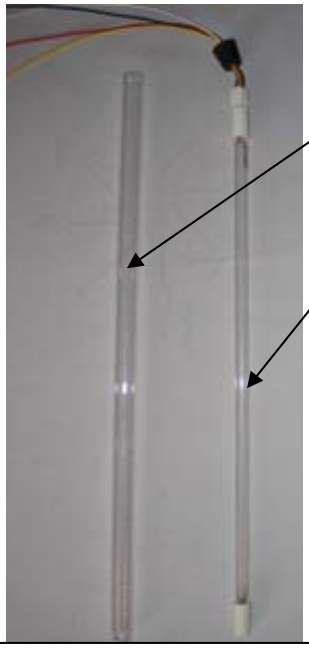

Photo No. 22. – Quartz Tube – UV Bulb Assembly

Photo No. 23. Top Support Rack – Showing One UV Bulb Assembly with its Connecting Wires

Photo No. 24. New Chamber Housing

UV-Technik
Electronic Ballast
Power Center

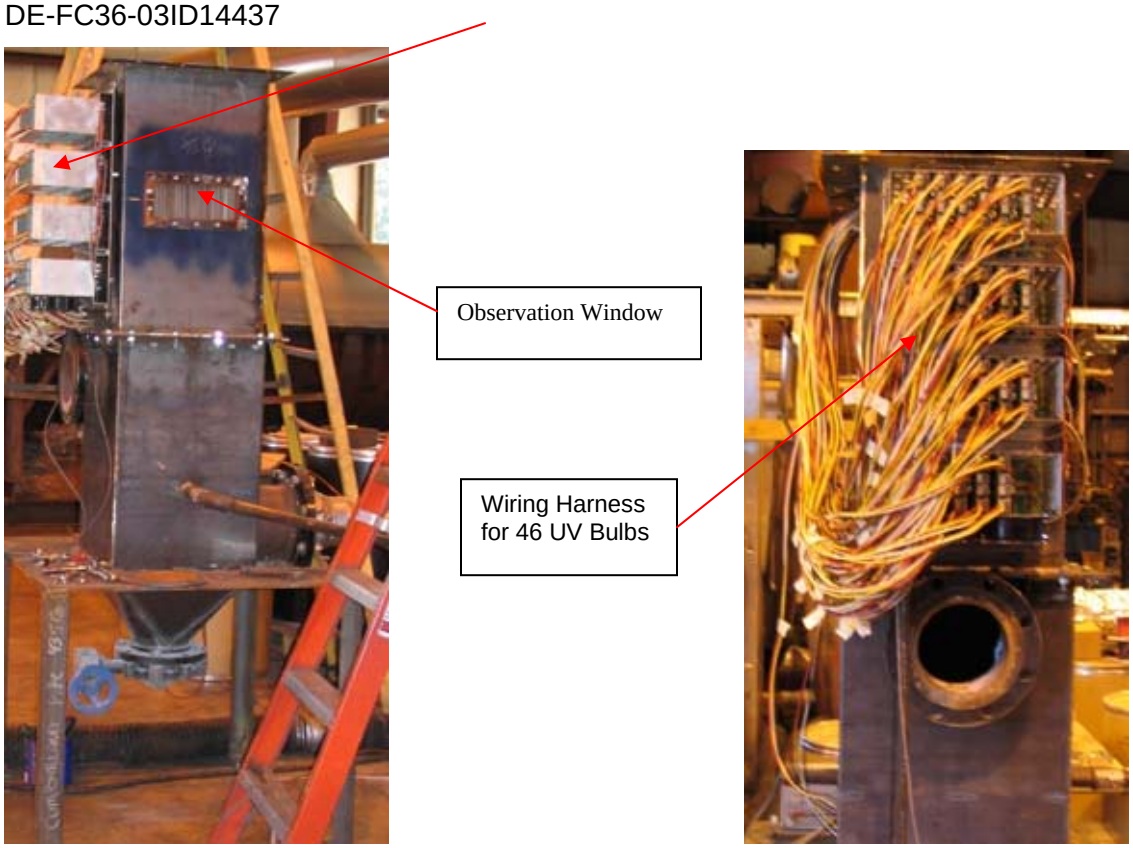

Photo No. 25. Reactor Housing

Photo No. 26. UV Bulb Wiring

Survey Tests to Correlate UV Intensity vs. Varying Voltage. Upon completion of modifications to the reactor, a survey was conducted to correlate UV radiation in relation to varying voltages by utilizing the UV-Technik Electronic Ballast Power Center.

The monitoring probe of a radiometer was positioned; so as, to allow it to “look-through” a port opening in the center of the new observation window that was part of the reactor modifications. Three different conditions of testing were employed, including: (a). “Cool” reactor just at startup of lamps with no air flowing through the reactor, (b). “Warm” reactor after about one-half hour of startup with no air flowing through the reactor, and (c). “Cool” reactor that is cooled by airflow passing through the reactor.

Figure 64 shows results of the test survey, which indicates a range of about 50 percent between the highest intensity to lowest intensity (the latter observed by the lowest potentiometer setting on the control system without any bulbs “flickering”).

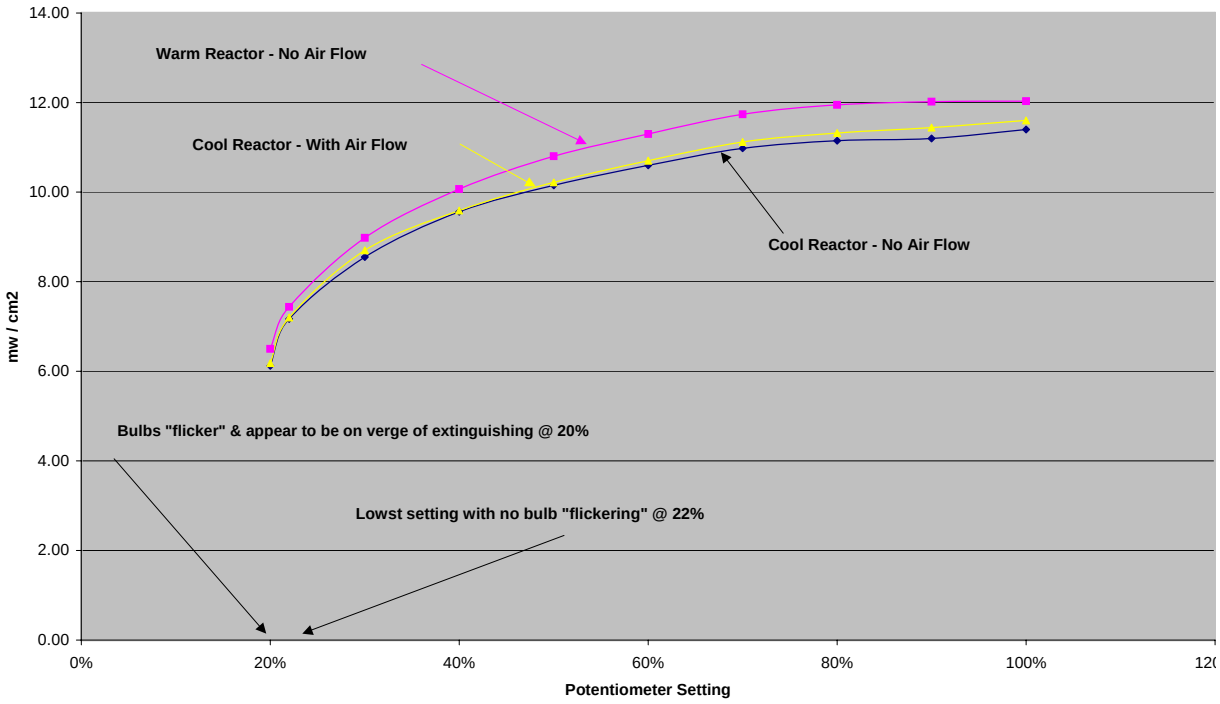

Figure 64. UV Intensity vs. Potentiometer Settings

Testing – STC Pellets in the Reactor. Following modifications to the PFBR and calibrating the UV bulbs, a series of tests were conducted to determine the performance efficiency of the system.

The test criteria, was similar to previous testing, and included: (a). Creating a known mass airflow containing a specified concentration of methanol and moisture content approaching saturation that was sent directly to the reactor, (b). Monitoring the methanol concentration entering and exiting the reactor, and (c). Determining the reactor's methanol recovery efficiency based on the measured reduction of methanol between inlet and outlet flows.

Test criteria, as established by Dr. Mazyck during laboratory testing, included:

- Residency time of airflow in reactor: 4.3 seconds.
- Inlet concentration of methanol: 50 ppm_v
- Moisture content in airflow: 95 –to- 99 percent.

A 24-hour test was conducted on November 1 –2, 2005. In addition to determining system performance efficiency, a primary objective was to determine at what time period the system reached steady state, which is the point that the incoming methanol is oxidized by UV radiation at a rate equal to its adsorption rate on the pellets. Steady state would be indicated by a constant and level methanol concentration on the reactor's outlet flow.

Test protocols were the same as previous tests, and included: (a). Inlet and outlet methanol concentrations measured using a ThermoElectron TVA-1000B Toxic Vapor Analyzer and the NCASI Chilled Impinger Method (NCASI, 1998), (b). Airflows controlled using variable frequency drive on the forced draft (FD) fan supplying air to the reactor, (c).Airflows measured using pitot tubes linked with manometers to measure static and velocity pressures in the connecting duct between the FD fan and reactor, (d). Thermocouple to monitor temperatures on the reactor's inlet and outlet for mass flow corrections, (e). Variable speed, positive displacement, pump calibrated to ensure the proper quantity of water/methanol mix injection into the air stream (i.e., 50 ppmv-methanol, and 95 –to- 99 percent moisture

content), and (f). high accuracy scale to monitor over time the weight distribution of water/methanol mix to the system.

For approximately the initial 16 hours of the test period, methanol removal rates ranged from 95 to 97 percent. During the last period of the test, removal rates decreased to 65 to 75 percent. The effluent formaldehyde concentration during the entire test was less than 1 ppm_v.

At steady state, the methanol on the surface of the silica is oxidized; therefore, regenerating the silica in-situ. The high removal efficiencies experienced during the initial test period is a result of the high rate of adsorption on the virgin surfaces of the silica. Over time, toward the latter period of testing, the rates of oxidation and adsorption become equal and in balance. Thus, the rate of methanol removal efficiency became dependent on the rate of methanol oxidation. This same trend was observed during lab-scale studies. The production of formaldehyde, which is a byproduct of methanol oxidation, was low; thus, indicating that the majority of methanol was oxidized to inert byproducts, which are primarily carbon dioxide and water vapor. Measured concentrations of formaldehyde, resulting from the test program, were similar to those measured in lab-scale studies. Thus, the scale-up of the system did not yield increased production of formaldehyde.

To improve the steady state removal efficiency of the system, the rate of methanol oxidation had to increase. It was thought that this could be accomplished by improving the efficiency of the UV bulbs, which are used to activate the titania that catalyzes the oxidation of methanol. The optimal operating temperature of the UV bulbs is 104 deg. F. Throughout the test, the temperature of the exiting reactor gas flow was approximately 160 deg. F, which indicated that lamps were less than 50 percent efficient.

It was thought that possibly if the voltage input to the bulbs would be decreased, it would decrease the bulb's temperature; thus, increasing their efficiency. Within the unique design of the reactor, it was anticipated that with a lower voltage input, the UV intensity could actually be greater than at a 100 percent setting, due to a higher efficiency resulting from cooler operation. Thus, it was thought that, the rate of methanol oxidation could increase. By increasing the rate of methanol oxidation, the percent removal achieved at steady state should increase.

Based on this theory, the next test, which was conducted on January 5-6, 2006, was to operate the UV bulbs at their minimum intensity, with an objective of observing the impact of: (a). Reducing the reactor bed temperature; thus, (b). increasing the methanol removal efficiency of the system. The intent of reducing the bed temperature from previous tests to "reach" the theoretic optimum operating temperature of UV bulbs, which is 104 °F. In addition to determining system performance efficiency, a primary objective was to determine at what time period the system reached steady state.

All other test criteria remained the same as previous tests, except that the inlet methanol concentration was increased to 100 ppm_v mixed with sufficient water to create a 95 –to- 99 percent moisture content.

Test results during the 24-hour test on January 5-6, 2006 indicated reactor outlet temperatures ranging between 131 and 143 °F, with an overall average of 139 °F.

Figure 65 presents the test results, showing the inlet vs. outlet methanol concentrations.

Figure 66 indicates the methanol removal efficiencies over the test time period.

As test results indicate, acceptable methanol removal efficiencies occurred for about the initial four hours of testing; but then were followed by a steady decrease in efficiency over time until steady state removal of about 20 to 40% was achieved.

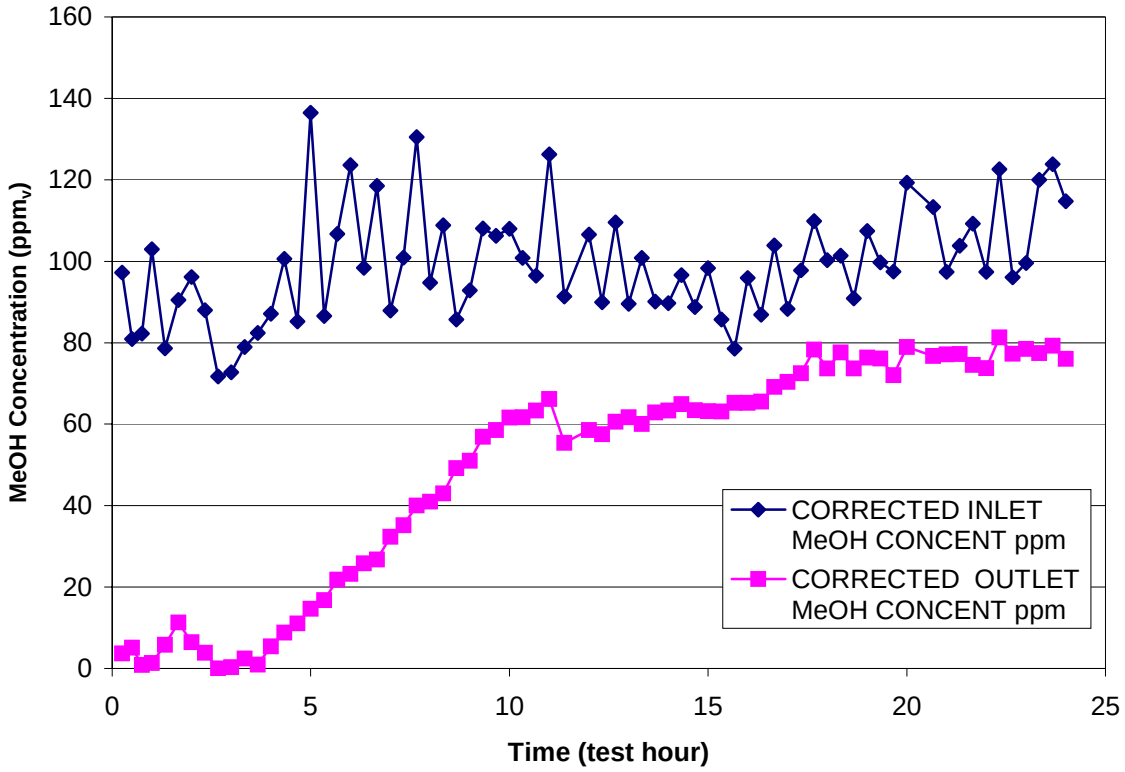

Figure 65. January 5-6, 2006 Test Results - Inlet and Outlet Methanol Concentrations for STC Illuminated with Minimum UV Intensity

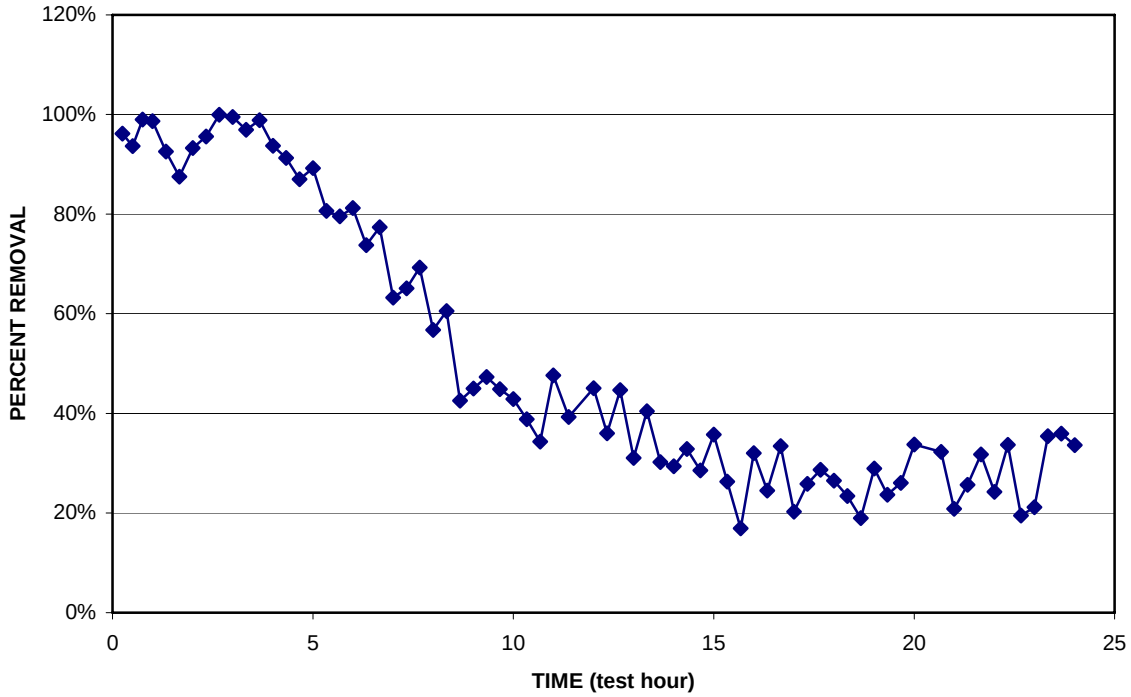

Figure 66. January 5-6, 2006 Test Results - Methanol Removal Efficiencies for STC Illuminated with Minimum UV Intensity

The test results indicated that decreasing the UV intensity did reduce the reactor bed temperature in comparison to previous tests; however, any efficiency gained by the temperature reduction was more than cancelled by the reduced UV intensity; which obviously decreased the overall methanol removal efficiency.

As previously indicated, the optimal operating temperature of the UV bulbs is 104 °F. Therefore, it was decided to conduct the next test at the maximum 100 percent UV intensity; but to modify the air inlet system to the reactor by implementing a system to chill the inlet air to a point that would result in an outlet reactor temperature closer to 104 °F (i.e., optimal operating temperature of the UV bulbs).

Utilizing this criterion, the next test was conducted on March 8-9, 2006. During the 24-hour test, indicated reactor outlet temperatures ranging between 111 and 127 °F, with an overall average of 116 °F.

The target inlet methanol concentration criterion during testing was 100 ppm_v.

Figure 68 presents the test results, showing the inlet vs. outlet methanol concentrations based on TVA-1000 readings. The influent methanol concentration was variable and ranged between 80 and 140 ppmv over the duration of the test. Figure 69 indicates the methanol removal efficiencies over the test time period based on TVA-1000 readings. As shown in Figure 66, high levels of methanol removal occurred for about the initial eight hours of testing and were followed by a steady decrease in efficiency to about 60% by the end of the 24-hour test period. Figure 70 indicates the methanol removal efficiencies over the test time period, based on impinger samples. This figure shows that the results monitored with the TVA-1000 correlated well to those measured by the chilled impinger method. Figure 71 shows that the production of formaldehyde, which is a byproduct of methanol oxidation, was low; thus, indicating that the majority of methanol was oxidized to inert byproducts, which are primarily carbon dioxide and water vapor. Measured concentrations of formaldehyde, resulting from the test program, were similar to those measured in lab-scale studies.

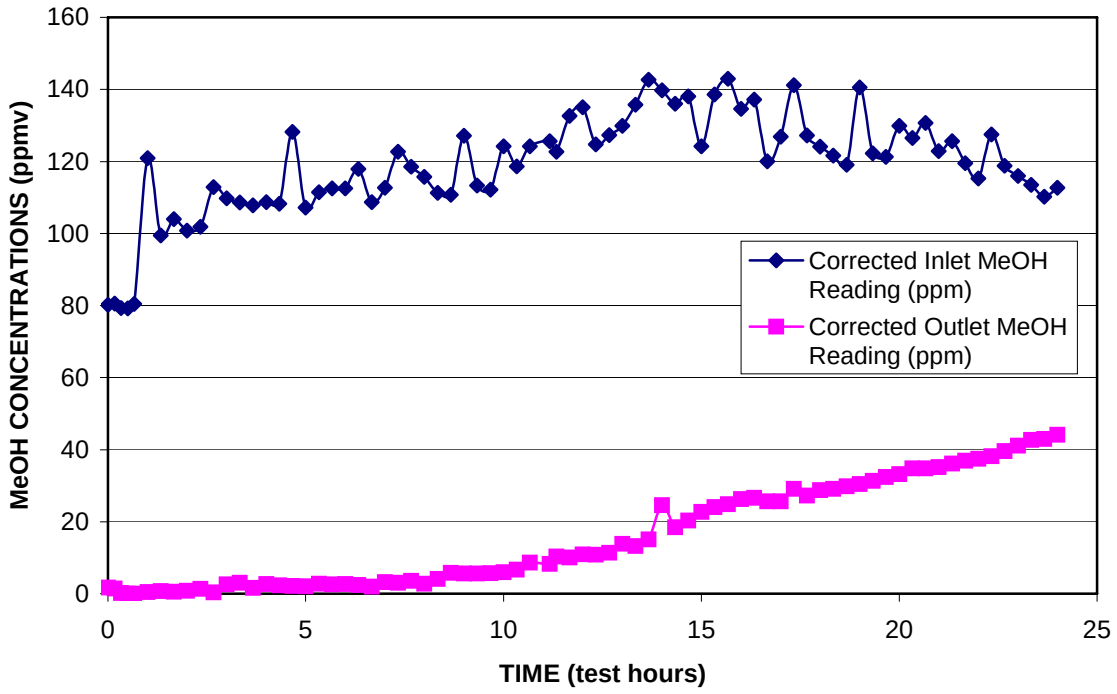

Figure 68. March 8-9, 2006 Test Results - Inlet vs. Outlet Methanol Concentrations (TVA-1000)

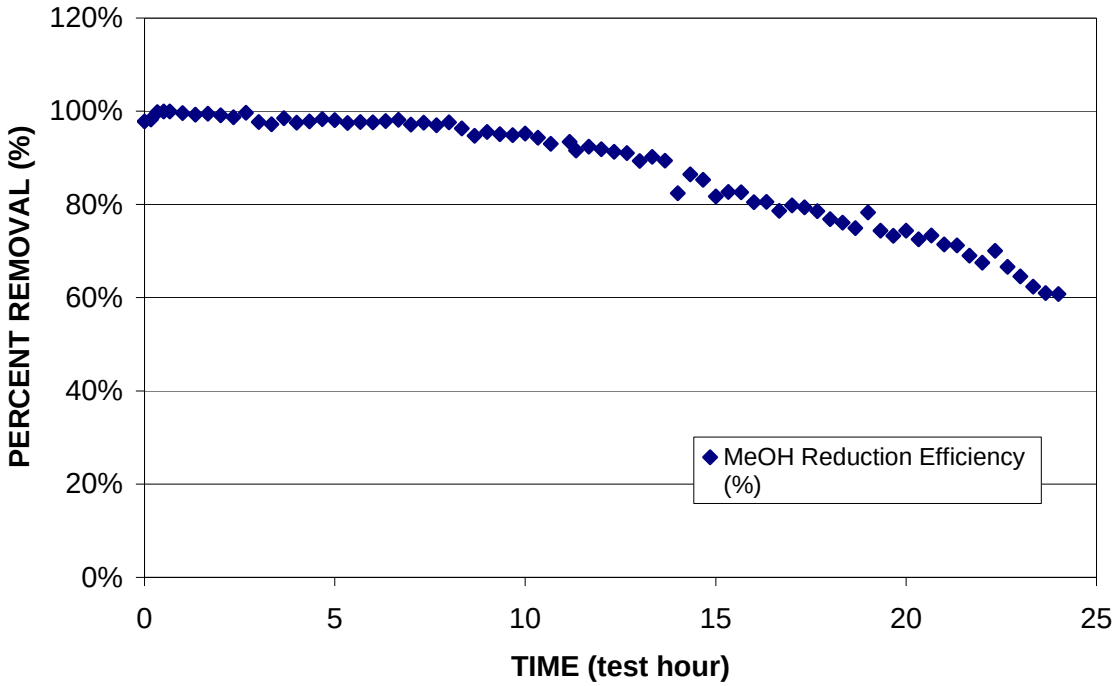

Figure 69. March 8-9, 2006 Test Results - Methanol Removal Efficiencies (TVA-1000)

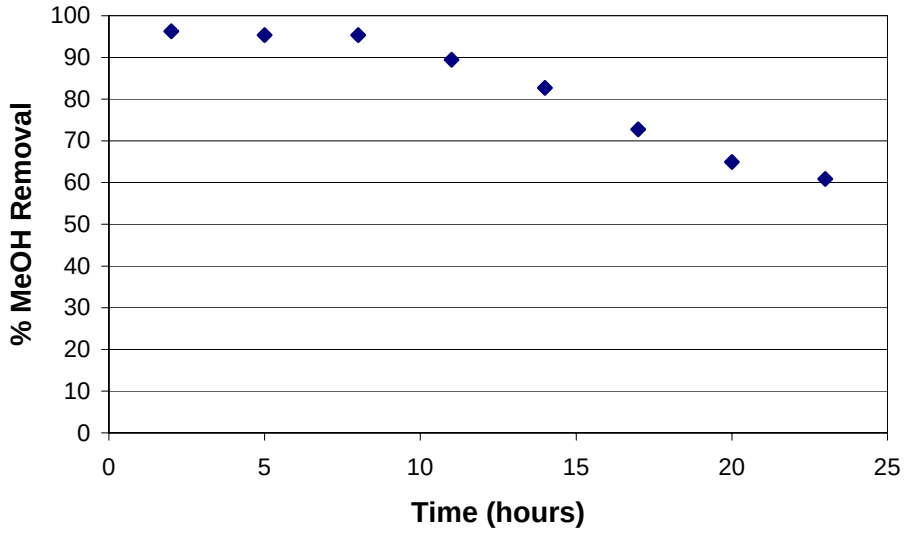

Figure 70. March 8-9, 2006 Test Results - Methanol Removal Efficiencies (based on impinger samples)

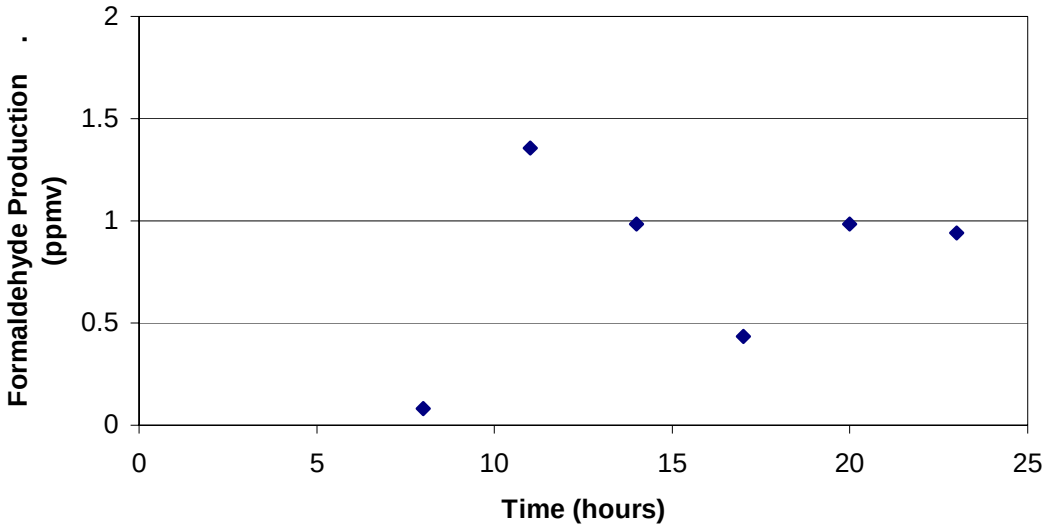

Figure 71. March 8-9, 2006 Test Results - Formaldehyde Formation during Testing (based on impinger samples)

Development of Silica-Titania Coated Packing (STCP)

In the studies reported so far, STC were employed as 3 mm by 5 mm cylindrical pellets in a packed bed. A packed bed of pellets is well suited for reactor configurations designed to treat low flow rates (e.g., less than 2,000 ACFM). However, when employing the technology for higher flow rates, such as the tens to hundreds of thousands of cubic feet per minute, a packed-bed reactor may not be ideal due to the pressure drop associated with a packed bed of pellets and the required number of UV lamps. In order to reduce the pressure drop and UV lamp requirement, a novel approach was designed that involves the STC coated on chemical tower packing material. This new coated material will hereon be referred to as Silica-Titania Coated Packing (STCP). An individual piece of packing material is approximately the size of a ping-pong ball. It has a large external surface area and high void space. Thus, the pressure drop associated with flow through a packed bed of STCP will be significantly less than that associated with a packed bed of pellets. In addition, the structure of the STCP will allow better UV light distribution within the packed bed, thereby reducing the quantity of UV lamps required. The STCP overcomes the limitations associated with typical thin film systems since the STC coating will be porous and have a high surface area. Thus, improved mass transfer and higher adsorption capacity compared to typical thin film systems will be realized.

Development of the STCP began with coating a titania slurry on commercially available chemical tower packing material. The STCP was optimized to ensure good adherence of the titania on the surface. A spray coating method was developed by using a Testers spray gun (shown in Photo 27) with compressed air as the propellant. Various solutions were mixed and sprayed on 304 stainless steel packing material. The effects of pre-oxidation of the surface, number of coatings, and pH of the titania solution were investigated. Pre-oxidation of the surface was achieved by heat treating the stainless steel substrate in air at 1000 deg. F for 45 minutes and resulted in poor adherence of the titania. Three coatings of titania was determined to be optimal since this number of coatings provided the greatest coverage of the titania on the surface without a negative impact on the adherence. The pH of the titania solution was varied by using acetic acid (for acidic solutions) or NaOH (for alkaline solutions). A 7%wt solution of acetic acid resulted in the best dispersion and adherence on the stainless steel surface. Examples of STCP showing good dispersion and adherence of the titania is shown in Photo 28.

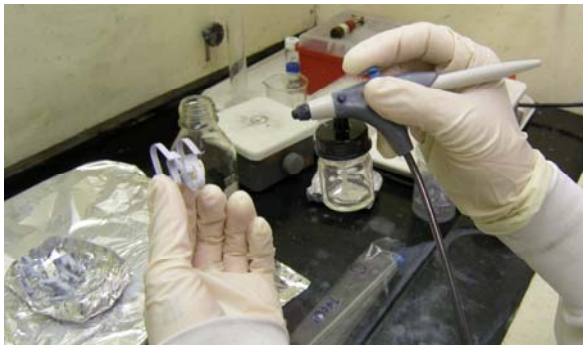

Photo 27. Spray gun used to coat the silica-titania composite on the stainless steel substrate

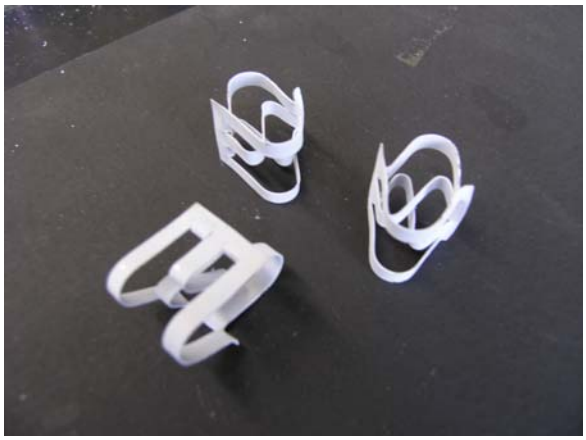

Photo 28. Example of STCP

Second Generation Pilot Reactor

A second generation pilot unit was fabricated for the testing of the STCP. This second generation pilot unit (3-D models are shown in Photos 29 and 30) was designed so that the UV lamps were positioned in a horizontal configuration. Since the bulbs in the previously described pilot reactor had a vertical orientation, the air flow could possibly "short circuit" through bed without seeing high intensity UV light (i.e., without coming in close contact with silica-titania pellets close to the UV lamp). The horizontal configuration in the second generation reactor should help further reduce this possible short-circuiting. The spacing of the lamps in the second generation reactor is similar to that of the original pilot reactor. However, an additional improvement incorporated into the second generation reactor is that lamps can be easily removed in order to change the spacing between the UV lamps, which is an important test parameter for the STCP since the goal is to not only increase performance of the reactor but also reduce the number of UV lamps required in a system. A picture of the second generation reactor is shown in Photo 29. A picture of the electrical cabinet, which houses the ballasts that drive the lamps in the reactor, is shown in Photo 30.

Figure 3. Photo of the Pilot Unit

Figure 4. Photo of the Electrical Cabinet for the Pilot Unit

Initial testing of the titania-coated STCP showed greater than 99% removal of methanol. More testing, including determination of required UV intensity and further development of the STCP, will be conducted in the future.

LIFE CYCLE ANALYSIS

Overview

A better understanding of the benefit of the technology developed in this DOE project can be realized by an environmental assessment using life cycle assessment (LCA), the systematic inventory and analysis of environmental impacts for the entire life of a process or product for comparison purposes. Without an understanding of the potential impacts associated with the production and operation of a full-scale photocatalytic oxidation and biofiltration system as compared to thermal oxidation, it is impossible to determine which technology actually represents the most environmentally preferable option. As the final technology developed in this work is finalized, this LCA is ongoing and is being conducted in accordance with ISO 14040 series guidelines, which call for four stages: 1) definition of the assessment goals and scope and system boundaries, 2) inventory of all material and energy inputs and outputs from the system, 3) assessment of environmental impacts associated with the inventoried system inputs and outputs, and 4) interpretation of the impacts according to the defined goal and scope.

Goal and Scope Definition

The goal of this LCA is to compare the environmental impact associated with the current state of volatile emissions from pulp and paper mills with that of two different treatment scenarios: (1) a common existing treatment option – incineration in a regenerative thermal oxidation; and (2) an innovative treatment option – photocatalytic oxidation and biofiltration. Specifically, the LCA scope includes an inventory of raw materials and energy required and air emissions and solid waste generated for each of these three scenarios. The emphasis of this study will be on emissions to air and their contribution to appropriate environmental impact categories, including global warming, smog formation, and acidification, as assessed using a variety of impact assessment methods (Babbitt and Lindner, 2007b).

All raw materials required, emissions produced, and environmental impacts created by the current VOC emissions or by the two treatment options will be referenced to the same functional unit, a parameter that describes the function to be carried out by the system of interest. For this LCA, the functional unit is HVLC effluent air in a volume of 350 scfm and containing methanol in a concentration of 50 ppm_v.

System Boundaries

This LCA focuses on air emissions from all unit operations that generate HVLC gases during the production of brownstock pulp at Kraft mills. These processes include digesting of wood chips to produce pulp; storage, washing and screening of the brownstock pulp; and recovery of chemical pulping liquors. Wood procurement, bleaching, drying, and finishing processes are excluded from this analysis, as they are not considered significant sources. For the two treatment options, the system includes raw materials required and emissions generated during all life cycle stages involved in production and operation of the treatment system, including raw material extraction, system production, system use, and waste disposal. Details of the system parameters for each of the three scenarios are shown in Table 23 and a schematic of the life cycle stages included is shown in Figures 72 and 73.

Table 23. Life Cycle System Parameters

A: No HVLC Control	B: Thermal Oxidation	C: Photocatalytic Oxidation and Biofiltration
• Emissions from Kraft mill brownstock pulp production • Two brownstock washers in series • 350 scfm air, 50 ppmv methanol, gas stream also contains other VOCs	• Regenerative thermal oxidation technology • Control parameters are gas temperatures of 1600 deg F and minimum of 75 seconds retention time • SO2 scrubber required • Stainless steel ductwork • 200 feet from emissions source to RTO	• Control parameter is 98% removal of methanol • 90% removal by PCO, remaining 8% by biofilter • PCO and biofilter located adjacent to emissions source • PCO uses silica-titania pellets and 75 watt UV-C lamps • Biofilter contains granular activated carbon

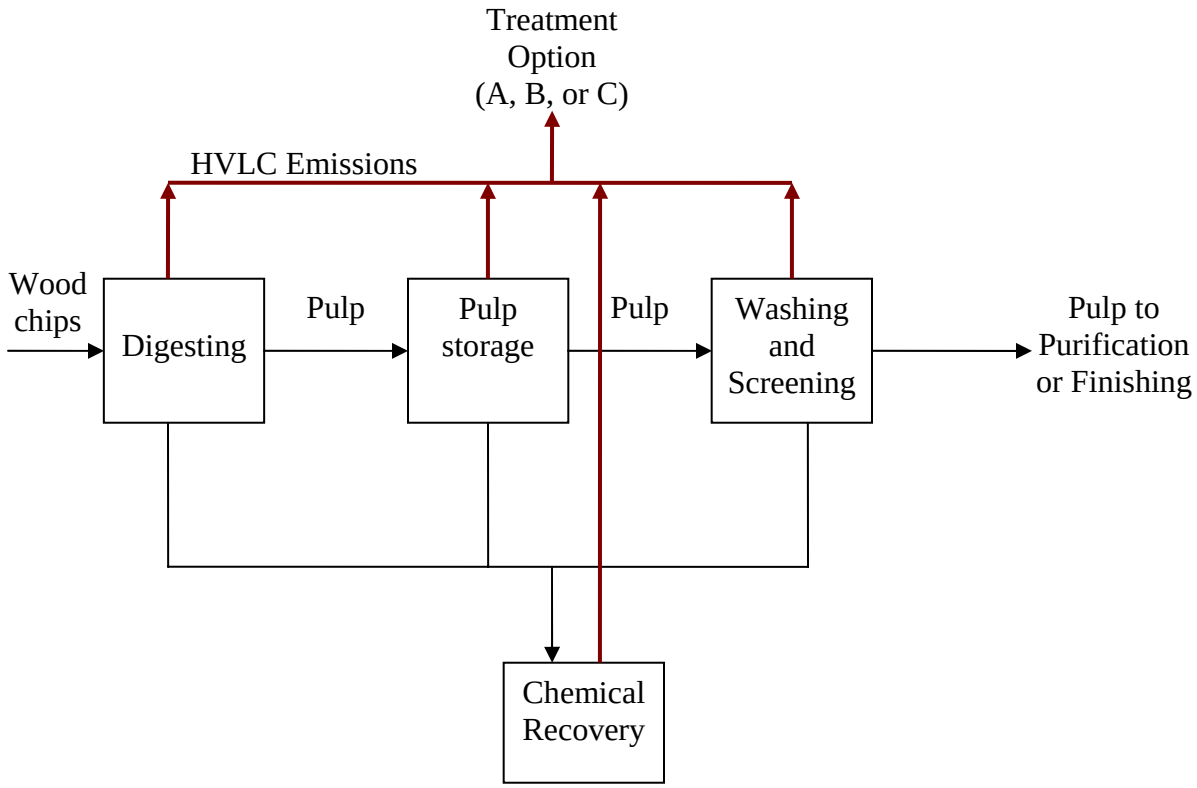

Figure 72. Life Cycle System Schematic

Data Collection

Data is being collected by interviews of environmental managers at pulp and paper mills participating in pilot scale installations of the PCO system, design and operational specifications of the PCO system, NCASI technical documents, literature, regulatory agencies, theoretical calculations, and from published databases (Franklin Associates, Prairie Village, Kansas, USA). SimaPro 7.0 software (PRé Consultants, The Netherlands) is being used to model the life cycle inventory of each scenario of interest as has been previously shown (Babbitt and Lindner, 2005 and 2007a). Life cycle environmental and human health impacts from the three scenarios will be compared to determine the most environmentally preferable HAPs control technology.

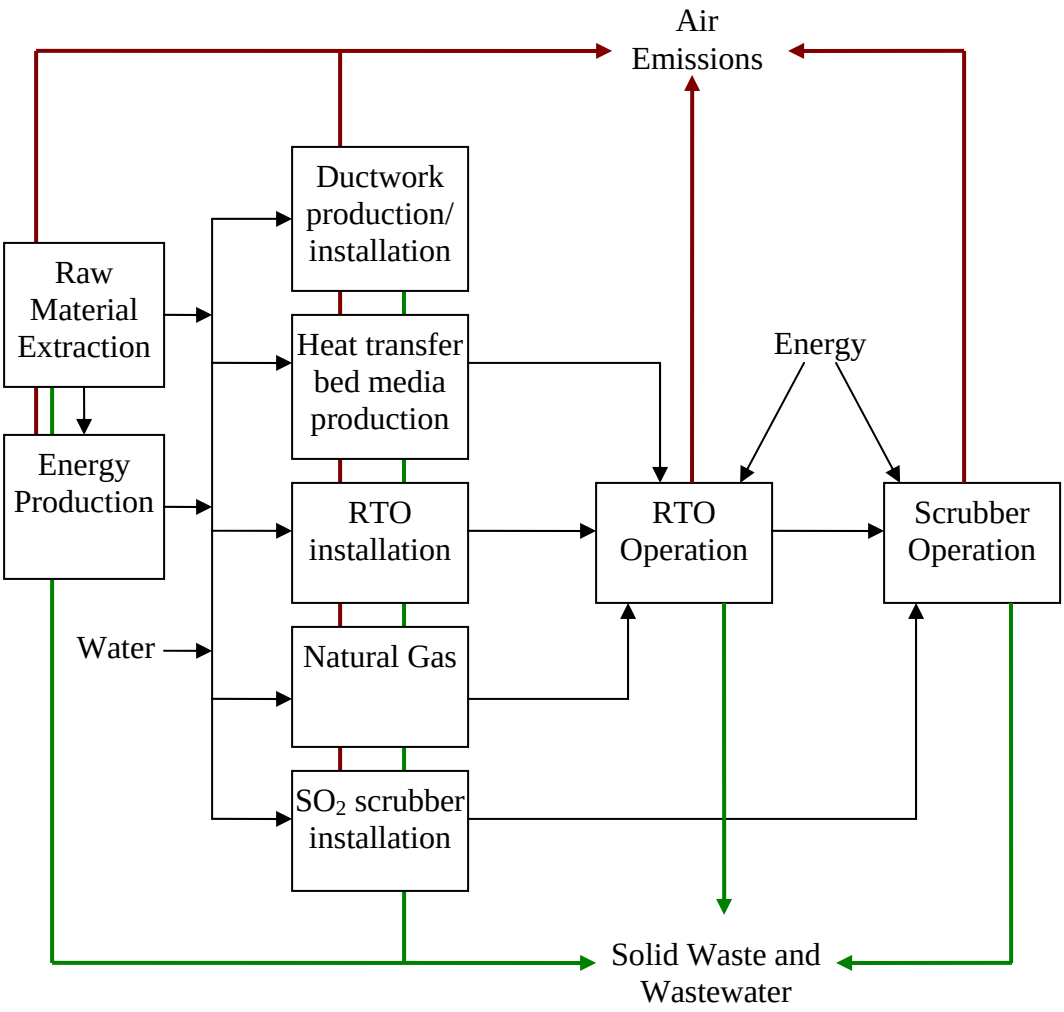

Figure 73A. Life Cycle Stages For the RTO System

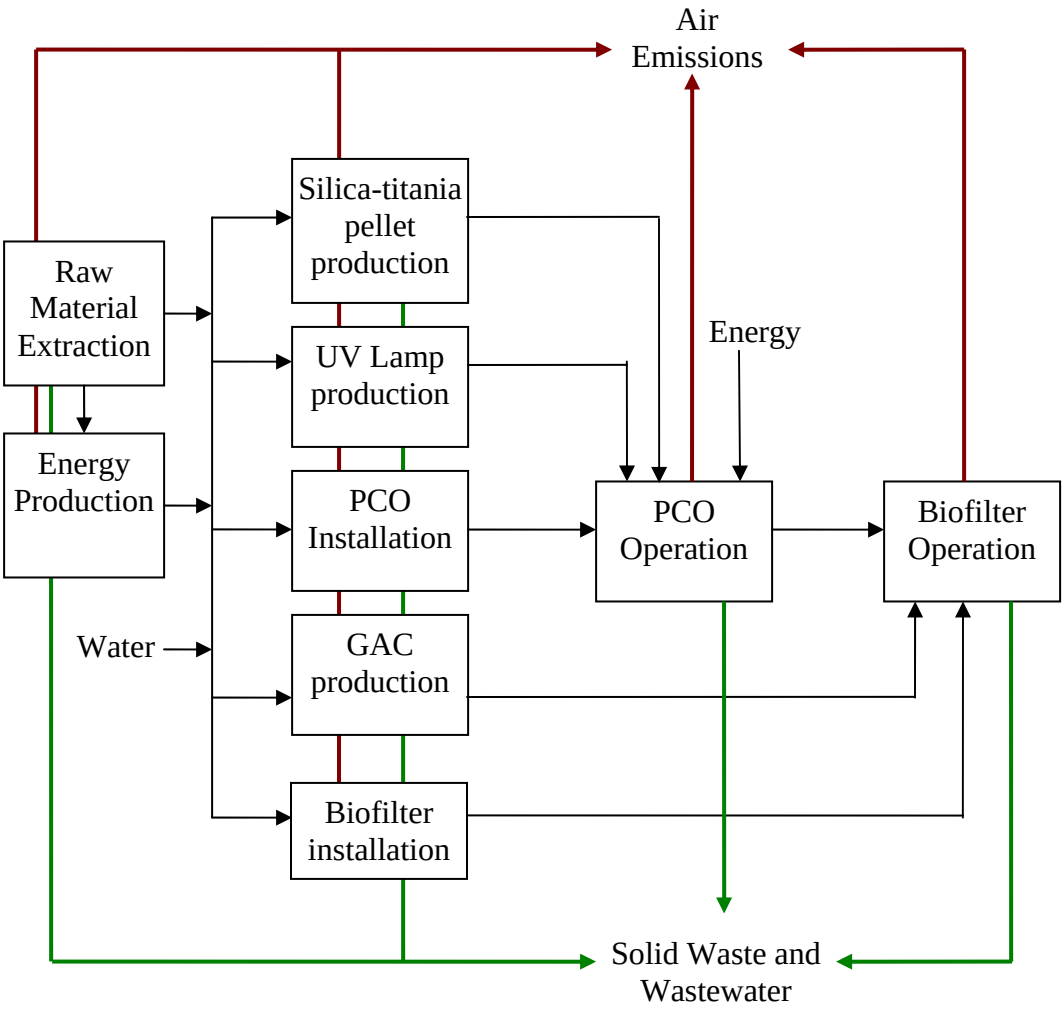

Figure 73B. Life Cycle Stages For the PCO-Biofilter System

Conclusions

Most of the data collection for the LCA has been completed, and currently, work is in progress to complete the inventory and impact assessment portions of the LCA.

REFERENCES

Babbitt, C.W., Lindner, A.S. 2005. A life cycle inventory of coal used for electricity production in Florida. J. Clean. Prod. 13: 903-912.

Babbitt, C.W., Lindner, A.S. 2007a. A life cycle comparison of disposal and beneficial use of coal combustion products in Florida; Part 1: Methodology and inventory of material, energy, and emissions. Int. J. Life Cycle Ass. Submitted.

Babbitt, C.W., Lindner, A.S. 2007b. A life cycle comparison of disposal and beneficial use of coal combustion products in Florida; Part 2: Impact comparisons of disposal and beneficial use options. Int. J. Life Cycle Ass. Submitted.

Bandosz, T. 2002. On the adsorption/oxidation of hydrogen sulfide on activated carbons at ambient temperatures. J. Colloid Interface Sci. 246, 1-20.

Cannon F.S., Dusenbury, J., Paulsen, D., Singh, J., Mazyck, D., Maurer, D. 1996. Advanced Oxidant Regeneration of Granular Activated Carbon for Controlling Air-phase VOCs. Ozone Sci. Engr. 18: 417-441.

Choi, W., Termin, A. and Hoffmann, M. R. 1994. Role of metal ion dopants in quantum-sized TiO2. Correlation between photoreactivity and charge carrier recombination dynamics. J. Phys. Chem. 98 (51): 13669-13769.

Crittenden, J. C., Suri, R. P. S., Perram, D. L., Hand, D. W. 1997. Decontamination of water using adsorption and photocatalysis. Wat. Res. 31: 411-418.

Dedysh, S.N., Smirnova, K.V., Khmelenina, V.N., Suzina, N.E., Liesach, W.; Trotsenko, Y.A. 2005a. Methylotrophic autotrophy in *Beijerinckia mobilis*. J. Bact. 187: 3884-3888.

Dedysh, S.N., Knief, C., Dunfield, P.F. 2005b. *Methylocella* species are facultatively methanotrophic. J. Bact. 187: 4665-4670.

Dijkstra, M., Panneman, H., Winkelman, J., Kelly, J., Beenackers, A. 2002. Modeling the photocatalytic degradation of formic acid in a reactor with immobilized catalyst. Chem. Eng. Sci., 57 (22-23), 4895-4907.

Doronina, NV., Ivanova, EG., Trotsenko, YA. 2005. Phylogenetic position and emended description of the genus Methylovorus. Int. J. Sys. Evol. Microbiol. 55: 903–906.

Dunfield, P.F., Khmelenina, V.N., Suzina, N.E., Trotsenko, Y.A., Dedysh, S.N. 2003. *Methylocella silvestris* sp. nov., a novel methanotroph isolated from an acidic forest cambisol. Int. J. Sys. Evol. Microbiol. 53: 1231-1239.

Fujii, T., Suzuki, T., Sakamoto, K.1997. Simultaneous Removal of Gases and Particulates by Photocatalyst and UV/Photoelectron Method. Kuki Seijo 35(3): 169-176.

Gribbins, M.J., Loehr, R.C. 1998. Effect of media nitrogen concentration on biofilter performance. J. Air Waste Manage. Assoc. 48: 216-226.

Hanson, R.S. 1998. Ecology of methylotrophic bacteria. In Techniques in Microbial Ecology. Burlage, R.S.; Atlas, R.; Stahl, D.; Geesey, G.; Sayler, G.; eds. Oxford

Hayek, L.C., Buzas, M.A. 1996. Surveying Natural Populations. Columbia University Press: New York City, New York.

Hayes, B. L. *Microwave Synthesis: Chemistry at the Speed of Light*; CEM Publishing: Matthews, NC, 2002.

Herrmann, J. M., Disdier, J., Deo, G. and Wachs, I. E. 1997. J. Chem. Soc., Faraday Trans. 93: 1655.

Kim, S. B., Hong, A. C. 2002. Kinetic study for photocatalytic degradation of volatile organic compounds in air using thin film TiO2 photocatalyts. Appl. Catal. B: Env. 35, 305-315.

Kumar, S., Tamura, K., Nei, M. 2004. MEGA3: Integrated software for Molecular Evolutionary Genetics Analysis and sequence alignment. Briefings in Bioinformatics 5:150-163.

Legendre, P., Legendre, L. 1998. *Numerical Ecology*. Second English Edition. Elsevier Science B.V., Amsterdam, The Netherlands.

Lidstrom ME. 2001. "Aerobic Methylotrophic Prokaryotes" in M. Dworkin et al., eds., The Prokaryotes: An Evolving Electronic Resource for the Microbiological Community, 3rd edition, release 3.7, Springer-Verlag, New York, <http://link.springer-ny.com/link/service/books/10125/> Accessed 3/31/06.

Perego, C., Villa, P., 1997. Catalyst preparation methods. Catal. Today 34, 281.

Sadeghi, M., Liu, W., Zhang, T., Stavropoulos, P., Levy, B., 1996. Role of photoinduced charged carrier separation distance in heterogeneous photocatalysis: oxidation degradation of CH3OH vapor in contact wit Pt/TiO2 and cofumed TiO2-Fe2O3. J. Phys. Chem., 100, 19466-19474.

Sutton, W. H., Brooks, M. H., Chabnsky, I. J., 1998. Microwave processing of materials. Materials Research Society, Pittsburgh, Pennsylvania. Volume 124.

Wu, C.Y., Lee, T.G., Tyree, G., Arar, E., Biswas P. 1998. Capture of Mercury in Combustion Systems by InSitu Generated Titania Particles with UV Irradiation. Env. Eng. Sci.15(2): 137-148.

Yang, H., Minuth, B., Allen, D.G. 2002. Effects of nitrogen and oxygen on biofilter performance. J. Air Waste Manage. Assoc. 52: 279-286.

PATENTS

None filed

PUBLICATIONS/PRESENTATIONS

Mazyck, D.W., Wu, C.Y., Lindner, AS., Sheahan, R., and Jain, A. TiO_2-coated carbon for the removal of VOCs. TAPPI Paper Summit, 2004.

Stokke J.M., Mazyck D.W., Wu C.Y. Comparison of titania-doped sorbents for VOC/HAP control (Paper #415). Air and Waste Management 98th Annual Conference and Exhibition. Minneapolis, MN. June 21-24, 2005.

Stokke J.M., Mazyck D.W., Wu C.Y., Sheahan, R. 2006. Photocatalytic Oxidation of Methanol Using Silica-Titania Composites in a Packed-Bed Reactor. Environ. Prog. 25(4): 312-318.

Stokke, J.M. and Mazyck D.W. Effect of Catalyst Support on the Photocatalytic Destruction of VOCs in a Packed-bed Reactor (Paper # 2007-01-3138). Accepted for the International Conference on Environmental Systems. Chicago, IL. July 9-12, 2007.

Stokke J.M., Mazyck D.W. 2007. Optimization of silica-titania composites for methanol removal from humid air streams. To be submitted.

Tao Y., Wu C.Y., Mazyck D.W. 2006. Microwave-assisted Preparation of TiO_2/Activated Carbon Composite Photocatalyst for Removal of Methanol in Humid Air Streams. Indust. Eng. Chem. Res. 45(14): 5110-5116.

Tao Y., Wu C.Y., Mazyck D.W. 2006. Removal of Methanol from Pulp and Paper Mills using Combined Activated Carbon Adsorption and Photocatalytic Regeneration. Chemosphere 65(1): 35-42.

Tao, Y., Wu, C.Y., Mazyck, D.W. 2005. Development of a TiO_2/AC composite photocatalyst by dry impregnation for the treatment of methanol in humid airstreams. Indus. Eng. Chem. Res. 44 (19): 7366-7372.

POSTER PRESENTATIONS

Babbitt, C. Lindner, A.S. A biological activated carbon reactor for reducing emissions of hazardous air pollutants from pulp and paper mills. Air and Waste Management 98th Annual Conference and Exhibition. Minneapolis, MN. June 21-24, 2005.

Mazyck, D., Lindner, A., Wu, C., Stokke, J. An Innovative Titania-Activated Carbon System for the removal of VOCs and HAPs from Pulp, Paper, Paperboard Mills, and Wood Products Facilities with In-situ Regeneration Capabilities. ITP Forest Products Peer Review. Atlanta, GA. April 2006.

Tao, Y., Wu, C.Y., Mazyck, D.W. Development of a TiO_2/Activated Carbon Composite Photocatalyst by Pore Volume Impregnation for Treatment of VOCs and HAPs. Air & Waste Management Association. Minneapolis, MN on June 21-24, 2005.

Tao, Y., Wu C.Y., Schwartz, S., Mazyck, D.W. Development of a TiO_2/Activated Carbon Composite Photocatalyst by Pore Volume Impregnation for Treatment of VOCs and HAPs. Air and Waste Management Conference. Orlando, FL. October 27, 2004.

PARTICIPATION

Students supported via this proposal:

Callie Babbitt (Ph.D. candidate)
Jennifer Stokke (Ph.D. candidate)
Yong Tao (received Ph.D. in 2006)
Christina Akly*
Gustavo Avila*
Brendon Blum*
Aly Byrne*
Heather Byrne*
Teri Lierman*
Paloma Rohrbaugh*
Sam Schwartz*

* undergraduate

MILESTONE STATUS TABLE

ID Number	Task / Milestone Description	Planned Completion	Comments
1	Development of Materials		
1.1	Literature Review	8/31/03	Review journals and patents
1.2	Assess Commercial Products	9/30/03	Characterize pros and cons
1.3	Tailor Products with Wood Biomass	11/31/03	Optimization for application
1.4	Assess silica as a sorbent	9/30/03	Characterize pros and cons
1.4	Optimize Coating Strategy	1/31/04	Focus on sol gel
1.5	Quantify Regeneration Efficiency	3/31/05	Performance testing
2	Pilot Design and Testing	9/30/03	
2.1	Site Visits	10/31/03	Mill assessments
2.2	Design System	12/31/03	Schematics/Bill of Materials
2.3	Construct and Evaluate Bench Apparatus	3/31/04	For prototype research
2.4	Construct Pilot Plant	12/31/04	For field site installation
2.5	Evaluate Pilot Plant	3/31/05	Shakedown tests
3	Field Tests	2/28/06	
3.1	Data Collection	2/28/06	Performance characterization
3.2	Assess bio/carbon synergies	11/31/05	
3.3	Modify Pilot Plant	12/31/06	Modified for STC technology
4	Life Cycle Analyses	3/31/07	
4.1	Environmental	3/31/07	
4.2	Energy	3/31/07	
4.3	Economic	3/31/07	

APPROVED BUDGET DATA

Phase / Budget Period			DOE Amount	Cost Share	Total
	From	To			
Year 1	4/03	3/04	434,629	156,643	591,272
Year 2	4/04	3/05	650,617	167,574	818,191
Year 3	4/05	3/06	553,503	143,744	697,247
Year 4					
Year 5					
Totals			1,638,749	467,961	2,106,710